THE UNIVERSITY
of EDINBURGH

Towards Understanding the Signalling Requirements of Thymic Epithelial Progenitor Cells

Dong Liu

Thesis submitted for the degree of Doctor of Philosophy

The University of Edinburgh

March 2018

Declaration

The work in this thesis is my own, except where otherwise stated.

Dong Liu

Acknowledgements

I would first like to thank my supervisor Prof. Clare Blackburn for the opportunity to work in her lab. I owe my academic progress to her constant guidance and encouragement in the last four years. I would like to express my gratitude for the valuable advice I received from my thesis committee: Dr. Sally Lowell, Dr. Simon Tomlinson and Dr. Henning Wackerhage. Moreover, I am deeply grateful to Dr. Kathy O'Neill for training me when I joined the lab, and so many enlightening discussions we had over the years.

I could not have completed my PhD without the help of Dr. Claire Cryer and Dr. Fiona Rossi in the flow lab, and Dr. Bertrand Vernay of the imaging facility. My sincere appreciation goes to Ron Wilkie for teaching me all about histology. Special thanks to all the technical staff at the CRM, especially Theresa, Helen and Marilyn in tissue culture, and Carol, John, Hollie and Laura in the animal unit. They made this institute such a great place to work in. I would also like to thank the School of Biological Sciences and Edinburgh Global Research for sponsoring my scholarship.

I am grateful to my collaborators Dr. Ute Koch and Prof. Freddy Radtke at the EPFL, and Dr. Francois Guillemot at the Francis Crick Institute. Much of this thesis is only possible because of their generosity. Thank you also to members of the Medvinsky lab, Kranc lab, Chambers lab and Wilson lab for all you help.

Thanks a million to Frances Stenhouse and Diana Peddie for looking after all aspects of my work in the lab. What's more, I could not have wished for better lab mates. I am glad to have shared this journey with Kathy, Svetlana, Harsh, Nick, Karen, Natasha, Paul, Tim, Alberto, Dominique and Joanna.

I am very fortunate to have worked with some wonderfully talented science communicators and podcasters during my PhD. The world is a noisy place. It's comforting to know that our research means something to somebody.

Being so close to my Scottish family, Lisa, Ron and Aidan, I never felt that I was alone. And I won't ever forget the joyous time I spent with so many dear friends and colleagues in Edinburgh – you are the colours of my life.

Finally, I would like to thank my parents for their support every step of the way. No matter how far away, you are always on my mind.

Abstract

Thymic epithelial cells (TECs) are indispensable for the development of T cells in the thymus. Two subtypes of TECs exist in the thymus, medullary mTECs and cortical cTECs. Both mTECs and cTECs originate from endodermal thymic epithelial progenitor cells (TEPCs) in the embryo, but how the differentiation of TEPCs is regulated is not well understood. The aims of this thesis were to establish the role of Notch signalling in TEPC differentiation, and how it interacts with known regulators such as FOXN1 and the NFκB pathway. Gene expression data showed that Notch is active in TEPCs and exhibits a correlation with the mTEC lineage. Loss of Notch function led to a significant reduction in the number of mTECs in the thymus, and this can be attributed to aberrant mTEC specification. Furthermore, the duration of Notch activity in determining mTEC number appears limited to the early phase of organogenesis, and precedes RANK/NFκB mediated mTEC proliferation. Gain of Notch function resulted in a considerable shift to a primitive, TEPC-like phenotype, and subsequently a latent increase in mTEC frequency. Finally, transcriptomic and functional analyses pointed to a cross-repressive mechanism between Notch and FOXN1 in TEPCs. Taken together, these results identified Notch as a novel regulator of mTEC specification, likely through maintaining the potency of fetal TEPCs, a pre-requisite for mTEC lineage commitment.

Lay summary

T cells comprise an important part of the immune system. The development of T cells in the thymus is controlled by thymic epithelial cells (TECs). TECs can be broadly divided into those residing in the cortex (cTECs), and those in the medulla (mTECs). The role of cTECs is to select for T cells that are capable of recognizing antigens, whereas mTECs are responsible for preventing T cells that can harm one's own tissues from entering the bloodstream. It is known that cTECs and mTECs originate from a common progenitor population in development, but how these progenitors decide to become either cTECs or mTECs is not well understood. The aim of this thesis was to investigate whether a cell-to-cell communication mechanism, known as the Notch signalling pathway, is involved in controlling the cell fate decision of early TECs. By removing a key component of the Notch pathway, or by treating embryonic thymus with a chemical that prevents Notch signalling, I showed that Notch is required for the emergence of mTECs. Furthermore, using a genetic system that activates Notch signalling in all developing TECs, I concluded that Notch facilitates cell fate regulation by promoting the maintenance of TEC progenitors. High throughput gene expression analysis identified several potentially significant target genes, and demonstrated that Notch activity in developing TECs is self-reinforcing. Incorporating the results obtained from these work, I proposed an updated model for TEC progenitor differentiation by integrating Notch with other known regulators of early TEC development.

Table of Contents

Abbreviations

3PP – Third pharyngeal pouch

BMP – Bone morphogenetic protein

bp – base pair

cDNA – Complementary DNA

cKO – Conditional knockouts

CLDN – Claudin

CMJ – Cortico-medullary junction

Cq – Quantification cycle

cTEC – Cortical thymic epithelial cells

DAPI – 4',6-Diamidino-2-phenylindole

DAPT – γ-secretase inhibitor

DC – Dendritic cells

DEL – Deleted allele

dGuo – 2’ Deoxyguanosine

DLL – Delta-like (Notch ligand)

DMSO – Dimethyl sulfoxide

DN – Double negative

DP – Double positive

ECM – Extracellular matrix

EGFR – Epidermal growth factor receptor

FACS – Fluorescence-activated cell sorting

FGF – Fibroblast growth factor

FL – Floxed allele

FMO – Fluorescence minus one

FTOC – Fetal thymus organ culture

GFP – Green fluorescence protein

GRN – Gene regulatory networks

IHC – Immunohistochemistry

IL – Interleukin

JAG – Jagged (Notch ligand)

K – Keratin

mTEC – Medullary thymic epithelial cells

NICD – Notch intracellular domain

PC – Principal component

PCA – Principal component analysis

RANK – Receptor activator of nuclear factor kappa-B

RANKL – Receptor activator of nuclear factor kappa-B ligand

RBPJ – Recombining binding protein suppressor of hairless

RT-qPCR – Real-time quantitative polymerase chain reaction

Seq – Sequencing

Shh – Sonic hedgehog

SP – Single positive

TCR – T-cell receptor

TEC – Thymic epithelial cells

TEPC – Thymic epithelial progenitor cells

TNFSF – Tumor necrosis factor superfamily

TRA – Tissue restricted antigens

Treg – Regulatory T cells

MHC –Major histocompatibility complex

RTOC – Reaggregate thymic organ culture

Chapter I: Introduction

1.1 The thymus

T lymphocytes develop exclusively in the thymus (Male et al., 2013). In mammals the thymus is a bi-lobed organ situated above the heart (Miller, 1961). The organ is found in all jawed vertebrates (Boehm and Swann, 2014), reflecting the increased complexity in the vertebrate adaptive immune system. The complexity of cellular and molecular interactions during T cell development is also highlighted by the fact it is the only haematopoietic lineage that requires a dedicated organ.

The purpose of thymopoiesis is to generate a T cell receptor (TCR) repertoire capable of engaging self major histocompatibility complexes (MHC) that display foreign but not self antigens (Male et al., 2013). The need to acquire sufficient TCR specificities to recognize an immense range of foreign antigens presents a formidable challenge to the immune system. Random rearrangement of the TCR loci ensures that a diverse repertoire is generated (Krangel, 2009), with the compromise that such process is highly energetically expensive: more than 99% of T cells undergo cell death during positive and negative selection (Krueger et al., 2017). Defects in establishing the thymic microenvironment result in T cell immunodeficiency (Nehls et al., 1996), whereas failure to eliminate self-antigen recognizing T cells can cause autoimmunity (Kajiura et al., 2004).

Developing T cells, or thymocytes, account for more than 99% of the cells in the adult thymus, with the other 1% composed of various cell types of the stroma (Gray et al., 2006). The cells making up the stroma are thymic epithelial cells (TECs), dendritic cells (DCs), endothelial cells, fibroblasts, macrophages, natural killer cells and thymic B cells (Figure 1.1A). Of these, TECs are of central importance, since fully functional thymi can be formed from grafts whose potential stromal contribution is restricted to TECs (Gordon et al., 2004). Unlike most types of epithelial cells, TECs form neither simple nor stratified epithelium. Rather, they lack apparent apico-basal polarity and form three-dimensional reticular meshwork that maximizes contact area with thymocytes (van Ewijk et al., 1999).

The interior of the thymus is divided into two major regions, known as cortex and medulla, through which thymocytes migrate in a highly stereotypical fashion to encounter unique signals at each stage of their development (Blackburn and Manley, 2004). The two compartments contain two subtypes of resident TECs, cortical TEC (cTEC) and medullary TEC (mTEC). Localization aside, the distinction of cTEC and mTEC also concerns their functions and developmental lineages (reviewed in Takahama et al., 2017). The area where outer cortex meets inner medulla is termed cortico-medullary junction (CMJ) and has characteristic histological and molecular features. It has been shown that certain TECs located at the CMJ exhibit progenitor activity (Klug et al., 1998; Ulyanchenko et al., 2016; Wong et al., 2014).

Perhaps related to the metabolically expensive nature of thymopoiesis, or the selective pressure to minimize cancer risks, the thymus begins to degenerate from an early age (1-year after birth in humans), in a highly regulated process known as age-related thymic involution (Boehm and Swann, 2013; Chaudhry et al., 2016). Involution is defined by several hallmarks: decrease of thymus size, reduction of T cell production, loss of cortico-medullary architecture and the invasion and replacement of the tissue by adipose cells (reviewed in Chinn et al., 2012). It contributes to the immuno-senescence phenomenon where elderly people become more prone to novel infections and cancer, due to poorer immuno-surveillance (Palmer, 2013). In circumstances where a new T cell repertoire is required, such as following bone marrow transplantation, the lack of significant thymic capacity poses a more acute challenge (Chaudhry et al., 2016). Therefore, interventions to regenerate the thymus are of considerable clinical value.

Thymus regeneration strategies belong to two broad categories: (1) tissue regeneration rooted in chemical stimulation of residual TEC progenitors, and (2) tissue replacement. Fibroblast Growth Factor 7 (FGF7), Interleukin 22 (IL22) and enforced Forkhead Box Protein N1 (FOXN1) expression have all been shown to promote thymus regeneration (Alpdogan et al., 2006; Bredenkamp et al., 2014a; Dudakov et al., 2012). Alternatively, TECs can be generated from directed differentiation of pluripotent stem cells or trans-differentiation from unrelated tissues (Bredenkamp et al., 2014b; Parent et al., 2013; Sun et al., 2013), underlying the potential of tissue replacement. Importantly, in order to constitute a viable therapy,

such tissue needs to contain long-term self renewing TEC progenitors, and both cTEC and mTEC compartments (reviewed in Bredenkamp et al., 2015). In this regard, our understanding of thymus development, the way embryos build the thymus for the first time, will provide valuable insights for attempts to regenerate the thymus, during which the need to rebuild the organ arises.

1.2 T cell development

Haematopoietic progenitors enter the adult thymus at the CMJ. The earliest intrathymic progenitors can differentiate into T cells, B cells and myeloid cells (Luc et al., 2012). The initial seeding of the thymic primordium by progenitors is dependent on FOXN1 and its direct targets, Chemokine (C-C motif) Ligand 25 (CCL25), C-X-C Motif Chemokine 12 (CXCL12) and Kit ligand (Calderon and Boehm, 2012; Luis et al., 2016). In the thymus, thymocytes go through sequential stages of differentiation characterized by cell surface marker expression. Those stages are $CD4^-$ $CD8^-$ (double negative, DN), $CD4^+$ $CD8^+$ (double positive, DP), and finally $CD4^+$ $CD8^-$ or $CD4^-$ $CD8^+$ (single positive, SP). The DN stages can be further divided by the expression of CD44 and CD25 into DN1 ($CD44^+$ $CD25^-$), DN2 ($CD44^+$ $CD25^+$), DN3 ($CD44^-$ $CD25^+$) and DN4 ($CD44^-$ $CD25^-$) stages (reviewed in Shah and Zuniga-Pflucker, 2014). The importance of cTECs, mTECs and cortico-medullary architecture for the differentiation and selection of developing T cells is discussed here (Summarized in Figure 1.1A,B).

The specification of T cells is regulated by Notch signalling. Activated by ligand Delta-like 4 (DLL4) on cTECs, early thymic progenitors (ETPs) upregulate *Hes1*, *Gata3*, *Tcf7* and *Bcl11b,* and these factors steer ETPs into the T cell lineage (Shah and Zuniga-Pflucker, 2014). Once the Notch signal is received, DN2 thymocytes in the cortex begin rearranging the V(D)J region of the T Cell Receptor β (*Tcrb)* locus by RAG1 and RAG2 recombinases, and by the DN3 stage assemble the pre-TCR complex with invariant pre-TCRα and CD3. DN2 thymocytes can also rearrange TCRγδ chain and become γδ-T cells (Krangel, 2009). Successful TCRβ rearrangement triggers ligand-independent pre-TCR signalling, resulting in extensive proliferation at the subcapsular cortical region, followed by rearrangement of TCRα

locus and the upregulation of CD4 and CD8 (Yamasaki and Saito, 2007). These DP cells migrate through deep cortex to undergo positive selection by engaging self peptide-MHC complexes displayed on cTECs.

Affinity between TCR and MHC is crucial for the outcome of positive selection, since only weak engagement promotes cell survival, while the lack of physical binding leads to death by neglect, and strong affinity to apoptosis, respectively (reviewed in Klein et al., 2014). DP thymocytes further differentiate into CD4 or CD8 SP T cells in the cortex as they become restricted to either MHCII or MHCI. cTECs orchestrate these processes too with β5t (a component of thymoproteasome) and Cathepsin L (CtsL) (Takada et al., 2017). Thymoproteasome is important for the generation of high affinity MHCI ligands, and consequently the number of $CD8^+$ SP T cells was considerably hampered in β5t deficient mice (Murata et al., 2007). Moreover, Cathepsin L catalyzes the processing of MHCII in endosome as well as the production of self peptide to be loaded on MHCII in lysosome. In the absence of these combined actions, CD4 SP T cells in *CtsL* mutants were severely impaired (Honey et al., 2002; Nakagawa et al., 1998).

Thymocytes passing the positive selection checkpoint then migrate from cortex to medulla. This migration occurs in a chemokine receptor CCR7-dependent manner (Ueno et al., 2004). Although negative selection against ubiquitously expressed self antigens also proceeds in the cortex (Krueger et al., 2017), the selection against tissue restricted antigens (TRAs), proteins expressed in specific peripheral tissues, only occurs in the medulla (Klein et al., 2014). The vast antigen diversity is the results of promiscuous gene expression mediated by Autoimmune Regulator (AIRE) and FezF2 in mTECs (Anderson and Su, 2016; Takaba et al., 2015). TRAs can be directly presented on mTECs, or on DCs via transfer from mTECs. Interestingly each TRA is only expressed in 1-3% of mTECs, and it takes 200-500 mTECs to represent the full TRA repertoire (Klein et al., 2014). It has been estimated that SP T cells encounter hundreds of antigen presenting cells before exiting the thymus, thus minimizing the risk of autoreactivity (Klein et al., 2014).

Peripheral T cells that escape negative selection are controlled by regulatory T cells (Tregs), and the initial development of $CD4^+$ $CD25^+$ $Foxp3^+$ regulatory T cells also

occurs in the thymic medulla (reviewed in Lio and Hsieh, 2011). CD4 SP T cells differentiate via either of two progenitor states, $CD25^{+}$ $Foxp3^{-}$ or $CD25^{-}$ $Foxp3^{+}$, before acquiring the fully mature phenotype (Lio and Hsieh, 2008; Tai et al., 2013). Functional mTECs are instrumental to Tregs generation in the thymus, since mTEC deficient $Relb^{-/-}$ thymus grafts contain dramatically reduced precursor and mature Tregs (Cowan et al., 2013). Striking similarities exist between Treg generation and negative selection, although autoreactive TCRs on Tregs are of lower affinity (Klein et al., 2014). A recent study found that both precursor and mature Tregs in thymus, defined by CD25 and Foxp3, consist of both de novo and recirculating Tregs from the periphery (Cowan et al., 2016). Thus aspects of Treg development may require reassessment.

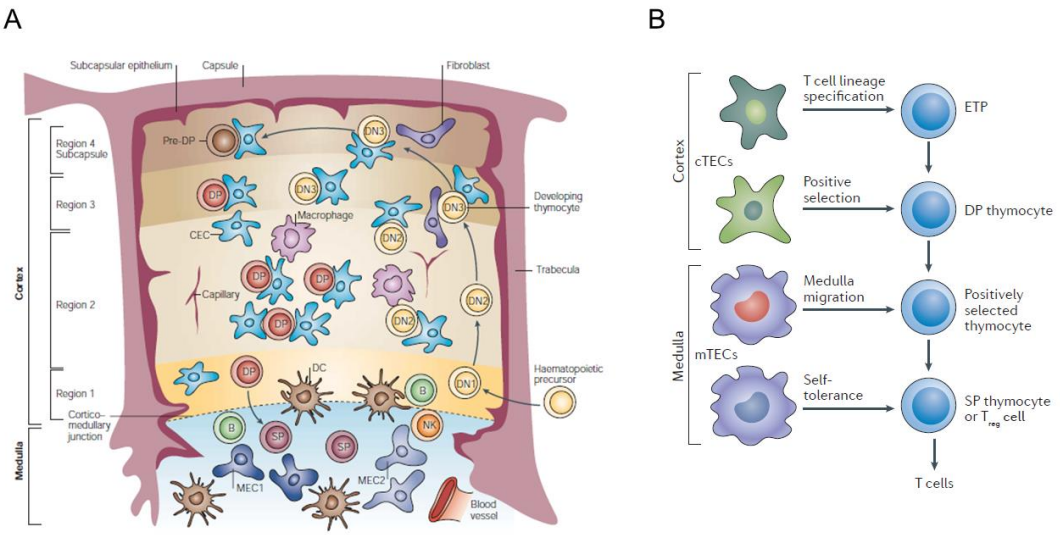

Figure 1.1 T cell development is coupled to the orderly migration of thymocytes in the thymus.

(A) The stereotypical route of thymocyte migration in the thymic stroma. CEC – cTEC, MEC – mTEC, B – thymic B cell, NK – natural killer cell, DC – dendritic cells. (Blackburn and Manley, 2004)

(B) cTECs and mTECs orchestrate progression to increasingly mature thymocytes (Takahama et al., 2017).

1.3 Overview of thymus development

The thymus anlage forms from the third pharyngeal pouches (3PPs), a pair of evaginations of the pharynx, which exist from E9.5 to E11.5 in the mouse embryos. The 3PPs are the common primordia for the thymus and the parathyroid, which are clearly demarcated by the expression of ventral *Foxn1* and dorsal Glial Cells Missing 2 (*Gcm2)* respectively by E11.25 (Gordon et al., 2001). The common primordia separate from the pharynx at E11.5, and the thymus and parathyroid separate from each other at E12.5. The two thymus lobes then migrate caudally from the neck region and join above the heart, where further growth and differentiation will proceed (reviewed in Gordon and Manley, 2011). Of note, both the thymic primordia and TECs dramatically change their morphology in early organogenesis. First, from E10.5 to E11.5 the two dimensional (2D) endodermal layer thickens, transforming from a simple to a more stratified epithelium. In the following two days the 3PP lumen collapses, TECs lose apico-basal polarity and form an extensive meshwork underpinning a fully three-dimensional (3D) rudiment (Itoi et al., 2001).

The origin of TECs, thymocytes and other thymic cell types was first probed using the chick-quail chimera system. Quail pharyngeal endoderm transplanted into chick hosts gave rise to TECs in the chimeric thymus, whereas T cells and thymic mesenchyme were of host origin (Le Douarin and Jotereau, 1975). This indicates that TECs originate from the endoderm. Moreover, the potency of murine thymic cells can be studied by transplanting tissue or reaggregated thymic organ culture (RTOC) under the kidney capsule (Blackburn and Manley, 2004; Sheridan et al., 2009). Dissected E9.0 3PP endoderm, when grafted, grew into an ectopic thymus composed of normal cortico-medullary architecture and capable of supporting T cell development, establishing the endoderm as the sole origin of TECs (Gordon et al., 2004). Crucially this study suggested that the thymic fate is inherent to a subset of cells in the 3PP endoderm, even though definitive markers such as *Foxn1* are not yet switched on.

Two laboratories independently identified Placenta-expressed Transcript 1 (PLET1), the antigen targeted by MTS20 and MTS24 monoclonal antibodies (Depreter et al., 2008), as a marker for a fetal TEC population that can reconstitute the thymus in

RTOC grafts (Bennett et al., 2002; Gill et al., 2002). Improved flow cytometry techniques led to the finding that nearly all TECs express PLET1 at E12.5, and the proportion of PLET1^{+} TECs declines subsequently in organogenesis (Nowell et al., 2011). The differentiation of TECs has also been characterized with cytokeratin expression. In the early thymus rudiment most TECs are cytokeratin K5^{+} K8^{+}, and later downregulate either marker to become K5^{+} K8^{-} mTECs or K5^{-} K8^{+} cTECs (Bennett et al., 2002; Gill et al., 2002; Klug et al., 2002). Of interest, K5^{+} K8^{+} TECs are also found in the CMJ and were thought to be a likely source of TEC progenitors in adult thymus (Klug et al., 1998).

The maturation of TECs is dependent on signals from mesenchymal cells and developing T cells (Auerbach, 1960; van Ewijk et al., 1994). Neural crest-derived mesenchyme coalesces around the thymic lobes to form the capsule, and these cells secrete FGF factors to stimulate the proliferation of immature TECs (Jenkinson et al., 2003; Revest et al., 2001). Colonization of the thymus by haematopoietic cells begins at E11.5 (Luis et al., 2016), coinciding with the onset of *Foxn1* expression and the shift of epithelial morphology. In the hCD3ε transgenic mice where thymopoiesis was blocked at DN1 stage, TECs were found to be in a 2D configuration and predominantly K5^{+} K8^{+}, and large cysts were present in the hypoplastic thymi (Klug et al., 1998; Van Ewijk et al., 2000). This likely represents failure to maintain organization as haematopoietic progenitors are not required for the initial patterning of fetal epithelium (Klug et al., 2002). In contrast, in Rag1$^{-/-}$ mutants where T cell development was blocked at the DN3 stage, cTEC organization was reticular and differentiated K5^{-} K8^{+} cTECs were found, although mTECs were barely detectable (Klug et al., 1998). Indeed, the elaboration of the mTEC sub-lineage occurs in the presence of more mature, positively selected T cells (Hikosaka et al., 2008). Taken together these results show that TEC differentiation past the initial establishment stage contains several checkpoints and requires non cell-autonomous interactions to progress.

1.4 Molecular regulation of thymus organogenesis

1.4.1 FOXN1

The investigation of FOXN1 began with the description of the 'nude' mutant phenotype (Flanagan, 1966), in which thymus development is arrested very early in organogenesis and thymopoiesis does not occur (Cordier and Haumont, 1980; Pantelouris, 1968; Pantelouris and Hair, 1970). Positional cloning and targeted gene disruption confirmed *Foxn1*, which encodes a DNA-binding protein, as the *nude* gene and the mutation is a single nucleotide deletion in *Foxn1* exon 3 (Nehls et al., 1996; Nehls et al., 1994). Elegant cross-transplantation studies of thymus and bone marrow between *nude* and wildtype mice showed that the thymic phenotype in *nude* mice was due to stromal rather than haematopoietic defects (Wortis et al., 1971). Furthermore, chimera analysis showed that *nude* TECs could be incorporated into a wildtype thymic epithelium, but they retain immature markers, suggesting that FOXN1 acts cell-autonomously to promote TEC differentiation (Blackburn et al., 1996). Indeed, the potency of *Foxn1* knockout TECs resembles that of undifferentiated bipotent TEC progenitors, since quasi-clonal postnatal activation of *Foxn1* in these cells was sufficient to resume the formation of a patterned and functional thymus (Bleul et al., 2006).

The targets of FOXN1 in TECs can be broadly divided into genes that are responsible for thymocyte development in the thymus, and those that act cell autonomously to regulate TEC differentiation. Several studies have shown that FOXN1 directly activates genes essential for nurturing T cell migration, selection and maturation, including *Dll4*, *Ccl25*, *Cxcl12*, *Psmb11* and *Cd83* (Bajoghli et al., 2009; Uddin et al., 2017; Zuklys et al., 2016). Of these targets, DLL4 activates Notch receptors on haematopoietic progenitors, committing them to the T cell lineage while suppressing the alternative B cell fate (Koch et al., 2008). CCL25 and CXCL12 are chemokines that direct the cell migration within the thymus (Hu et al., 2015). *Psmb11* encodes the β5t unit of thymoproteasome and is required for MHCI function and selection of CD8 SP T cells (Murata et al., 2007). Knockout of cell surface protein CD83 is known to stabilize surface MHCII and boost the positive selection of $CD4^+$ SP T cell (Fujimoto et al., 2002). Forced expression of some of these targets

in *Foxn1*$^{-/-}$ TECs rescued certain aspects of T cell development, while TECs remain undifferentiated (Calderon and Boehm, 2012). This showed that the two distinct roles of FOXN1 can be uncoupled. Abnormal endothelial and mesenchymal cells phenotypes have also been observed in *Foxn1* mutant thymi (Bryson et al., 2013; Mori et al., 2010), indicating that FOXN1 regulates other components of the stroma.

Foxn1 gene expression in TECs is initiated at E11.25, when the thymic identity of the domain is already determined (Gordon et al., 2001; Gordon et al., 2004). Using hypomorphic *Foxn1* strains, it has been demonstrated that TEC differentiation occurs in a progressive manner, with each step forward requiring higher levels of FOXN1 (Nowell et al., 2011; Su et al., 2003). The specification of the mTEC lineage, however, takes place even in TECs expressing little or no *Foxn1*, suggesting that TEC lineage divergence precedes, or is independent of, *Foxn1* expression (Baik et al., 2016; Nowell et al., 2011). In terms of regulatory mechanisms, FOXN1 appears to exert a mitogenic effect on TEC progenitors (Itoi et al., 2001), and this is indeed consistent with the observations in postnatal thymus (Bredenkamp et al., 2014a; Chen et al., 2009). Furthermore, though not definitively proved, several transcription factors associated with FOXN1, such as P63 and PAX1 (Nowell et al., 2011; Zuklys et al., 2016), are candidates that may account for the differentiation block in *Foxn1* mutants. What is more, TEC differentiation also requires crosstalk with thymocytes (van Ewijk et al., 1994). Through facilitating T cell development, FOXN1 is indirectly involved in regulating TEC maturation by ensuring that thymic crosstalk occurs normally.

1.4.2 Transcription factor network

A genetic regulatory network (GRN) of transcription factors defines thymic identity prior to, and eventually leads to, the initiation of *Foxn1* expression (Figure 1.2). It was postulated that, based on a number of single or compound knockout mice, this GRN consists of *Hoxa3*, *Pax1*, *Pax9*, *Eya1*, *Six1* and *Tbx1* (Blackburn and Manley, 2004; Hollander et al., 2006). More recent data have largely confirmed this theory, although the specific role of *Tbx1* has been revised (Reeh et al., 2014). Moreover,

gene expression analysis has suggested additional components in this GRN, notably *Foxg1* and *Islet1* (Wei and Condie, 2011).

In the foregut/pharyngeal region, Homeobox A3 (*Hoxa3*) is expressed in both the endoderm and the surrounding mesenchyme (Manley and Capecchi, 1995). Deletion of *Hoxa3* resulted in the lack of thymus, parathyroid and a greatly reduced thyroid gland in newborns, which can be traced to the malformation of E10.5 3PP/4PP (Chisaka and Capecchi, 1991; Manley and Capecchi, 1995). In *Hoxa3*$^{-/-}$ mice, *Foxn1* expression is delayed but nevertheless initiated, thus *Hoxa3* alone does not define thymic identity (Chojnowski et al., 2014). A rise in apoptosis was observed in *Hoxa3*$^{-/-}$ 3PP prior to *Foxn1* activation, suggesting that the lack of thymus in mutant neonates is due to enhanced cell death (Chojnowski et al., 2014). Conditional deletion of *Hoxa3* in the endoderm led to a more severe thymic phenotype than deletion in mesenchyme, and this may be explained by the fact that *Bmp4* expression is dependent on *Hoxa3* only in the endoderm (Chojnowski et al., 2014).

Paired Box 1 (PAX1) and Paired Box 9 (PAX9) are related transcription factors that share high degrees of homology (reviewed in Blake and Ziman, 2014). Both genes are expressed in the E10.5 3PP (Peters et al., 1998; Wallin et al., 1996), however their knockout phenotypes are considerably different. The *Pax9*$^{-/-}$ mice display a 3PP/4PP growth defect at E11.5 (Peters et al., 1998) and instead of undergoing normal migration, a highly hypoplastic mass of thymic tissue remains in the neck region (Hetzer-Egger et al., 2002). These ectopic pharyngeal polyps express *Foxn1*, support initial thymocyte colonization, but diminish after E16.5 due to pervasive apoptosis (Hetzer-Egger et al., 2002). In contrast, thymic rudiments migrate normally in *Pax1* mutants, albeit exhibiting mild growth retardation, large cysts and delay in DN-to-DP thymocyte transition (Wallin et al., 1996).

Of note, the maintenance of *Pax1* expression following initiation is *Hoxa3*-dependent (Manley and Capecchi, 1995), yet *Hoxa3* expression is unaffected in *Pax1 Pax9* double knockouts (Zou et al., 2006), suggesting that *Hoxa3* is upstream of *Pax1*. What is more, losing one *Hoxa3* allele exacerbated the *Pax1* mutant phenotype (Su et al., 2001; Su and Manley, 2000). The compound phenotype of *Hoxa3*$^{+/-}$ *Pax1*$^{-/-}$ thymus consists of more severe aberrations detected in *Pax1* mutants – hypoplasia,

cysts and DP arrest, and additional defects – stalled migration, low epithelial MHCII expression and low DN count. These data indicate that HOXA3 regulates thymus organogenesis through both PAX1 and other independent mechanisms.

Eyes Absent Homolog (EYA) and Sine Oculis Homeobox Homolog (SIX) factors form transcriptional complexes in a highly conserved fashion. *Eya1* and *Six1* are expressed in the pharyngeal pouch and subsequently in fetal thymus (Xu et al., 2002; Zou et al., 2006). The thymus-parathyroid primordium is not formed in $Eya1^{-/-}$ mice (Xu et al., 2002), whereas in $Six1^{-/-}$ or $Six1^{-/-}$ $Six4^{-/-}$ double knockout the 3PP rudiment forms but rapidly degenerates due to apoptosis (Zou et al., 2006). Notably, *Six1* expression is reduced in $Eya1^{-/-}$ primordia, and $Eya1^{-/-}$ $Six1^{-/-}$ double mutants exhibit additional aberrations compared to either single knockout, such as lower expression of *Pax1*, *Fgf8* and *Wnt5b* (Xu et al., 2002; Zou et al., 2006). Since EYA1 lacks DNA-binding capacity (Rebay et al., 2005), taken together these data reflect that there may be redundancy between SIX1 and SIX4 regarding EYA1 binding, and that EYA1 may act through alternative mechanisms, possibly via its phosphatase activity.

Deletion of chromosome region 22q11.2 causes DiGeorge syndrome (DGS), in which patients present a diverse range of symptoms including immune compromise as a result of thymus hypoplasia or aplasia (reviewed in Hollander et al., 2006). Knockout of the T-box 1 (*Tbx1*) gene in mice recapitulated the DGS phenotype, confirming that its deletion is largely responsible for the abnormalities (Jerome and Papaioannou, 2001; Lindsay et al., 2001). *Tbx1* is expressed in the pharyngeal pouch endoderm and arch mesenchyme in the pharyngeal region (Lindsay et al., 2001), however endoderm specific knockout of *Tbx1* is sufficient for the loss of posterior pharyngeal pouches and their derivatives (Arnold et al., 2006). Interestingly, *Tbx1* gain-of-function also led to thymus hypoplasia (Vitelli et al., 2009), underlining the importance of dynamic *Tbx1* expression in thymus organogenesis. Constitutively active *Tbx1* triggered by $Foxn1^{Cre}$ demonstrated that TBX1 specifically represses *Foxn1*, and that *Tbx1* downregulation is necessary for TEC differentiation (Reeh et al., 2014). Using live imaging, a recent study showed that pharyngeal pouch formation, the pre-requisite for thymus development, fails in mutant tbx1 zebrafish (Choe and Crump, 2014). In conclusion, *Tbx1* plays a temporary role to regulate

pharyngeal pouch patterning and morphogenesis, partly by activating *Fgf8* and *Pax9* (Arnold et al., 2006; Okubo et al., 2011). It is then repressed to permit TEC differentiation.

It is evident that components of this proposed GRN of thymic anlage cross-interact extensively. This may explain the fact that despite severe abnormalities in the mutants of *Pax1*, *Pax9*, *Hoxa3* and *Six1*, a thymic anlage initially formed nonetheless. Indeed, this relative stability is a hallmark of gene networks (Payne and Wagner, 2015). Contrary to the *nude* phenotype, in which thymic rudiments survive well into adulthood, the thymic primordia in most of these knockouts degenerate through apoptosis, with the exception of *Pax1*. This indicates that TEC differentiation can be divided into two phases, the pre-FOXN1 and the post-FOXN1 (Nehls et al., 1996). In the pre-FOXN1 phase, the GRN ensures that specified TEC progenitors reach a stable state in which they are poised for differentiation and robust from apoptosis. Once FOXN1 is activated, it mediates the differentiation of both mTEC and cTEC sub-lineages, as well as substantial proliferation.

1.4.3 Hedgehog (Hh)

Sonic Hedgehog (*Shh*) and its receptor Patched1 (*Ptc1*) are expressed in E10.5 3PP (Moore-Scott and Manley, 2005). In the $Shh^{-/-}$ null mutants, reduced pouch size was detected as a result of cell death, and whilst the parathyroid marker *Gcm2* was lost, the thymic domain in 3PP marked by *Bmp4* and later *Foxn1* appeared expanded (Moore-Scott and Manley, 2005). Constitutively active Hh signalling in pharyngeal endoderm did not convert epithelial cells into $GCM2^{+}$ parathyroid fate. Rather, it induced TBX1 which in turn repressed *Foxn1* expression (Bain et al., 2016; Reeh et al., 2014). Therefore, Hh activity patterns the primordium by regulating the competence of cells to become thymic or parathyroid.

Hh signalling continues to be active in the developing thymus following the initial patterning. Smaller thymi are present in $Shh^{-/-}$ nulls until development fails around E16.5 (Shah et al., 2004). Fetal culture of $Shh^{-/-}$ thymi, or blocking Hh signalling with antagonist Hhip, revealed that Hh-deficient FTOC exhibit decreased numbers of cTECs and mTECs, with the latter more severely affected (Saldana et al., 2016).

What is more, ablation of the pathway, genetically or chemically, led to increased levels of MHCII accompanied by a reduced frequency of $AIRE^{+}$ mTECs (Saldana et al., 2016). This evidence points to a role of Hh in regulating TEC differentiation, although it is uncertain whether the effects are entirely cell autonomous, or partly indirect through thymic crosstalk, since SHH is also a potent regulator of thymocyte development (Barbarulo et al., 2016).

1.4.4 WNT

Wnt ligands WNT1, WNT4 and WNT5b are expressed in the thymic anlage as early as E10.5, with WNT4 persisting robustly into adulthood (Balciunaite et al., 2002). Using cell lines derived from primary cTECs, it was shown that both Wnt activation by lithium chloride and co-culture with WNT4-transfected thymocytes led to elevated *Foxn1* expression (Balciunaite et al., 2002). These data support the hypothesis that Wnt pathway may initiate *Foxn1* and consequently TEC differentiation. A later study provided further evidence by co-culturing E15.5 thymi with supernatant from a WNT4-secreting cell line (Kvell et al., 2014); TECs isolated after culture exhibited elevated expression of *Foxn1*.

Moreover, Heinonen and colleagues analyzed the fetal thymi of $Wnt4^{-/-}$ knockout mice. TEC cellularity in WNT4 deficient mice is reduced by half compared to wildtypes, and mTEC frequency in the epithelium appears lower. Interestingly, conditional deletion of *Wnt4* at neonatal stages produced a stronger phenotype (lower TEC count and mTEC frequency) than deletion in adult mice, suggesting that the WNT4 effect on TECs is temporally restricted (Heinonen et al., 2011). In addition, TEC specific knockout of *Gpr144*, required for WNT ligand transport to the cell surface, exhibited reduced thymocyte cellularity apparent by birth (Brunk et al., 2015). T cell development was not blocked, however a significant decrease in TEC number and increased TEC apoptosis rate were observed (Brunk et al., 2015). Thus, the pathway may function in an autocrine fashion, where WNT ligand secreted by TECs activates WNT signalling in TECs to enhance cellular survival.

On the other hand, elevated Wnt activity can also have a profound impact on the thymic epithelium. Loss of the Wnt antagonist *Kremen1* enhanced Wnt activity, and

as a result the cortico-medullary architecture was gradually lost in fetal and postnatal thymus (Osada et al., 2006). An even more dramatic collapse was observed in two independent studies where the canonical Wnt effector β-catenin was stabilized specifically in TECs (Swann et al., 2017; Zuklys et al., 2009). Typical reticular thymic epithelial structure was disrupted in the fetal thymus, and *Foxn1* expression was either lost or reduced. The remaining epithelium appeared small, cystic and unable to be colonized by haematopoietic cells. In comparison, overexpression of WNT4 alone produced milder defects in primordium migration and TEC differentiation (Swann et al., 2017). Of note, various Wnt antagonists were activated in the gain-of-function model, indicating an intrinsic negative feedback loop in fetal TECs (Zuklys et al., 2009).

In the context of thymic homeostasis, the induction of Wnt antagonist Dickkopf Homolog 1 (DKK1) resulted in a significant but reversible fall in thymus size and cellularity (Osada et al., 2010). The inducible DKK model also showed decrease in *Foxn1* expression and perturbed epithelial architecture, reminiscent of age-related involution (Osada et al., 2010). The expression of many Wnt genes in TECs declines with age, but can be restored by the overexpression of *Foxn1* to the levels of young TECs (Bredenkamp et al., 2014a).

In conclusion, Wnt ligands, especially WNT4, may have a role in activating *Foxn1* expression in thymus organogenesis. The appropriate range of Wnt activity is crucial to safeguard the differentiation and architecture of the thymic epithelium.

1.4.5 Bone Morphogenetic Proteins (BMP)

The morphogens BMP2, BMP4, BMP7 and their antagonists Chordin, Noggin and Twisted Gastrulation (Tsg) are all expressed during thymus organogenesis, either by endodermal progenitors/TECs or by neural crest derived mesenchyme (Bleul and Boehm, 2005; Graf et al., 2002; Patel et al., 2006; Scott et al., 2000). Expression of NOGGIN driven by the *Foxn1* promoter led to stalled migration of the thymus, as well as a significant reduction in thymus size (Bleul and Boehm, 2005). Sustained exposure to NOGGIN also triggered part of the epithelium to lose *Foxn1* expression and revert to cystic structure indicative of immature precursor cells (Soza-Ried et al.,

2008). Specific deletion of *Bmp4* using Foxg1^{Cre}, which is active as early as E9.5 in the 3PP endoderm and surrounding mesenchyme, resulted in morphogenetic aberrations and smaller thymi, a phenotype not dissimilar to that observed of misexpression of *Noggin* (Gordon et al., 2010). Moreover, deletion of *Bmp4* with Wnt1^{Cre} and Foxn1^{Cre}, which specifically target neural crest derived mesenchyme and committed TECs respectively, showed that while the requirement for BMP4 for thymus size continues after *Foxn1* is switched on, migration of the rudiments only requires an early pulse of BMP4, possibly to ensure that the mesenchymal cells mature normally and form organized thymic capsule (Gordon et al., 2010).

The relationship between BMP signalling and *Foxn1* expression in development is complex. The addition of BMP4 in FTOC medium increased the expression of *Foxn1* in TECs (Tsai et al., 2003). In our hands, the combination of BMP4 and FGF8, but not BMP4 alone, led to *Foxn1* upregulation in E10.5 3PP culture (Popis, unpublished). However, neither forced *Noggin* expression nor Foxg1^{Cre} induced *Bmp4* deletion completely abolished *Foxn1*, although in the former case part of the thymic rudiment indeed lost *Foxn1* and exhibited a cystic structure (Bleul and Boehm, 2005; Gordon et al., 2010; Soza-Ried et al., 2008). Remarkably, when BMP signalling is suppressed by NOGGIN, *Bmp2* and *Bmp4* are activated in a negative feedback fashion (Bleul and Boehm, 2005). This, and redundancy shared by other BMP factors, may account for the relatively normal *Foxn1* expression in the Foxg1^{Cre} *Bmp4* deletion model. In addition, *foxn1* downregulation was observed in the zebrafish larval thymus subsequent to Noggin misexpression or BMP inhibitor treatment (Soza-Ried et al., 2008). *Foxn1* initiation in avian thymic rudiments can also be abolished by Noggin, though this effect is lost later in development (Neves et al., 2012). Taken together, these studies revealed an evolutionarily conserved role of BMP signalling in positively regulating *Foxn1* expression, but this effect is likely to depend on the maturation status of TECs, as well as the overall signalling environment TECs encounter.

Some aspects of the BMP loss-of-function models resemble those of WNT gain-of-function, such as incomplete thymic rudiment migration, reduced cellularity and *Foxn1* suppression (Bleul and Boehm, 2005; Gordon et al., 2010; Soza-Ried et al., 2008; Swann et al., 2017; Zuklys et al., 2009). By simultaneously overexpressing

Wnt4 and *Noggin*, Swann and colleagues observed a more severe phenotype – smaller rudiment size and poor migration – than *Noggin* alone (Swann et al., 2017). Therefore, the proliferation and maturation of early TECs likely require a BMP^{high} $WNT^{low/med}$ environment. What is more, a number of studies concluded that BMP ligand treatment results in the arrested development of thymocytes (Graf et al., 2002; Hager-Theodorides et al., 2002; Tsai et al., 2003). Since BMP ligands are soluble morphogens, this highlights the importance of intricate BMP pathway regulation in thymic organogenesis, namely the initial high activity to establish TEC program and morphogenesis, and a following phase of modest expression compatible with T cell progression.

1.4.6 Fibroblast Growth Factors (FGF)

The expression of FGF ligand *Fgf8* can be detected in the pharyngeal pouch endoderm and surface ectoderm when these structures first appear at E9.5 (Crossley and Martin, 1995). Embryos carrying hypomorphic alleles of *Fgf8* exhibit a variety of thymus phenotypes linked to the rise in cell death in pharyngeal arches, ranging from hypoplasia to the complete absence of the thymus (Abu-Issa et al., 2002; Frank et al., 2002; Macatee et al., 2003). *Fgf8* is a TBX1 target and is downregulated in the *Eya1* knockout (Arnold et al., 2006; Zou et al., 2006), hence it may be an important effector of the early thymic GRN program. In this context, the requirement of FGF8 differs amongst the cells in the primordium. In contrast to promoting expansion of the thymic domain, sustained high FGF activity decreased parathyroid size and prevented pouch separation from the pharynx (Gardiner et al., 2012). Remarkably, modulation of FGF8 activity by FGF antagonists Sprouty1 and 2 also conditions the thymic capsule and mesenchymal cells to secrete FGF10 and thereby indirectly regulates the proliferation of fetal TECs (Frank et al., 2002; Gardiner et al., 2012).

Alternative splicing of the FGF Receptor 2 (*Fgfr2*) gene produces two isoforms, FGFR2IIIb and FGFR2IIIc. FGFR2IIIb serves as receptor for two FGF ligands, FGF7 and FGF10, in the developing thymus (Ohuchi et al., 2000; Revest et al., 2001). In E12-14 thymus, these FGF ligands are most prominently expressed in the capsule, which originates from earlier mesenchyme, while FGFR2IIIb expression is

restricted to the epithelium (Revest et al., 2001). Deficient FGF10, FGFR2IIIb, or blocking with soluble dominant negative FGF receptors produced the fetal thymic hypoplasia phenotype (Celli et al., 1998; Ohuchi et al., 2000; Revest et al., 2001). Combined with the facts that mitotic TECs are less abundant in the absence of FGF10 or FGFR2IIIb, and that the addition of FGF7 or FGF10 rescued proliferation in mesenchyme-deprived reaggregate cultures (Jenkinson et al., 2003; Revest et al., 2001), it appears that the FGF ligands act as mitogenic stimulants in mesenchymal-epithelial crosstalk. In addition, *Fgf7* is upregulated as thymocytes mature (Erickson et al., 2002), indicating that T cells could be an alternative source of FGF7 later in development.

In summary, FGF signalling occurs in two waves in thymus development. First, FGF8 promotes the survival of 3PP cells and, through negative feedback, governs the patterning and morphogenesis of the rudiments. This is followed by mesenchymal-epithelial interaction involving FGF7 and FGF10 to enhance TEC proliferation.

1.4.7 Tumour necrosis factor superfamily (TNFSF)

Several TNFSF factors have been shown to play synergistic roles in mTEC development through the canonical and non-canonical NFκB pathway (reviewed in Nitta et al., 2011). Briefly, the canonical pathway is dependent on the degradation of Inhibitor of κB (IκB), and the non-canonical pathway signals through NFκB inducing kinase (NiK) (reviewed in Dejardin, 2006). Mice with deletions in the NFκB components RelB (Burkly et al., 1995), NiK (Kajiura et al., 2004), lymphotoxin β receptor (LTβR) (Boehm et al., 2003), TRAF6 (Akiyama et al., 2005) and RANK receptor (Akiyama et al., 2008) develop autoimmunity, suggesting a prominent role of NFκB in regulating mTECs and central tolerance. Notably, T cell developmental arrest caused a similar mTEC phenotype, and this mutual dependence between thymocytes and the stroma was termed thymic crosstalk (van Ewijk et al., 1994).

LTβR signalling is specifically required for a subset of $AIRE^{-}$ $CCL21^{+}$ mTECs (Lkhagvasuren et al., 2013). $LT\beta R^{-/-}$ mice show disorganized, hypoplastic medulla and presented autoimmunity in multiple organs despite detectable levels of Aire and promiscuous gene expression (Boehm et al., 2003). This apparent contradiction may

result from AIRE-independent TRA expression mediated by FezF2, a proposed target gene of LTβR (Takaba et al., 2015). However, this conclusion has also been challenged, as another study found FezF2 expression in LTβR deficient TECs (Cosway et al., 2017). Instead, the autoimmune phenotype in LTβR$^{-/-}$ mice seems to originate from impaired medullary dendritic cell function in negative selection, which is regulated separately from mTECs (Cosway et al., 2017).

RANK ligand (RANKL, also known as TNFSF11) is a major facilitator of thymic crosstalk. Positively selected T cells secrete RANKL which promotes the proliferation of immature mTECs, the upregulation of maturation markers MHCII and CD80, and the activation of *Aire* (Hikosaka et al., 2008). Lymphoid tissue inducer cells (LTi, defined as CD4^{+} CD3^{-}) also secrete RANKL (Rossi et al., 2007b), however this contribution seems minor since mice lacking LTi cells exhibit only a marginal proportional reduction in mTECs (Hikosaka et al., 2008). Given the vital importance of AIRE in negative selection, these results are fully consistent with the autoimmune phenotype of NFκB mutants. Two independent reporter lines showed that RANK receptor expression is negligible in E13.5 rudiments, which contain few mTECs, but increases afterwards as mTECs expand and mature (Akiyama et al., 2016; Baik et al., 2016), in line with its role in instructing these processes. Furthermore, mTECs secrete osteoprotegerin (OPG) (Akiyama et al., 2014; Hikosaka et al., 2008), a soluble decoy receptor of RANKL that in effect functions as an antagonist of the pathway, thus preventing the hyper-stimulation of RANK.

More recent investigations have established a framework of the mechanisms and temporal sequence of various TNFSF factors in mediating mTEC development. Agonist LTβR antibodies in FTOC raised the expression of *Rank* within 6 hours (Mouri et al., 2011), suggesting that LTβR is upstream to RANK in the cascade and conditions mTECs to respond to RANKL. A similar approach revealed that RANKL can activate CD40 in mTECs, making these cells receptive to CD40L secreted by thymocytes (Desanti et al., 2012). Double mutants of these three receptors again placed RANK at the epistatic centre, with LTβR/RANK and RANK/CD40 double knockouts exhibiting more severe mTEC hypoplasia than single knockouts alone (Akiyama et al., 2008; Mouri et al., 2011), but LTβR and CD40 showed no evidence of interaction (Mouri et al., 2011). It has also been shown that the ligands upregulate

largely distinct subsets of genes, and that only RANKL is responsible for activating AIRE (Bichele et al., 2016). Indeed, functional NFκB binding sites have been found in the regulatory region of *Aire* (Haljasorg et al., 2015).

In terms of the intracellular pathway, RelB and TRAF6 mark two distinct checkpoints in the mTEC lineage. *Relb* deficient mTECs are arrested at a more primitive stage ($RANK^{lo}MHCII^{lo}CD24^{hi}$) than in *Traf6* mutants ($RANK^{+}$ $MHCII^{mid}$), and the transition between the two progenitor states requires the combined stimulation of LTβR and RANK (Akiyama et al., 2016; Baik et al., 2016). Full maturation to $MHCII^{hi}$ $AIRE^{+}$ mTECs requires both TRAF6 and RANK stimulation (Akiyama et al., 2016). Crucially, Claudin (CLDN) $3,4^{hi}$ $SSEA1^{+}$ cells, the most primitive mTEC progenitors identified to date (Hamazaki et al., 2007; Sekai et al., 2014), are present even in the more severe *Relb* mutant (Baik et al., 2016), hence mTEC specification occurs independently of thymic crosstalk.

Along with TNFSF ligands, recent reports also shed light on novel regulators of mTEC development following the initial expansion of mTEC. An EGFR-STAT3 axis appears to promote postnatal mTEC cellularity without affecting their maturation status (Satoh et al., 2016). The histone deacetylase HDAC3 is required for mTEC cellularity, maturation and the capacity to suppress autoimmunity, partly by repressing excessive Notch activity in postnatal mTECs (Goldfarb et al., 2016). In contrast, TGFβ ligand, through receptor TGFβR2, inhibits proliferation of postnatal mTECs (Hauri-Hohl et al., 2014). Together, these discoveries highlight that mTECs reside in a complex and dynamic chemical microenvironment.

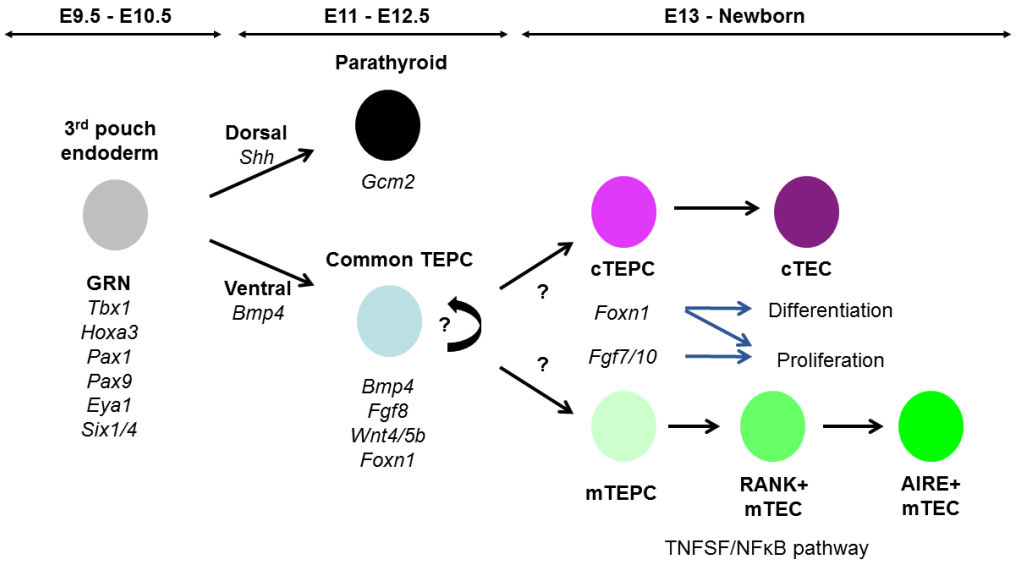

Figure 1.2 The time frame of TEC lineage progression, and the underlying regulatory mechanisms. Third pharyngeal pouch (3PP) endoderm identity is established in the presence of the gene regulatory network (GRN). Some genes (e.g. *Pax1*) continue to express in more differentiated TECs, while others (eg. *Tbx1*) are gradually downregulated. Polarized expression of signalling molecules (*Shh* and *Bmp4*) likely patterns 3PP into dorsal parathyroid and ventral thymic domains. The combined influence of the GRN and signalling pathways switches on *Foxn1*, the key regulator of TEC differentiation. Moreover, mesenchymal cells directly promote the proliferation of early fetal TECs by releasing mitogenic FGF7/10 ligands. If and how common TEPCs with cTEC and mTEC potential are maintained is unclear. How bipotent TEPCs are specified to become cTECs or mTECs also remains elusive. Having committed to the two lineages, the further maturation of mTECs into AIRE-expressing cells requires TNFSF/NFκB ligands, predominantly secreted by thymocytes in thymic crosstalk.

1.5 Potency of TEC progenitors (TEPCs)

The bipotency of E12.5 EPCAM$^+$ PLET1$^+$ progenitors capable of giving rise to both mTECs and cTECs was demonstrated using a single cell transplantation assay (Rossi et al., 2006). The proportion of TECs expressing PLET1 reduces as thymus organogenesis advances, but a higher proportion of the emerging mTECs than cTECs are PLET1$^+$ (Sheridan, unpublished), and remains so in adults (Ulyanchenko et al., 2016). The murine *Plet1* gene is of unknown function, poorly conserved (Depreter et al., 2008), and both PLET1$^+$ and PLET1$^-$ E14.5/16.5 TECs show similar reconstitution activity (Rossi et al., 2007a). Thus, unlike the functional maturation marker MHCII, PLET1 represents a 'neutral' marker for TEC differentiation.

Unipotent mTEC progenitors have been shown to contribute to the long-term maintenance of mTECs. Chimera analysis showed that the mTEC 'islets' (clusters of cells occupying single medullary regions) in fetal and young thymi are the products of clonal expansion from single progenitors (Rodewald et al., 2001). Unipotent mTEC progenitors can be isolated from E13.5 primordia using CLDN3/4 and SSEA1 (Hamazaki et al., 2007; Sekai et al., 2014). These mTEC progenitors not only show long term reconstitution activity, but are able to correct autoimmunity in a mTEC-deficient background (Sekai et al., 2014). Interestingly, CLDN3/4 were shown to localize specifically in the luminal side of E10.5 3PP (Hamazaki et al., 2007). Although this seems to suggest that apico-basal polarity may mark mTEC-biased progenitor, or directly regulate cell fate, the potency of CLDN3/4$^+$ TECs prior to E13.5 has not been reported. Also, a clonal resolution lineage tracing has not been performed using CLDN3/4.

In contrast, the separation of putative bipotent TEPCs from committed cTECs in developing thymi has proved more difficult, since early fetal TECs express high levels of mature cTEC markers such as β5t and CD205 (Baik et al., 2013; Ohigashi et al., 2015; Ohigashi et al., 2013). Indeed, the earliest TEPCs share a number of functions generally attributed to cTECs: instructing the homing of haematopoietic progenitors, providing Notch ligands, and supporting positive selection. Therefore a 'serial progression' model has been proposed for the TEC lineage hierarchy: whereas cTEC represents a default fate for bipotent TEPCs since they share molecular and

functional similarities, specification of the mTEC lineage requires a currently unidentified signalling cue (reviewed in Alves et al., 2014).

In adults, the MHCII^{lo} cTEC (cTEC^{lo}) population expressing α6 integrin and Sca-1 was shown to contain TECs that contribute to mTEC and cTEC lineages when reaggregated with fetal thymus cells and grafted under the kidney capsule (Wong et al., 2014). Such bipotent reconstitution potential was also illustrated for Ly51^{+} PLET1^{+} TECs in adult thymus, and limiting dilution analysis estimated that approximately 1 in 90 cells in this minor population (<1% total TEC) accounted for this stem/progenitor cell behaviour (Ulyanchenko et al., 2016). Histological analysis revealed that individual Ly51^{+} PLET1^{+} TECs can differentiate into both mTECs and cTECs, and their progeny remained 9 months after reconstitution (Ulyanchenko et al., 2016). Although there are certain discrepancies between the two studies, such as the MHCII status, the stem/progenitor cells identified in each case nevertheless share the expression of cortical marker and a common localization (CMJ). What is more, the method adopted for these studies aimed to assay cellular potency, therefore the behaviour of these cells in homeostasis remains unclear.

Regarding committed mTEC progenitors, the clonogenic activity of CLDN3/4^{+} SSEA1^{+} TECs is greatly reduced in the first month after birth, reflecting an altered self-renewing potential in this population (Sekai et al., 2014). As mTECs continue to turn over rapidly in adults (Gray et al., 2007), this raises the question as to how mTECs are maintained in homeostasis. The MHCII^{lo} mTEC subset possibly contains transit amplifying cells, since they could differentiate into post-mitotic, functionally mature MHCII^{hi} AIRE^{+} mTECs (Gray et al., 2007), but lack long term self-renewal capacity (Ulyanchenko et al., 2016; Wong et al., 2014). Interestingly, Podoplanin (PDPN) expressing cells residing at the CMJ gave rise to mTECs but not cTECs in lineage tracing, and may thus represent a source of steady state mTEC progenitors (Onder et al., 2015). As PDPN^{+} junctional TECs (jTECs) differentiate into mTECs, they typically downregulate PDPN and acquire mTEC markers (Onder et al., 2015). The common location of adult bipotent TEPCs and PDPN^{+} jTECs at the CMJ may be relevant to their role in maintaining thymic epithelium during homeostasis. Future interrogations of their progenitor-progeny relationship will shed light on this hypothesis.

Currently, how fetal TEC progenitors relate to their counterparts in the adult epithelium is not well understood. There are two broad hypotheses: either that adult TEPCs are set aside during development from ontogenetic TEPCs, or that they arise due to proximity to the niche environment (likely CMJ). All adult TECs are derived from β5t-expressing fetal progenitors, and such progenitors can contribute to both mTECs and cTECs until postnatal 1-week (Ohigashi et al., 2015; Ohigashi et al., 2013). Moreover, while fetal and neonatal TECs cycle frequently, label-retaining cells have been identified in adult TECs (Dumont-Lagacé et al., 2014), although their cellular phenotype remains controversial. Based on the very scarce number of studies, we can infer that, in terms of cellular hierarchy, the thymic epithelium undergoes profound changes as expansion slows and cTEC/mTEC cell-fate boundary becomes less fluid in the first few postnatal weeks. Nonetheless, some rare CMJ-localized TECs appear to either retain or acquire bipotency.

Going forward, it is of interest to identify niche factors (signalling and scaffold molecules) that may play a part in maintaining adult TEPCs. More precise lineage tracing will also produce accurate information on how progenitor populations are related. In particular, since CLDN3/4^{+} SSEA1^{+} cells exhibit drastically lower self-renewal activity in adults, it is probable that the progeny of these fetal mTEC progenitors may give rise to PDPN^{+} jTECs.

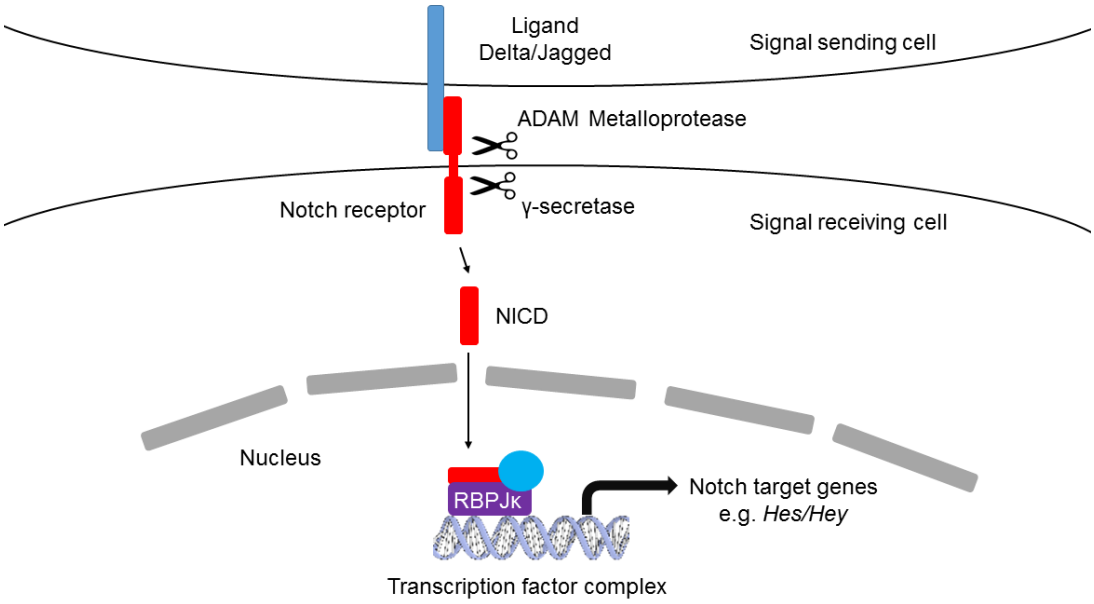

Figure 1.3 A simplified view of the canonical Notch signalling pathway. Interaction between membrane-bound Notch ligands and receptors on adjacent cells triggers the cleavage of the Notch receptor, first to release the extracellular domain, then to liberate the intracellular domain. Notch intracellular domain (NICD) can then form a protein complex by binding RBPJκ and other co-factors in the nucleus. This complex is required to effect the transcriptional changes downstream of Notch receptor activation.

1.6 Notch signalling

Cells in diverse invertebrate and vertebrate species communicate through a small number of signalling pathways in development. These pathways sense the physical and chemical environment the cells inhabit, often through ligand-receptor binding, and relay this information to the nucleus in order to facilitate transcriptional changes. Since each cell type or cell state has a distinct genetic and epigenetic make-up, the same pathway can be adopted multiple times and mediate unique responses in each cell type or at each developmental stage (reviewed in Gilbert, 2010). This list of pathways includes, but is not limited to, BMP/TGFβ, Hedgehog, Wnt, JAK/STAT, receptor tyrosine kinases, Hippo, and Notch. As discussed above, many of these pathways are relevant to thymus organogenesis (section 1.4).

In the case of Notch, both ligands (Delta or Jagged) and receptors (Notch) are membrane-bound proteins, hence restricting activation to cells in direct contact, often termed 'juxtacrine signalling'. Ligand binding triggers first the cleavage of Notch extracellular domain by ADAM protease, followed by Notch intracellular domain (NICD) by γ-secretase. Liberated cytosolic NICD fragments then translocate to the nucleus, where transcriptional complexes are formed to activate or repress genes downstream of Notch signalling (Figure 1.3). Importantly, NICD lacks DNA-binding capacity, thus its role as transcriptional co-factor relies on the partners in the complex, CSL (RBPJκ in mammals) and Mastermind (MAML). This sequence of events is regarded as 'canonical Notch signalling' (reviewed in Andersson et al., 2011). Notch activation facilitates the expression of many Hes/Hey family basic helix-loop-helix (bHLH) proteins, and these factors can relay Notch functions by further modifying gene expression or by protein-protein interactions (reviewed in Fischer and Gessler, 2007).

The Notch pathway is subject to extensive regulations, and several examples – by no means exhaustive – are discussed here. Notch is known to exhibit context-dependent positive or negative feedback through its target genes. Positive feedback, such as the activation of Notch receptor genes, reinforces the state of signal receiving cells and on tissue levels can lead to lateral inhibition (Greenwald, 1998). On the other hand, negative feedback via the expression of proteins antagonizing Notch signalling may

result in oscillatory behaviour (Hirata et al., 2002; Imayoshi et al., 2013). Apart from activating receptors *in trans*, Notch ligands can bind and inhibit receptors on the same cells, in a process called *cis*-inhibition (del Alamo et al., 2011). In addition, Fringe glycosyltransferases modify Notch receptors post-translationally to favour the binding of Delta ligands over Jagged (Panin et al., 1997; Visan et al., 2006). It is also well established that F-Box And WD Repeat Domain Containing 7 (FBXW7), the substrate recognition protein in SCF E3 ubiquitin ligase complex, is involved in fine tuning Notch signalling by degrading NICD (Carrieri and Dale, 2016; Matsumoto et al., 2011). Finally, Notch signalling components are increasingly shown to interact with pathways, for instance TGFβ and Wnt, further expanding its diversity of mechanisms (Andersson et al., 2011).

The multitude of regulatory mechanisms confers great diversity to how Notch acts in different tissue and organ systems. For example, in inner ear development, Notch is involved in regulating different events in different processes (Kiernan, 2013). First, early widespread expression of Notch ligand JAG1 determines the field of sensory patches. In this case the *Jag1* gene is activated by Notch, resulting in the lateral expansion of cells entering the sensory fate. Early misexpression of NICD converted non-sensory regions to sensory fate, indicating the pro-sensory function of Notch (Hartman et al., 2010). Later, cells in the sensory patches are sorted out into hair cells and supporting cells, the two sensory cell types in the inner ear, via the action of DLL1 and JAG2. This later wave of Notch dictates a salt-and-pepper pattern, in which ligand-expressing cells differentiate into hair cells where active Notch signalling in the adjacent cells leads to supporting cell fate (Kiernan et al., 2005). The difference in signalling outcome is due to ligand-dependent levels of Notch activation, since genes that require higher thresholds were activated by DLL1 but not JAG1 (Petrovic et al., 2014).

What is more, Notch is dynamically deployed in the differentiation of pancreatic progenitors. Loss of *Dll1*, *Rbpj* or canonical target *Hes1* in the early pancreatic primordium led to premature differentiation into the endocrine lineage, suggesting that Notch is a repressor of the endocrine fate (Apelqvist et al., 1999; Jensen et al., 2000). However, constitutive expression of NICD prevented the differentiation of both endocrine and exocrine lineages, thus high levels of Notch appears to favour

progenitor self-renewal over differentiation (Murtaugh et al., 2003). It was thought that the decision to self-renew or undergo endocrine differentiation depends on a lateral inhibition mechanism, in which Neurogenin 3 (*Ngn3*)-expressing endocrine progenitors display Notch ligands, and Notch activity in the adjacent signal receiving cells in turn upregulates HES1 to repress *Ngn3* and the endocrine potential (reviewed in Li et al., 2015). More recent studies have challenged this simple model. For example, Shih and colleagues have shown that two Notch targets, *Hes1* and *Sox9*, are activated by high and intermediate levels of Notch signalling, respectively. Variations in Notch activity produced two subsets of progenitors: $HES1^{+}$ $SOX9^{+}$ and $HES1^{-}$ $SOX9^{+}$. Although HES1 and NGN3 expression domains are mutually exclusive, in cells that experience intermediate Notch activity, SOX9 induces *Ngn3* to initiate endocrine differentiation (Shih et al., 2012). These observations suggest that, instead of an ON/OFF model, lineage decisions in pancreas development result from a graded response to Notch.

Notch signalling is of crucial importance to T cell development in the thymus (Shah and Zuniga-Pflucker, 2014). In comparison, its role on TECs is less well understood, and the few published reports came to contradictory conclusions. Knockout mice of Notch pathway genes rarely survive to mid-gestation, hindering the examination of thymus development. An exception is the gene encoding the ligand *Jagged2*, the absence of which is associated with reduced medullary area in the thymus (Jiang et al., 1998). In culture, the addition of T cells or B cells overexpressing the Notch ligand DLL1 to thymocyte-depleted fetal thymus drastically improved the medullary architecture (Masuda et al., 2009). In contrast, Notch activity in adult TECs is enriched in a small subset of cTECs and appears repressed in mature mTECs by Histone Deacetylase 3 (HDAC3), and the overexpression of NICD by $Foxn1^{Cre}$ led to postnatal thymus hypoplasia and a severe block in mTEC differentiation (Goldfarb et al., 2016). Of note, fetal thymi were not examined in the Goldfarb study, therefore the phenotype could indicate either a developmental defect, or alternatively the cytotoxicity of long term NICD exposure. Since preliminary data in our lab confirmed the expression of Notch receptors, canonical targets and cytoplasmic modulators in primitive TEC progenitors (Vaidya et al, unpublished), we decided to thoroughly investigate the role of Notch signalling in TEC development.

1.7 Comments on markers

It is the convention of the thymus field to conduct quantitative analysis using flow cytometry. Standard panels (Table 1.1 and 1.2) were designed in our lab for fetal and adult TEC flow analysis. The panels follow the rationale that there should be a distinction between live and dead cells (DAPI), lineage exclusion of non-TECs (LIN: CD45, CD31, TER119, CD11c), a pan-TEC marker (EPCAM), maturation markers (PLET1 and MHCII) and mTEC (UEA1) and cTEC (CD205/Ly51) markers. Note that for fetal analysis, CD205 is used to mark cTEC/TEPCs. This is switched to Ly51 for adult cTECs as is the standard practice in the field. Additional markers used in this thesis (NOTCH1, active Caspase3 etc.) were stained in addition to the standard panels. Some flow markers are optional for the appropriate stage; for instance, the very early TECs (E10-12.5) express little or no MHCII or UEA1, hence the omission of these markers.

The limited cellularity of fetal thymi occasionally precludes quantitative flow analysis. In order to overcome this challenge, as well as presenting tissue context, immunohistochemistry is often used as a complementary method to study TECs. These markers are summarized in Table 1.3.

Marker	Expression	Usage
EPCAM	Total TEC	Always
PLET1	Total E12.5 TEPC, then decrease in proportion	Optional for E17.5/18.5
CD205	TEPC/cTEC	E13.5 and older
UEA1	mTEC	E13.5 and older
MHCII	Functionally mature TECs	E14.5 and older
DAPI	Dead cells	Always
Lineage (CD45, CD11c, CD31, Ter119)	T cells, dendritic cells, endothelial cells, erythrocytes	Always

Table 1.1 Standard flow cytometry markers panel (fetal TEC).

Marker	Expression	Usage
EPCAM	Total TEC	Always
LY51	cTEC	Always
UEA1	mTEC	Always
MHCII	Functionally mature TECs	Always
PLET1	Minority of mTECs. LY51+ PLET1+ TECs show progenitor activity	Optional
DAPI	Dead cells	Always
Lineage (CD45, CD11c, CD31, Ter119)	T cells, dendritic cells, endothelial cells, erythrocytes	Always

Table 1.2 Standard flow cytometry markers panel (adult TEC).

Protein	Expression	Host species
Pan-keratin (panK)	General TEC	Rabbit
K5	mTEC and CMJ	Rabbit
K8	General TEC, highly expressed in cTEC	Rat
K14	Comitted mTEC	Rabbit
CD205	TEPC/cTEC	Rat
PLET1	E12.5 TEPC and a subset of developing and mature TECs	Rat
Claudin 3	Apical side of 3PP, mTEC progenitor and mature mTEC	Rabbit
AIRE	Mature mTEC, involved in tolerance induction	Rabbit
UEA1	mTEC	Biotin
DAPI	Nucleus	

Table 1.3 Standard immunohistochemistry (IHC) markers.

1.8 Aim

The overarching aim of this thesis was to elucidate the role of Notch signalling in the development of the epithelial compartment in the thymus. To achieve this goal, I analyzed the TEC phenotypes of loss-of-function and gain-of-function models of Notch, as well as gene expression datasets. I then incorporated the data presented here into an updated view of the signalling environment of early fetal TECs.

Chapter II: Material and Methods

2.1 Mice

2.1.1 Animal facilities

Wildtype (CBA and C57BL/6) and *Foxn1*^{Cre} (Gordon et al., 2007), *Rbpj*^{FL} (Han et al., 2002), CBF1:H2B-Venus (Nowotschin et al., 2013), silent GFP (Gilchrist et al., 2003) transgenic mice were housed in the animal unit at the MRC Centre for Regenerative Medicine (CRM), University of Edinburgh. The *Ascl1* null mice (Guillemot et al., 1993) were housed at the animal unit at the National Institute for Medical Research (Mill Hill), Francis Crick institute. The mice used for experiments in Chapter V – Foxn1^{Cre}, Rosa26$^{loxP\text{-}STOP\text{-}loxP\text{-}NICD\text{-}IRES\text{-}EGFP}$ (Murtaugh et al., 2003) and wildtype controls – were bred and housed at The École Polytechnique Fédérale de Lausanne (EPFL). Animal husbandry and treatments were carried out in accordance with Animal (Scientific Procedures) Act 1986.

2.1.2 Mating

Wildtype embryos used in this project were of CBAxC57BL/6 strain. CBA males were caged overnight with C57BL/6 females. Females were examined for vaginal plugs the next day, and the day the vaginal plug was found was taken as embryonic day 0.5 (E0.5).

For transgenic mice:

To produce Foxn1^{Cre}; Rbpj$^{FL/FL}$ conditional knockouts, Foxn1$^{Cre/+}$; Rbpj$^{FL/+}$ males were crossed to Rbpj$^{FL/FL}$ females. Conditional knockouts were produced in the progeny at approximately the expected Mendelian ratio of 1 in 4.

To produce Ascl1$^{-/-}$ null embryos, Ascl1$^{+/-}$ heterozygous males and females were mated.

To produce Foxn1^{Cre}; Rosa26$^{loxP\text{-}STOP\text{-}loxP\text{-}NICD\text{-}IRES\text{-}EGFP}$ double transgenic embryos, homozygous Foxn1$^{Cre/Cre}$ males were mated to Rosa26$^{NICD/NICD}$ females. C57BL/6 wildtypes were mated on the same day to generate controls.

2.1.3 Dissection of embryonic thymi

At the appropriate stage, pregnant females were sacrificed and the uterus was collected into ice cold Phosphate-buffered saline (PBS) buffer made up from PBS tablets (Sigma). E12.5 and older embryos were decapitated, and embryonic thymi were then collected into cold PBS under a dissecting microscope. Tissue waste was disposed of according to local institute regulations.

2.1.4 Embryo staging

E10.5 embryos were staged by the number of somites developed. The plug date was used to calculate the age of E12.5 and older embryos.

2.1.5 Genotyping

2.1.5.1 Genomic DNA isolation

Following microdissection of the embryonic thymus, embryonic tissue (head or appendage) was collected into Eppendorf tubes and digested overnight at 55°C in Embryo Buffer with 400µg/ml Proteinase K (Promega) in a shaking water bath. The next day the digested samples were incubated at 95 °C on a heat block for 10 minutes to deactivate Proteinase K. The samples were then centrifuged at 16.2g (13,000 RPM) for 10 minutes to collect the genomic DNA in the supernatant.

For genotyping FACS sorted TECs, the samples were resuspended in 25µl of 200µg/ml Proteinase K diluted in water. The following program was used to digest cells and extract genomic DNA:

55°C – 120min.

95°C – 7 min.

4°C – ∞.

2.1.5.2 Tissue lysis buffer ('Embryo Buffer')

10mM Tris-HCL, pH 8.3 (Roche)

50mM Potassium Chloride (KCl)

2.5mM Magnesium Chloride ($MgCl_2$)

0.1mg/ml Gelatin

0.45% NP40

0.45% Tween20

2.1.5.3 PCR mix

All genotyping carried out at the CRM used this reaction mix (Qiagen):

3µl 10x Reaction Buffer

6µl Q solution (optional on a reaction to reaction basis)

0.5µl Taq enzyme

0.5µl dNTP

1µl Primer 1 (20µM)

1µl Primer 2 (20µM)

Genomic DNA (volume varies)

Sterile water to a total volume of 30µl.

2.1.5.4 Genotype analysis

The genotyping of $Foxn1^{Cre}$ x $Rosa26^{loxP\text{-}STOP\text{-}loxP\text{-}NICD\text{-}IRES\text{-}EGFP}$ embryos was performed by Dr. Ute Koch at EPFL, Lausanne. All other genotyping was done by Frances Stenhouse, Diana Peddie and myself at the CRM, University of Edinburgh.

The genomic DNA was amplified with the appropriate PCR program (section 2.9) and primer pair (section 2.10). The amplified PCR product was analyzed by gel electrophoresis.

The composition of the gel was 2% agarose dissolved in x0.5 TBE buffer. 0.5µg/ml ethidium bromide was added to the gel allow the detection DNA. 5µl of 1X OrangeG loading dye was added to each amplified sample before loading. 10µl of 1kb ladder (Invitrogen) was also loaded to indicate the length of bands. The gels were run at 100V for approximately 30 minutes and were visualized using a UV transilluminator at 312nm (Gene Flash, Syngene, UK).

2.2 Tissue processing for analysis

2.2.1 Tissue embedding and sectioning for immunohistochemistry

Cultured explants, dissected thymi or embryo torsos were embedded in OCT (VWR) and snap frozen on dry ice. The OCT blocks were stored in a -80°C freezer and then cryo-sectioned into 7µm sections using a Leica cryostat at -15°C. Once the sections had been transferred to Polysine glass microscope slides (VWR), the slides were stored in a -80°C freezer until staining.

2.2.2 Preparation of postnatal thymi for flow cytometry

Thymi were cleaned up in RPMI 1640 medium (Gibco) prior to dissociation to remove blood, fat and connective tissue. The lobes were then cut up and dissociated.

First, the tissue was dissociated in 2ml of 1.25mg/ml collagenase D (Roche) and 0.05mg/ml DNaseI (Lorne) diluted in RPMI. After 15 minutes incubation the supernatant was transferred through a 70µm cell strainer (BD Falcon) to a 50ml Corning tube. Another 2ml of the dissociation buffer was added and the tissue was mechanically dissociated by pipetting in and out of the pipette tip. A total of three rounds of dissociation and collection were performed. The remaining pellet was further digested for 30 minutes in 1.25mg/ml collagenase/dispase (Roche) and 0.05mg/ml DNaseI diluted in RPMI. The incubation temperature was 37°C for the duration of dissociation.

After this final dissociation step the whole sample was transferred to the collection tube. The tubes were centrifuged for 5 minutes at 284g (1500 RPM) at 4°C to pellet cells. The pellet was resuspended in PBS (Sigma) with 2% fetal calf serum ('FACS wash'), and a small volume was diluted in FACS wash 100 times, and cells were counted using a BioRad cell counter and slides. Trypan blue was used to distinguish dead cells from live cells.

Antibody staining for T cell analysis proceeded directly after cell count. However for TEC analysis, T cell depletion was first performed using anti-mouse CD45 microbeads (Miltenyi). The beads were diluted 1/20 in FACS wash with 0.05mg/ml DNaseI, and used at the concentration of 5µl per 10^7 cells. After 15 minutes incubation on ice, with vigorous shaking midway through the incubation, the cell suspension was spun down for 5 minutes at 284g (1500 RPM) at 4°C and resuspended in 3ml of FACS wash with DNaseI. The cell suspension was then passed through a LS column (Miltenyi) fitted inside a strong magnet into a 15ml Corning tube on ice. Once the entire suspension had passed, 3ml of FACS wash with DNaseI was added in the columns to fully recover cells not bound by the magnetic beads. The Corning tubes were then centrifuged for 5 minutes at 284g (1500 RPM) and the pellet was resuspended in FACS wash with DNase. The samples can then be counted again, and TEC marker staining was carried out.

2.2.3 Preparation of fetal thymi and cultured explants for flow cytometry

Fetal tissue was collected into Eppendorf tubes containing 200-500µl of PBS with magnesium (Mg) and calcium (Ca) (Sigma). The tubes were spun down briefly to pellet the tissue. The supernatant was removed and replaced with 500-800µl of pre-warmed (37°C) embryonic dissociation buffer, which consisted of 1.25mg/ml collagenase D, 1.4mg/ml hyaluronidase (Sigma) and 0.05mg/ml DNaseI diluted in PBS with Mg and Ca.

The tissue was then dissociated in the buffer for 20 minutes at 37°C. Every four minutes the sample was mixed up and down with a pipette to aid the mechanical

detachment of cells. After 20 minutes the samples were spun down at 3.5g (6000 RPM) for two minutes to pellet cells. The supernatant was collected in a 50ml Corning tube through a 70μm cell strainer. The pellet was resuspended and further incubated in 1X Trypsin (Invitrogen) for two minutes, and then collected in the Corning tube. The tubes were spun down at 284g (1500 RPM) for 5 minutes at 4°C to pellet cells.

The pellet was resuspended in FACS wash with DNaseI. This cell suspension was then stained according to the antibodies panel for each individual experiment.

2.3 Flow cytometry

2.3.1 Antibody staining

The antibodies used to stain cells were listed in section 2.10. Most flow antibodies targeting cell surface antigens were directly conjugated to fluorophores. The exceptions were PLET1 and UEA1.

PLET1 antibody (1D4 supernatant) was not conjugated, therefore was stained alone first, and then with Goat anti-Rat Alexa 647 secondary antibody. Before other markers could be stained, a 15 minutes blocking in 20% rat serum was conducted.

UEA1 is lectin which binds carbohydrate modifications on an unidentified cell surface protein on mTECs. UEA1 is conjugated with biotin, hence the secondary reagent streptavidin Brilliant Violet (BV) 650 was used. Primary UEA1 staining was performed singly, while streptavidin BV650 was applied along with the directly conjugated fluorescent antibodies.

All cell surface antibody staining was carried out at 4°C for 15 minutes. For steps which involved incubation, FACS wash with DNaseI were used as buffer. Between two staining steps, 2ml of FACS wash was added to the cell suspension, and the samples were centrifuged at 284g (1500 RPM) for 5 minutes at 4°C to wash the cells. The supernatant was removed, and the pellet was resuspended in the buffer for the next step.

After surface markers had been stained, the samples were washed twice in FACS wash and DAPI (1/20000, Molecular Probes) was added to distinguish live cells ($DAPI^-$) from dead cells ($DAPI^+$).

For intracellular staining (Foxp3 and active Caspase3), cell surface markers were stained as above. The cells were then washed twice in PBS and stained with fluorescent viability dye eFluor™ 450 (Thermo) diluted 1/1000 in PBS for 30 minutes. Then the cells were fixed in Fixation/Permeabilization buffer (eBioscience) for 30 minutes, before staining with the antibodies against intracellular markers diluted in Perm buffer (eBioscience) for 30 minutes. After the intracellular staining, samples were washed in FACS wash twice before flow analysis.

2.3.2 Staining controls

Around 10% of cells were set aside for controls. In the cases where positive and negative populations were poorly resolved, fluorescence minus one (FMO) controls, in which cells were stained for all antibodies except for the one in question, were also established. Compensation for spectrum overlap was calculated by the software. For this purpose, Ultracomp beads (Invitrogen) stained with single fluorophores were run on the flow cytometer to determine the spectrum of each fluorophore. For DAPI and fluorescent viability dye, single stains were done on cells.

2.3.3 Performing analysis

Flow analyses were run on BD LSR Fortessa (4-laser and 5-laser system). Unstained and full stained sample were analyzed to determine suitable voltages, followed by single stained samples to calculate compensation. FMO and experimental samples were then recorded. Finally, the compensation matrix was examined and inaccuracies were manually corrected.

Flow cytometry data were analyzed using FlowJo Version 9.7.6. All gating strategies are displayed in appendices.

2.3.4 Cell sorting

Cell sorting was performed on a BD FACS Aria II under my instruction, by the CRM Flow Cytometry Facility staff Dr. Fiona Rossi and Dr. Claire Cryer, and by Dr. Romain Bedel and Dr. Andreia Ribeiro at the University of Lausanne, Epalinges. Compensation was performed before sorting.

2.4 RT-qPCR

2.4.1 Cell sorting

Small cell number (50-200 cells) FACS sorting was performed to isolate fetal TEC populations. Cells were directly sorted into PCR tubes containing the Reaction Buffer. Reaction Buffer, which consisted of 10µl CellsDirect 2X Reaction Mix (Cells Direct kit, Invitrogen) and 0.2µl SUPERase-In (Applied Biosystems). Sorted samples were briefly spun down and frozen on dry ice. Total $EPCAM^+$ TECs of equal number were sorted and used as controls. The sorted samples were stored in a -20°C freezer for no longer than one week before pre-amplification of candidate genes.

2.4.2 Primer design

Primer pairs for genes of interest were designed using the Roche Universal Probe Library (UPL) assay design software. One of the intron spanning designs with the highest score was selected. The primers (standard DNA oligonucleotides) were ordered from Sigma.

2.4.3 Pre-amplification

2.4.3.1 PreAmp Master Mix

5µl Primer Mix (pooled Forward and Reverse primers for all test genes, each diluted to 200nM in water)

1µl SuperScript III RT/Platinum Taq mix (Cells Direct kit)

4µl Water

Note that the 2X Reaction Mix, into which the cells were sorted, contained the required PCR buffer, therefore it is not provided in the PreAmp Master Mix.

For negative controls (without reverse transcriptase), the SuperScriptIII enzyme was substituted with Taq (Qiagen). Up to 32 primer pairs were multiplexed for each RT-qPCR analysis.

2.4.3.2 PreAmp reaction

10µl of PreAmp Master Mix was added to the sorted samples. For negative controls the Taq substituted Master Mix was added.

The pre-amplification PCR program (section 2.9) was run to first reverse transcribe cDNA and amplify the DNA fragments targeted by the primer pairs. The amplified samples were used directly for RT-qPCR analysis or stored in a -20°C freezer until analysis.

2.4.4 Quantitative PCR

2.4.4.1 Loading qPCR Master Mix

For each well of the 384-well plate (Roche), the following Master Mix (7.5µl) was loaded.

5.0µl 2X Master Mix (Roche)

0.1µl UPL probe (Roche)

0.225µl 20µM Forward+reverse primers

2.175µl Water

Each gene/population combination was loaded in triplicates.

2.4.4.2 Loading cDNA samples

The pre-amplified cDNA samples were diluted in sterile water to the concentration required. Usually for 16 genes 120µl water was added to 20µl pre-amplified sample.

2.5µl of diluted cDNA was loaded to each well of the plate. As the Master Mix was loaded first, pipette tips were changed between each loading.

2.4.4.3 Real time fluorescence detection

The loaded 384-well plate was sealed with a transparent film (Roche). The plate was then centrifuged at 170g (1000 RPM) for 60 seconds to mix the Master Mix with the cDNA. The PCR reaction was run on LightCycler 480-II (Roche) using the RT-qPCR program in section 2.9.

The Cq value of each well was calculated on the LightCycler 480-II software using the function 'Abs. Quant/2nd Derivative Max'. The values were exported as text files.

2.4.5 Calculation of normalized gene expression levels

If no great variation was observed, the numerical average of the triplicate Cq values was calculated. If, however, one of the three values deviated substantially (by larger than 1), this datum was discarded, and the other two values were used to calculate the average. The average Cq values were used to calculate the initial quantity of cDNA on the assumption that fluorescence emitted by the probe doubles in each PCR cycle. The geometric mean of three housekeeping genes (*Hprt, Hmbs* and *Ywhaz*) for each cDNA sample were taken as baseline. The relative expression value of all other genes was normalized to this baseline.

2.5 RNA sequencing

2.5.1 Cell sorting

Prior to sorting, ethanol and subsequently sterile water were run through the BD Aria II sorter. The sorting area was cleaned with 70% IMS and RNaseZap (Ambion).

100 TECs per population were sorted into 4µl of Smartseq2 buffer in sterile PCR tubes. Rbpj conditional knockout and littermate control TECs were collected at the CRM, University of Edinburgh. Inducible NICD TECs were collected at University

of Lausanne, Epalinges. Each transgenic embryo was genotyped retrospectively. Sorted samples were briefly spun down and frozen on dry ice. These samples were kept in a -80°C freezer until library preparation.

Tissue preparation for FACS was as described above. The antibody panel used for cell surface marker staining was:

PLET1 – AlexaFluor 647

EPCAM – PE

Lineage (CD45, CD11c, CD31 and TER119) – PerCP Cy5.5

Viability – DAPI

2.5.2 Smartseq2 buffer

2µl 0.2% Triton X-100 (Sigma) with RNase inhibitor (1:20, Takara)

1µl 10µM oligo-dT primer (Biomers.net)

1µl 10mM dNTP mix (Thermo)

The Smartseq2 buffer was prepared as described by Picelli and colleagues (Picelli et al., 2013). Triton X-100 was diluted in sterile water (Gibco).

The oligo-dT primer sequence was 5'-AAGCAGTGGTATCAACGCAGAGTACT30VN-3'.

2.5.3 Precautions regarding buffer preparation

Preparation of the buffer was carried out in a UV hood at the CRM, Edinburgh, and in a tissue culture hood at EPFL, Lausanne. In the case of the UV hood, UV lamp was kept on for 60 minutes to sterilize the handling area. Surfaces inside the hoods were cleaned with 70% ethanol, DNA-OFF (Takara Bio), and RNaseZap (Ambion). A disposable lab coat, sleeves and gloves were worn during buffer preparation.

2.5.4 Library preparation and sequencing

Samples were shipped on dry ice to the Weatherall Institute of Molecular Medicine, University of Oxford for library preparation by Dr. Neil Ashley. 75bp paired-end sequencing on Illumina HiSeq4000 was overseen by Dr. Jerome Nicod at the Wellcome Trust Centre for Human Genetics, University of Oxford.

2.6 Immunohistochemistry (IHC)

2.6.1 Staining protocol

For regular TEC markers (pan-keratin, K5, K8, K14, CD205, CLDN3, AIRE, PLET1 and UEA1), the following standard protocol was adopted.

Glass slides were retrieved from the -80°C freezer and warmed to room temperature. Intact sections were identified under a compound microscope. Sections were then fixed for two minutes in acetone (Fisher) which had been pre-chilled in a -20 °C freezer. The selected sections were ringed with hydrophobic pen (Vector Laboratories) and air dried for 30 minutes.

Sections were blocked in 100µl of 5% serum of the secondary antibody species diluted in 1X PBS (made up from Sigma tablets) for 30 minutes. After incubation the blocking solution was removed and replaced by 100µl of primary antibodies diluted in 1% secondary serum in PBS. Sections were stained with primary antibodies or IgG controls for 60 minutes at room temperature. Primary antibody cocktail was removed, and the sections were washed three times in PBS-Tween (PBS with 0.1% Tween-20) for five minutes. Afterwards, each section was stained at room temperature for 45 minutes with 100µl of fluorescent secondary antibodies made up in 1% secondary serum. The sections were shielded from light during his staining step. Three washes of five minutes in PBS-Tween were done before DAPI (1:1000 in water) was applied to the sections for approximately one minute. The slides were dipped briefly in distilled water and air dried. A drop of Vectorshield hard set mounting medium for fluorescence (Vector Laboratories) was applied to each section. Slide mounting was conducted by gently lowering the coverslip onto the slides. Mounted slides were kept at 4°C and shielded from light until imaging.

2.6.2 Adjustments for specific antibodies

For antibodies targeting NOTCH2, NOTCH3 and JAGGED1, sections were blocked with 10% goat serum for 60 minutes and stained with these primary antibodies alone in a moist staining chamber overnight at 4°C. On the second day the slides were washed three times in PBS-Tween before other TEC markers were stained as described above.

2.6.3 Imaging

Leica SP2, SPE and SP8 confocal microscopes were used to image immunofluorescence. Gain and offset for each fluorescence channel were adjusted prior to imaging based on stained sections and negative controls. Exported images were analyzed using Fiji or Photoshop. Only brightness and contrast of the images were altered.

2.6.4 Image quantitation (Chapter IV)

Every E14.5 thymic sections were collected and stained for image analysis on Fiji. The thymic area on each section was designated as the number of pixels defined by DAPI. A threshold was manually set for each section, above which the pixels were regarded as positive for the marker. 'Percentage positive for a marker' is defined as pixels positive for that marker divided by pixels that composed the thymic area. Each datum used for statistical analysis was the total percentage positive for the marker in a whole embryonic thymus.

2.7 Fetal thymus tissue culture (FTOC)

2.7.1 Culturing third pharyngeal pouch (E10.5) and embryonic thymic tissue (E12.5 and E14.5)

The culture was set up in 48-well plates (Figure 2.1A). A thin layer of matrigel (Corning) was coated onto the bottom of the wells. 300µl of N2B27 medium

supplemented with 20ng/ml human FGF8 (PeproTech) and 20ng/ml murine BMP4 (PeproTech) was then added to each well.

Microdissected tissue was transferred to plates using forceps and incubated at 37°C in 5% carbon dioxide. In the first 24 hours of culture the explants would submerge in the medium and mesenchymal cells would form attachment with the matrigel beneath. The culture medium was changed daily for the duration of the culture, unless otherwise indicated.

2.7.1.1 N2B27-based 'TEPC medium'

N2B27 medium:

1X DMEM/F12-N2 (Gibco)

1X Neurobasal medium-B27 (Gibco)

[DMEM/F12-N2 and Neurobasal-B27 were mixed at 1:1 ratio]

1mM L-Glutamine (Invitrogen)

0.114mM β-mercaptoethanol (Sigma)

Supplemented with:

20ng/ml murine BMP4 (PeproTech)

20ng/ml human FGF8 (PeproTech)

1μg/ml heparin (Sigma)

Penicillin (100U/ml) & streptomycin (100μg/ml) (Invitrogen)

Where DAPT (Tocris) was used, an equal volume of DMSO was added to the control condition.

2.7.1.2 Matrigel coating

Upon arrival, matrigel was thawed on ice and divided into 100µl aliquots in Eppendorf tubes. These tubes were frozen and stored in a -20°C freezer. Before coating, matrigel aliquots were thawed on ice for at least 30 minutes.

P200 pipette tips were cooled on ice before being used to transfer matrigel from Eppendorf tubes to 48-well plates. For thin coating, 90µl of matrigel was transferred to cover the surface of each well. After approximately 10 seconds, matrigel was removed, leaving only a thin surface at the bottom of the well.

2.7.2 Culturing older embryonic thymic tissue (E15.5 and E16.5)

The culture was set up in 24-well plates (Figure 2.1B). 600µl of 'FTOC medium' was added to each well. An isopore membrane filter (Millipore) was placed at the air-liquid interface. Microdissected tissue was transferred onto the membrane with forceps. The plates were then incubated for three days at 37°C with 5% carbon dioxide. The medium was not refreshed during incubation.

2.7.2.1 FTOC medium

DMEM (Gibco)

10% Fetal Calf Serum (FCS) (Life Technologies)

2mM L-Glutamine (Invitrogen)

Penicillin (100U/ml) & streptomycin (100µg/ml)

Additional reagents: 1.35 mM 2-deoxyguanosine (dGuo, Sigma), 500 ng/ml murine RANK ligand (PeproTech) and DAPT (Tocris) were included as indicated. Where DAPT was used, an equal volume of DMSO was added to the control condition.

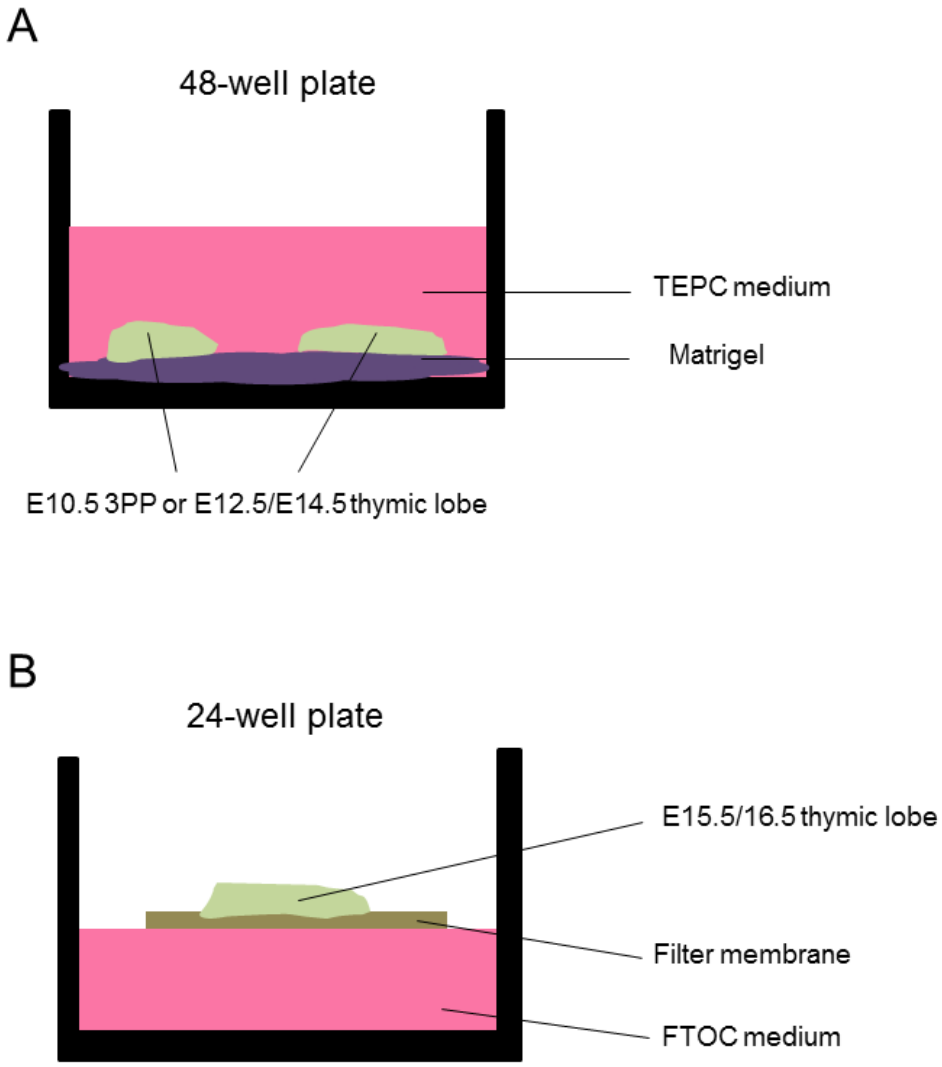

Figure 2.1 FTOC experimental set-up for younger (A) and older (B) embryonic thymic tissue. (A) E10.5 third pharyngeal pouches (3PPs) or E12.5/14.5 thymic lobes were submerged in TEPC medium on a thin layer of matrigel. 300µl of medium was transferred to each well in the 48-well plate. A maximum of three explants were cultured in each well. (B) E15.5/16.5 thymic lobes were cultured on filter membrane over FTOC medium. 600µl of medium was transferred to each well in the 24-well plate. For DAPT treatment 3 wildtype lobes were placed in each well. For RANKL stimulation of transgenic thymi, each pair of thymic lobes from an individual embryo was cultured in one well.

2.8 Statistics

2.8.1 Wet lab data

The raw data used for quantitation are presented in full in appendices. All error bars on histograms were plotted with standard deviations.

Statistical tests were carried out using the GraphPad Prism 7.02 software. For data where N is 3 or larger, pairwise comparisons were conducted using unpaired, two-tailed Student's T-test. For multiple comparisons one-way ANOVA test (two tailed) was performed, as appropriate for normally distributed data. For wildtype FTOC data, Tukey's test was used to generate multiple comparison matrix as N was uniform for all culture conditions. For the transgenic FTOC experiments N could not be controlled, thus a stepwise method (Holm-Sidak) was used to determine P-values in multiple comparisons. $P<0.05$ was taken as significant.

2.8.2 RNA-seq data

Bioinformatics analysis of the RNA-seq data was performed by Anastasia Kousa (CRM, University of Edinburgh).

Briefly, raw data were trimmed to remove adaptor contamination and low quality reads. Sequence reads that passed quality control were aligned with STAR mouse genome assembly (GRCm28 – Ensembl 87) and assigned to genes. Differential expression analysis was performed on R using the LIMMA package and voom from Bioconductor. A threshold of FDR ≤ 0.05 was set as significant between the different datasets. Pathway analysis was then analyzed using Gene Set Enrichment Analysis (GSEA). Pathways were defined as enriched where FDR ≤ 0.25 (the default significance criteria for GSEA).

2.9 PCR programs

2.9.1 Genotyping Foxn1^{Cre} allele

94°C – 3min.

30 cycles of: 94°C – 15s; 63°C – 15s; 72°C – 1min.

72°C – 10 min.

4°C – ∞.

2.9.2 Genotyping Rbpj^{+}, Rbpj^{FL} and Rbpj^{DEL} alleles

94°C – 5min

30 cycles of: 94°C – 30s; 56°C – 30s; 72°C – 1min.

72°C – 10 min.

4°C – ∞.

2.9.3 Genotyping silent GFP allele

94°C – 5min.

30 cycles of: 94°C – 30s; 59°C – 30s; 72°C – 1min.

72°C – 7 min.

4°C – ∞.

2.9.4 Genotyping CBF1:H2B-Venus allele

94°C – 5min.

30 cycles of: 94°C – 30s; 59°C – 30s; 72°C – 1min.

72°C – 10 min.

4°C – ∞.

2.9.5 Genotyping Ascl1^{+} and Ascl1^{-} alleles

94°C – 5min.

35 cycles of: 94°C – 1min; 60°C – 1min; 72°C – 1min.

72°C – 10 min.

4°C – ∞.

2.9.6 Genotyping Rosa26^{NICD} allele

94°C – 2min.

35 cycles of: 94°C – 30s; 60°C – 30s; 72°C – 30s.

72°C – 10 min.

4°C – ∞.

2.9.7 Pre-amplification of mRNA

50°C – 15min.

95°C – 2min.

18 cycles of: 95°C – 15s; 60°C – 4min.

4°C – ∞.

2.9.8 RT-qPCR

95°C – 5min.

45 cycles of: 95°C – 10s; 60°C – 20s*.

40°C – 10s.

(*The point at which fluorescence was quantified in each cycle.)

2.10 Tables

2.10.1 Primary antibodies for IHC

Antigen	Host species	Clone	Supplier
Pan-keratin	Rabbit	Z0622	DAKO
Cytokeratin5 (K5)	Rabbit	AF138	BD
Cytokeratin8 (K8)	Rat	Troma1	DSHB
Cytokeratin14 (K14)	Rabbit	AF64	Covance
Claudin3 (CLDN3)	Rabbit	AB15102	Abcam
NOTCH2	Rabbit	25-255	Santa Cruz
NOTCH3	Rabbit	AB23426	Abcam
JAG1	Rabbit	H114	Santa Cruz
AIRE	Rabbit	M300	Santa Cruz
PLET1	Rat	1D4	Homemade
CD205	Rat	NLDC-145	AbD Serotec
UEA1	Biotin	#L-1060	Vector
Rat IgG isotype	Rat	RTK4530	BioLegend
Rabbit IgG isotype	Rabbit	#550875	BD

2.10.2 Secondary antibodies for IHC

Antibody	Supplier	Catalogue number
Goat anti-rabbit Alexa488	Invitrogen	#A11034
Goat anti-rat Alexa 647	Life Technologies	#A21247
Goat anti-rat Alexa568	Invitrogen	#A11077
Streptavidin Alexa647	Life Technologies	#S21374

2.10.3 Flow cytometry antibodies

Antigen	Conjugate	Clone	Supplier
EPCAM	APC	G8.8	eBioscience
EPCAM	PE	G8.8	Biolegend
EPCAM	APCCy7	G8.8	Biolegend
MHCII	PE	M5/114.15.2	BD Pharmingen
MHCII	APCeFluor780	M5/114.15.2	eBioscience
MHCII	PECy7	M5/114.15.2	eBioscience
CD45	APC	30-F11	eBioscience
CD45	APCeFluor780	30-F11	eBioscience
CD45	PerCP Cy5.5	30-F11	eBioscience
NOTCH1	APC	22E5	eBioscience
UEA1	Biotin	#L-1060	Vector
CD205	PECy7	205yetka	eBioscience
LY51	PE	6C3	eBioscience
CD4	BV650	RM4-5	Biolegend
CD4	PECy7	RM4-5	eBioscience
CD8a	PerCP Cy5.5	53-6.7	eBioscience
CD25	PE	PC61.5	eBioscience
CD44	APC	IM7	Biolegend
CD11c	PerCP Cy5.5	N418	Biolegend
CD31	PerCP Cy5.5	390	Biolegend
TER119	PerCP Cy5.5	Ter119	eBioscience
B220	FITC	RA3-6B2	eBioscience
TCRβ	PerCP Cy5.5	H57-597	Biolegend
CCR6	PECy7	G034E3	Biolegend
FOXP3	PE	FJK-16S	eBioscience
PLET1	None	1D4	Homemade
Caspase3	PE	#51-68655X	BD Pharmingen
Streptavidin	BV650	#405231	Biolegend

2.10.4 Genotyping primers

Protocol	Orientation	Sequence
$Foxn1^{Cre}$	Forward (F)	5'-GACCAGGTTCGTTCACTCATGG-3'
	Reverse (R)	5'-CCTTAGCGCCGTAAATCAATCG-3'
$Rbpj^{WT}$	F	5'-GTTCTTAACCTGTTGGTCGGAAAC-3'
	R	5'-GCTTGAGGCTTGATGTTCTGTATTGC-3'
$Rbpj^{FL}$	F	5'-GTTCTTAACCTGTTGGTCGGAAAC-3'
	R	5'-GGGCTGCTAAAGCGCATGCT-3'
$Rbpj^{DEL}$	F	5'-CCTTGGTTTGTTGTTTGGGTT-3'
	R	5'-GTGGCTCTCAACTCCCAATCGT-3'
sGFP	F	5'-ACATGGTCCTGCTGGAGTTC-3'
	R	5'-TCAGGTTCAGGGGGAGGT-3'
$Rosa26^{NICD}$	F	5'-AAAGTCGCTCTGAGTTGTTAT-3'
	R	5'-GCGAAGAGTTTGTCCTCAACC-3'
$Rosa26^{WT}$	F	5'-AAAGTCGCTCTGAGTTGTTAT-3'
	R	5'-GGAGCGGGAGAAATGGATATG-3'
CBF1:H2B-Venus	F	5'-AAGTTCATCTGCACCACCG-3'
	R	5'-TGCTCAGGTAGTGGTTGTCG-3'
$Ascl1^{WT}$	F	5'-CTCCGGGAGCATGTCCCCAA-3'
	R	5'-CCAGGACTCAATACGCAGGG-3'
$Ascl1^{null}$	F	5'-GCAGCGCATCGCCTTCTATC-3'
	R	5'-CCAGGACTCAATACGCAGGG-3'

2.10.5 RT-qPCR primers and UPL probes

Gene	Orientation	Sequence	Probe
Notch1	F	5'-GGATGCTGACTGCATGGAT-3'	93
	R	5'-AATCATGAGGGGTGTGAAGC-3'	
Notch2	F	5'-TGCCTGTTTGACAACTTTGAGT-3'	6
	R	5'-GTGGTCTGCACAGTATTTGTCAT-3'	
Notch3	F	5'-AGCTGGGTCCTGAGGTGAT-3'	9
	R	5'-AGACAGAGCCGGTTGTCAAT-3'	
Jag1	F	5'-GAGGCGTCCTCTGAAAAACA-3'	6
	R	5'-ACCCAAGCCACTGTTAAGAGA-3'	
Dll4	F	5'-AGGTGCCACTTCGGTTACAC-3'	106
	R	5'-GGGAGAGCAAATGGCTGAT-3'	
Foxn1	F	5'-TGACGGAGCACTTCCCTTAC-3'	68
	R	5'-GACAGGTTATGGCGAACAGAA-3'	
Plet1	F	5'-CATCCGTGAAAATGGAACAA-3'	20
	R	5'-TCACAGTTGGAGTCGTGTTTATG-3'	
Hes1	F	5'-ACACCGGACAAACCAAAGA-3'	99
	R	5'-CGCCTCTTCTCCATGATAGG-3'	
Heyl	F	5'-CTGAATTGCGACGACGATTGGT-3'	25
	R	5'-GCAAGACCTCAGCTTTCTCC-3'	
Ascl1	F	5'-GCTCTCCTGGGAATGGACT-3'	38
	R	5'-CGTTGGCGAGAAACACTAAAG-3'	
Hes6	F	5'-GGATCAACGAGAGTCTTCAGGA-3'	66
	R	5'-TTCTCTAGCTTGGCCTGCAC-3'	
Fbxw7	F	5'-CTCAGACTTGTCGATACTGGAGAA-3'	73
	R	5'-GATGTGCAACGGTTCATCAAT-3'	
Tbx1	F	5'-GCTGTGGGACGAGTTCAATC-3'	104
	R	5'-ACGTGGGGAACATTCGTCT-3'	
Il7	F	5'-CTGCTGCAGTCCCAGTCAT-3'	10
	R	5'-TCAGTGGAGGAATTCCAAAGAT-3'	
Id1	F	5'-TCCTGCAGCATGTAATCGAC-3'	78

	R	5'-GGTCCCGACTTCAGACTCC-3'	
Hprt	F	5'-TCCTCCTCAGACCGCTTTT-3'	95
	R	5'-CCTGGTTCATCATCGCTAATC-3'	
Hmbs	F	5'-TCCCTGAAGGATGTGCCTAC-3'	79
	R	5'-AAGGGTTTTCCCGTTTGC-3'	
Ywhaz	F	5'-CTTCCTGCAGCCAGAAGC-3'	74
	R	5'-GGTTTCCTCCAATCACTAG-3'	

2.10.6 Tissue culture growth factors

Reagent	**Supplier**	**Catalogue number**	**Reconstitution solvent**
Recombinant murine BMP4	PeproTech	#315-27	10mM citric acid in water
Recombinant murine RANK ligand	PeproTech	#315-11	Water
Recombinant human FGF8	PeproTech	#100-25	Water
DAPT	Tocris	#2634	DMSO
2'-Deoxyguanosine monohydrate	Sigma	#D7145	DMSO

Chapter III Candidate gene expression in early fetal thymus

In order to theorize the functions of Notch signalling in regulating fetal TEC development, I first determined if the pathway is active in the early thymic epithelium. To this end, E12.5-14.5 TECs were characterized using RT-qPCR, immunohistochemistry (IHC), and a Notch reporter line. For gene expression, I specifically analyzed the expression pattern of Notch receptors, ligands, canonical targets and modulators, since these genes provide clues as to which cells are receptive to signalling, and which cells are actively transducing. As the early rudiments lack obvious histological features, rather than the more conventional *in situ* hybridization approach, populations of TECs were FACS sorted for mRNA analysis based on established cell surface markers.

3.1 Expression profile of mRNA and proteins

To detect Notch activity in the early thymus rudiments, RT-qPCR was performed for Notch pathway components, target genes and potential regulators. E12.5, E13.5 and E14.5 TEC populations were studied. These are crucial stages in the differentiation of early TEPCs, since relevant literature suggests that the restriction of some bipotent TEPCs to the medullary fate occurs during this time window (Hamazaki et al., 2007; Rossi et al., 2006).

The standard FACS sorting markers panel (EPCAM, PLET1, CD205, UEA1, MHCII, DAPI and lineage) for fetal TECs can be found in Table 1.1 in Chapter 1. For the stages I characterized, some of the markers were omitted due to their low frequency or levels of expression.

For E12.5 and E13.5 samples, in addition to viability marker DAPI and lineage exclusion markers, only EPCAM and PLET1 were stained to highlight cell populations (Fig 3.1). For E12.5 TECs, their $EPCAM^{+}$ $PLET1^{+}$ phenotype is relatively homogeneous and was thus sorted as a single population. PLET1 expression is gradually downregulated in TEC differentiation, and PLET1 heterogeneity is first apparent at E13.5 (Nowell et al., 2011). Since very few E13.5

TECs are positive for the mTEC marker UEA1, I decided to separate E13.5 TECs into PLET1^{hi} and PLET1^{lo} populations, which represent less and more differentiated TECs, respectively.

For E14.5 TECs, I used EPCAM, PLET1, UEA1, lineage and DAPI as the FACS sorting panel. The increased frequency of UEA1-expressing TECs allowed these prospective mTECs to be isolated separately. As the mature cTEC marker CD205 also marks some bipotent TEPCs at this developmental stage (Baik et al., 2013), it was not used to facilitate cell sorting. Instead, the UEA1^{-} E14.5 TECs were further divided into PLET1^{+} and PLET1^{-} fractions, again to represent more and less primitive cTEC/TEPC subsets.

200 cells were isolated for each population and analyzed by RT-qPCR. The sorting strategy is summarized in Appendix 8.1.1. Sorted samples are shown with asterisks in Fig 3.1, along with negative FMO controls for PLET1 and UEA1.

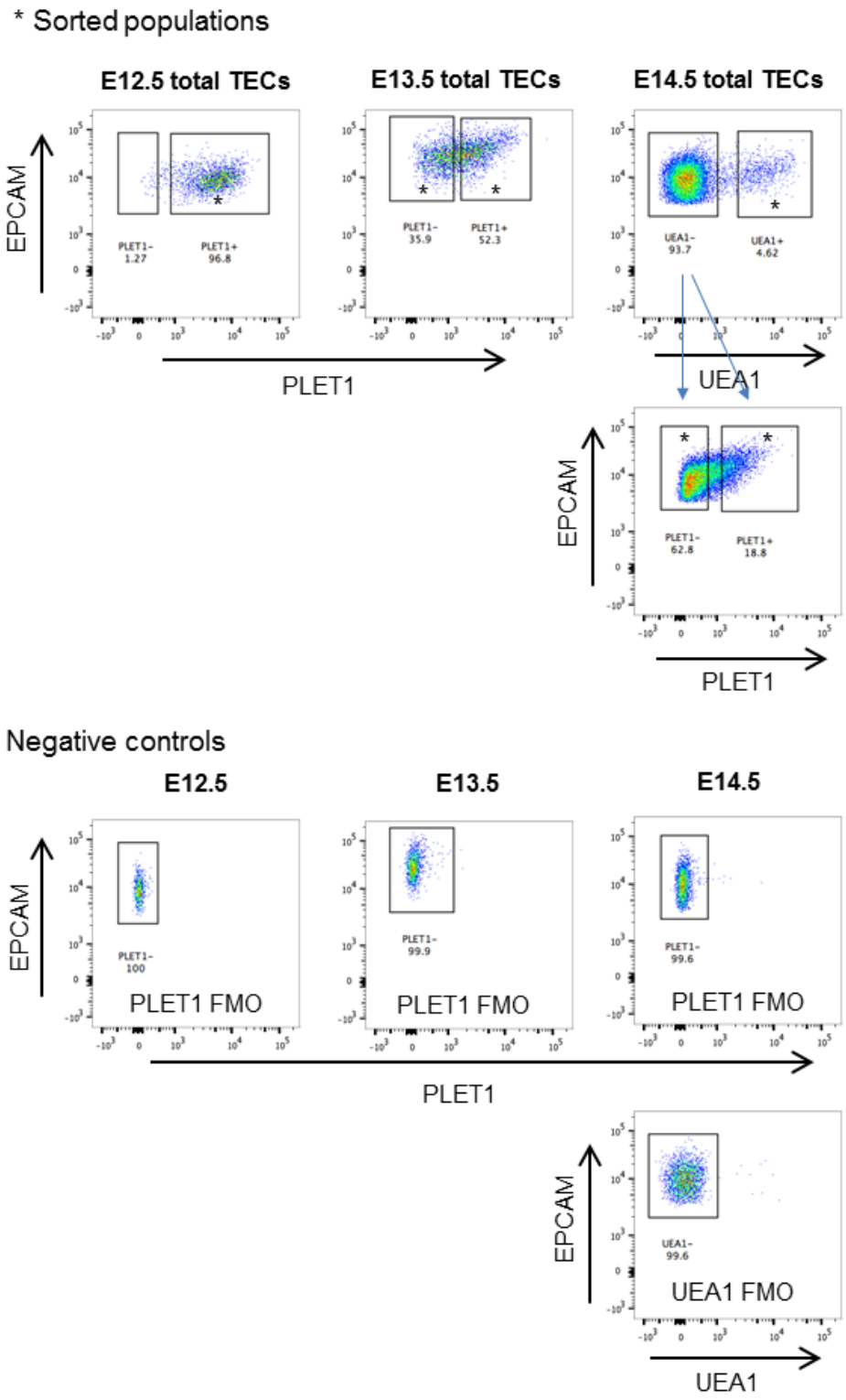

Figure 3.1 Legend on the next page.

Figure 3.1 The FACS sorting strategy for E12.5, E13.5, and E14.5 TEC populations analyzed by RT-qPCR. Positive and negative gates were established using FMO controls for UEA1 and PLET1. Gating strategy preceding the ‘total TECs’ population for all fetal TEC analyses is shown in Appendix: ‘Gating strategy (Fetal TEC)’.

3.1.1 mRNA expression

I first analyzed the expression pattern of all Notch family receptors and ligands. Of these, the expression of *Notch1*, *Notch2*, *Notch3*, *Dll4* and *Jagged1 (Jag1)* was detected at the stages analyzed (Fig 3.2), whereas the levels of *Notch4*, *Dll1* and *Jag2* were negligible. *Notch1* and *Notch2* were both enriched by two-fold specifically in the E14.5 $UEA1^+$ mTECs compared to E14.5 $UEA1^-$ populations. In comparison *Notch3* expression was initially high in E12.5 TECs, and decreased over the next two days, with the rate of decrease being noticeably more rapid in $PLET1^-$ cells. *Jag1* exhibited a very similar expression pattern to *Notch3*, but is distinct from *Dll4,* which was enriched in E13.5 $PLET1^-$ and E14.5 $UEA1^-$ populations. *Dll4* is an established FOXN1 target (Zuklys et al., 2016) and the correlation in their temporal expression pattern, especially in E14.5 TEC subsets, reflects this relationship.

The expression of several *Hes/Hey* genes was also addressed (Fig 3.2), as their expression is often associated with Notch activity (Fischer and Gessler, 2007). *Hes1* and *HeyL* were expressed most highly in E12.5 TECs and went down with developmental progression. *HeyL* also showed a slight enrichment in E14.5 mTECs. The expression of the recently identified FOXN1 target *Hey1* (Zuklys et al., 2016) was essentially unchanged during the timeframe examined. In contrast, *Hes6* expression fell from E12.5 to E14.5 specifically in the emerging mTECs (Fig 3.3). HES6 has been shown to antagonize the downstream effectors of Notch (Gratton et al., 2003), therefore its downregulation may reflect a fine-tuning mechanism to maintain Notch signalling strength in early mTECs. What is more, *Hes5* was not found to be expressed by fetal TECs. I established in Chapter VI that the expression of *Hes1* and *HeyL* is sensitive to Notch perturbation. Therefore, it seems that Notch activity is downregulated from E12.5 to E14.5.

Several other genes of interest were characterized similarly using RT-qPCR (Fig 3.3). Achaete-Scute Complex-Like 1 (*Ascl1)* encodes a bHLH transcription factor and is often repressed by Notch (Axelson, 2004). *Ascl1* is uniquely and strikingly activated in the E14.5 mTEC population, suggesting that it is a marker of early mTECs, or that it plays an active role in mTEC development. *Fbxw7* expression at E13.5 was enriched in the $PLET1^-$ fraction and by E14.5 the mRNA is almost

depleted in mTECs. FBXW7 has been implicated in the degradation of NICD (Carrieri and Dale, 2016) and is also a FOXN1 target (Zuklys et al., 2016). Moreover, ID proteins are bHLH factors often associated with BMP signalling (Ruzinova and Benezra, 2003), and can also enhance *Hes1* expression (Bai et al., 2007). *Id1* was found to be expressed highly in E12.5 TECs and indiscriminately downregulated in the next two days, likely indicating the waning strength of BMP signalling.

The agarose gels showing the PCR products can be found in Appendix 8.3.

3.1.2 Protein expression

Flow cytometry and IHC were also used to elucidate the protein expression of a number of Notch receptors and ligands. NOTCH1 expression was quantified in three E13.5 litters using flow cytometry, as a good antibody was available, with each litter pooled to maximize the abundance of $UEA1^+$ mTECs (Fig 3.4A). The proportion of $NOTCH1^+$ cells among mTECs was 51.5% ± 8.4%, significantly higher than 24.7% ± 10.4% among TECs that did not express definitive mTEC marker. This may reflect enriched receptiveness of emerging mTECs for NOTCH1 activation.

In the absence of good flow antibodies, I undertook IHC to study the expression of NOTCH2, NOTCH3 and JAG1. Like NOTCH1, NOTCH2 and JAG1 also largely co-stained with UEA1 on E14.5 thymic sections, whereas NOTCH3 was broadly expressed at a low level (Fig 3.4B-D).

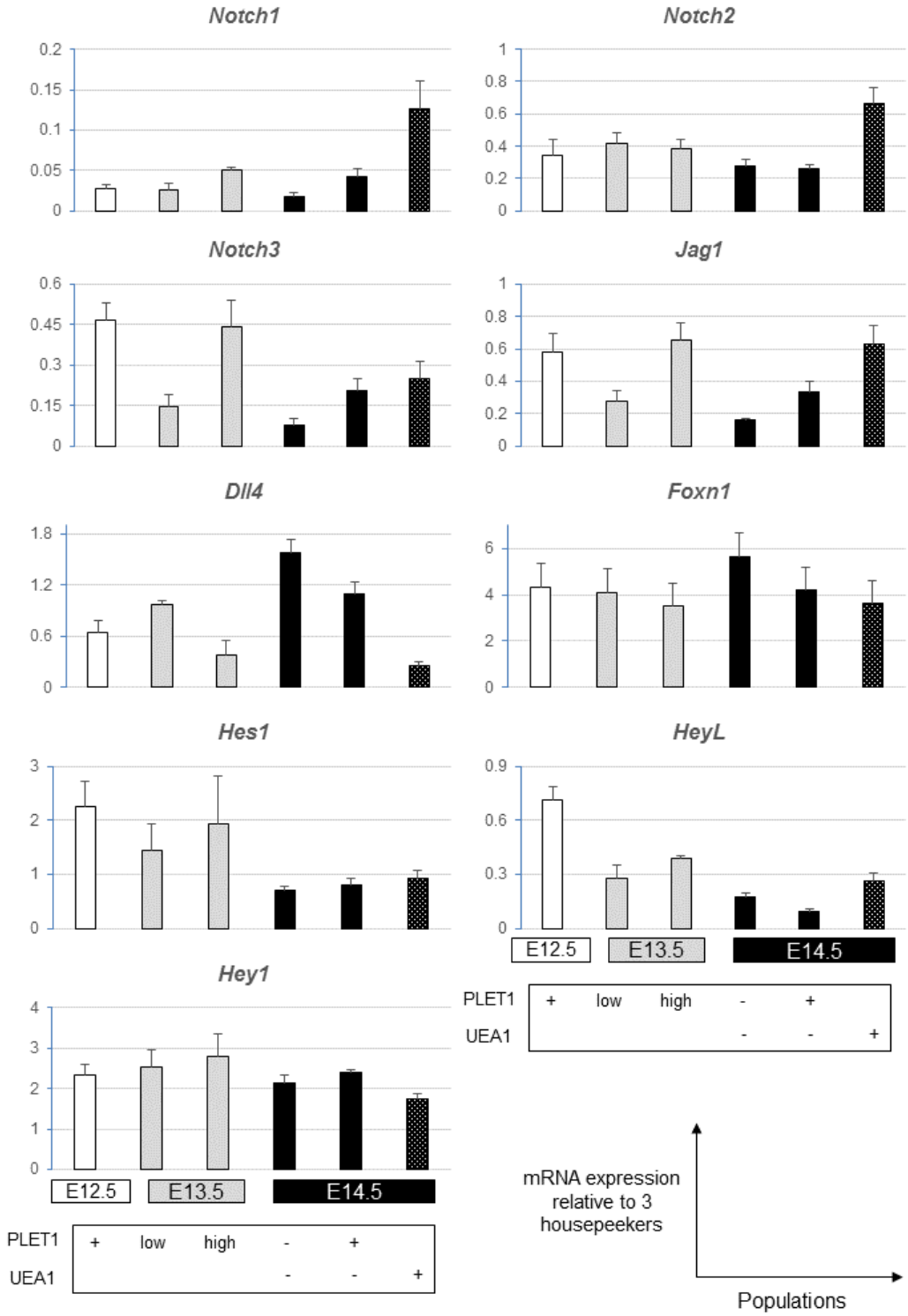

Figure 3.2 Legend on the next page.

Figure 3.2 mRNA expression of candidate genes in fetal TEC populations. E12.5, E13.5 and E14.5 populations were presented in white, grey and black bars, respectively. The E14.5 mTEC population ($UEA1^+$) was shown in dotted pattern to distinguish it from E14.5 non-mTEC populations.

For *Foxn1, Notch1, Ascl1, Fbxw7, Hes1, Hes6* and *Hey1*, N=6 for E12.5 and E13.5 populations, and N=3 for E14.5 populations.

For *Notch2*, N=5 for E12.5 and E13.5 populations, and N=3 for E14.5 populations.

For *Id1, Jag1, Dll4, Notch3* and *HeyL*, N=3 for all populations.

For *Plet1*, N=2 for all populations.

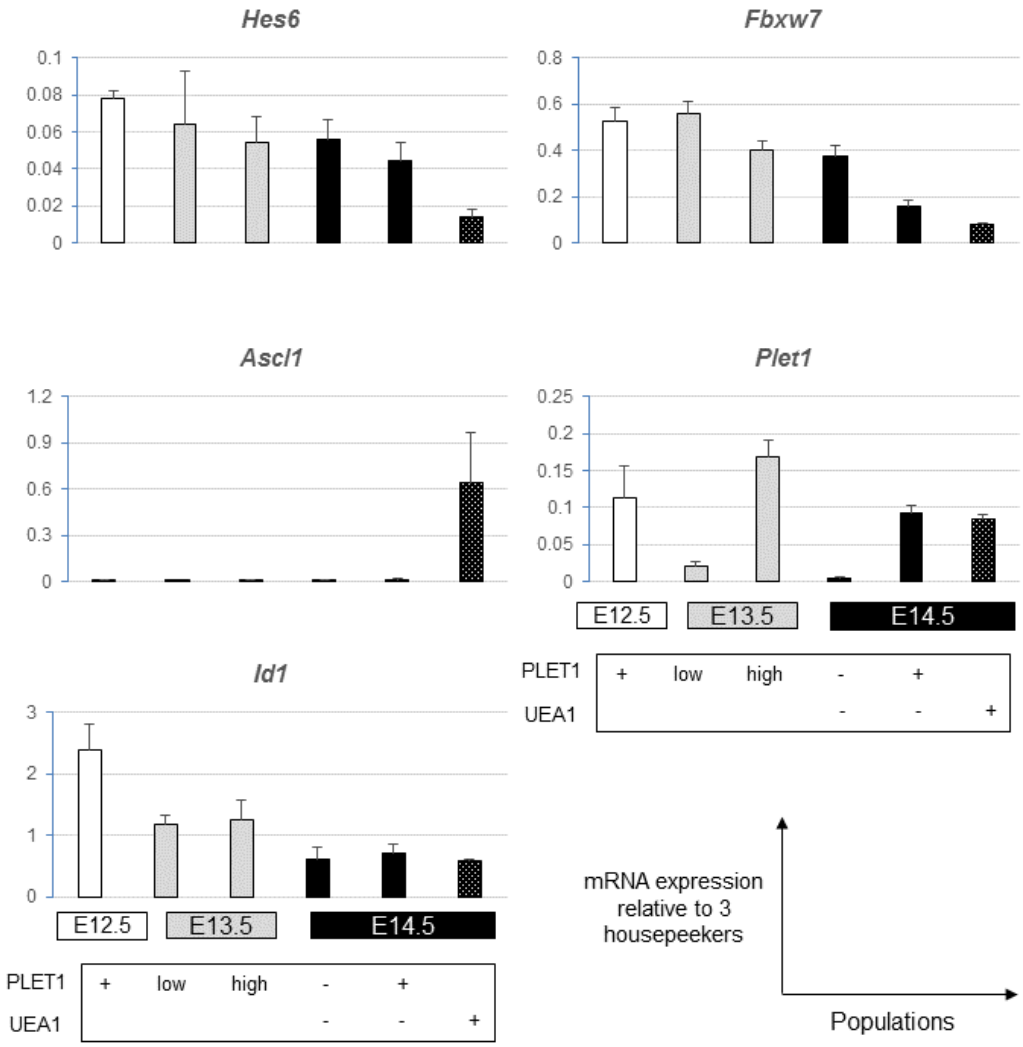

Figure 3.3 mRNA expression of candidate genes in fetal TEC populations (continued from Figure 3.2).

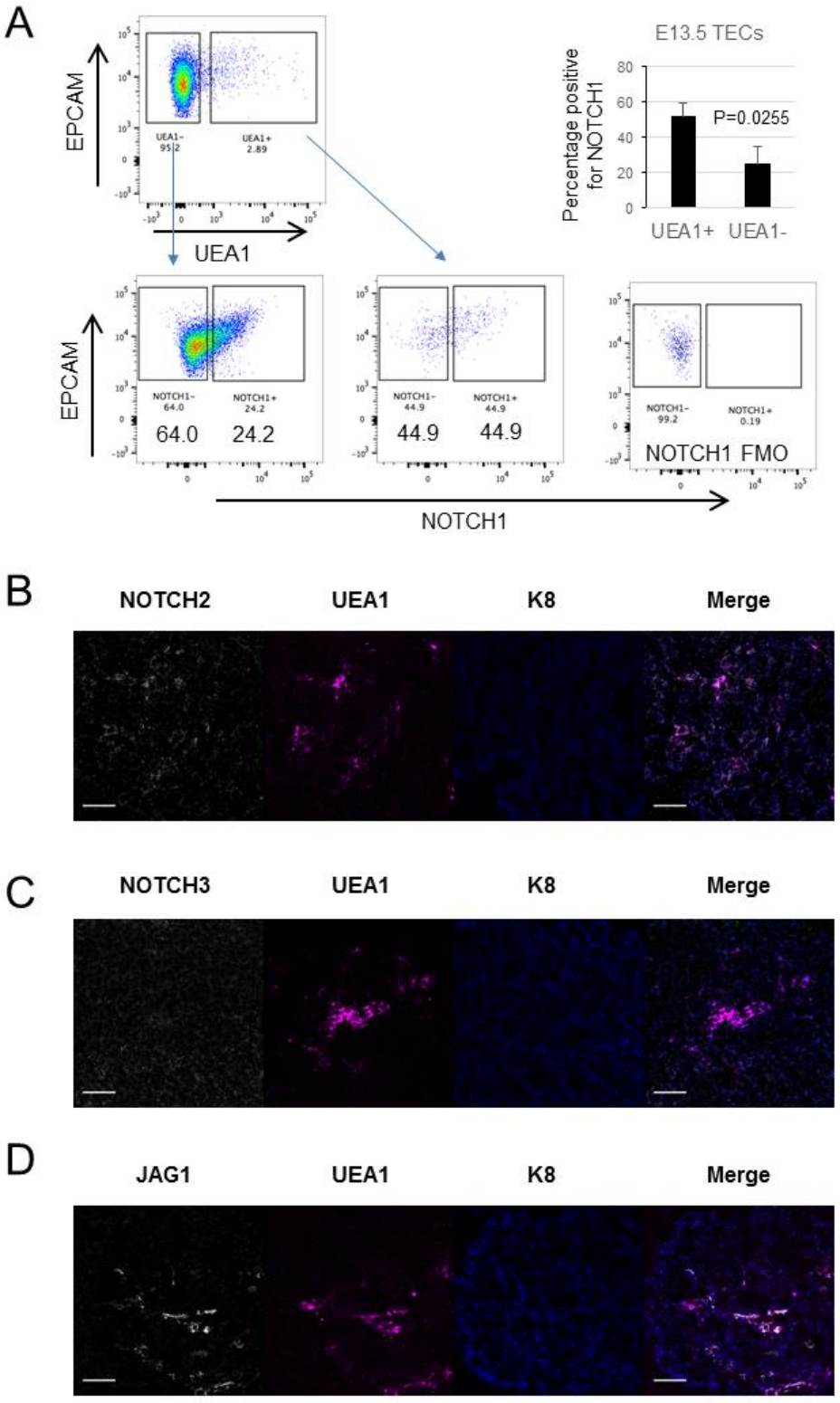

Figure 3.4 Legend on the next page.

Figure 3.4 Protein expression of NOTCH1, NOTCH2, NOTCH3 and JAG1 in embryonic TECs.

(A) The expression of NOTCH1 in E13.5 TECs, divided by UEA1 expression. Each independent litter of embryos was used to generate a data point used to quantify the percentage $UEA1^{+}$ or $UEA1^{-}$ TECs expressing NOTCH1. N=3.

(B-D) Immunohistochemistry staining of NOTCH2 (B), NOTCH3 (C) and JAG1 (D) on E14.5 thymus sections. Counter stained with mTEC marker UEA1 and epithelial marker K8. Scale bar=50μm.

3.2 Analysis of a Notch reporter line

To further characterize Notch activity in fetal TECs, I also analyzed CBF1:H2B-Venus thymi at E14.5. The logic of the reporter line is as follows (Nowotschin et al., 2013). When NICD-RBPJ complex binds the CBF1 Response Elements inserted before the SV40 promoter, expression of the histone H2B-Venus fusion protein is activated. Cells with a recent history of Notch activity could therefore be identified through the detection of Venus fluorescence.

At E14.5, the mTEC and cTEC populations were clearly identifiable based on the expression of UEA1 and CD205, although the $CD205^+$ subset may still contain some bipotent TEPCs (Figure 3.5A). At this stage about 5% of total TECs were $Venus^+$. A striking disparity in Venus expression was found between prospective mTECs and cTECs. Whereas half of mTEC (47.7% ± 6.7) were $Venus^+$, only a small minority of $CD205^+$ cTECs/TEPCs (3.4% ± 1.1%) expressed Venus (Figure 3.5A). There was also heterogeneity of Venus expression in terms of MHCII profile. When total TECs were divided into the more primitive $MHCII^-$ and the more differentiated $MHCII^+$ populations, a higher proportion of $MHCII^+$ cells were $Venus^+$ (8.4% ± 1.9% compared to 2.4% ± 1.4%) (Figure 3.5B).

While analyzing the Venus expression in adult TECs, I noted that the frequency of $Venus^+$ TECs was considerably higher than that reported by Goldfarb and colleagues using a different reporter strain (Goldfarb et al., 2016). The CBF1:H2B-Venus line is not without flaws, including the slow turnover of H2B-Venus proteins and the fixation of transgene expression in cells no longer signalling (Hadjantonakis, personal communications). Thus, caution shall be exercised in the interpretation of these results.

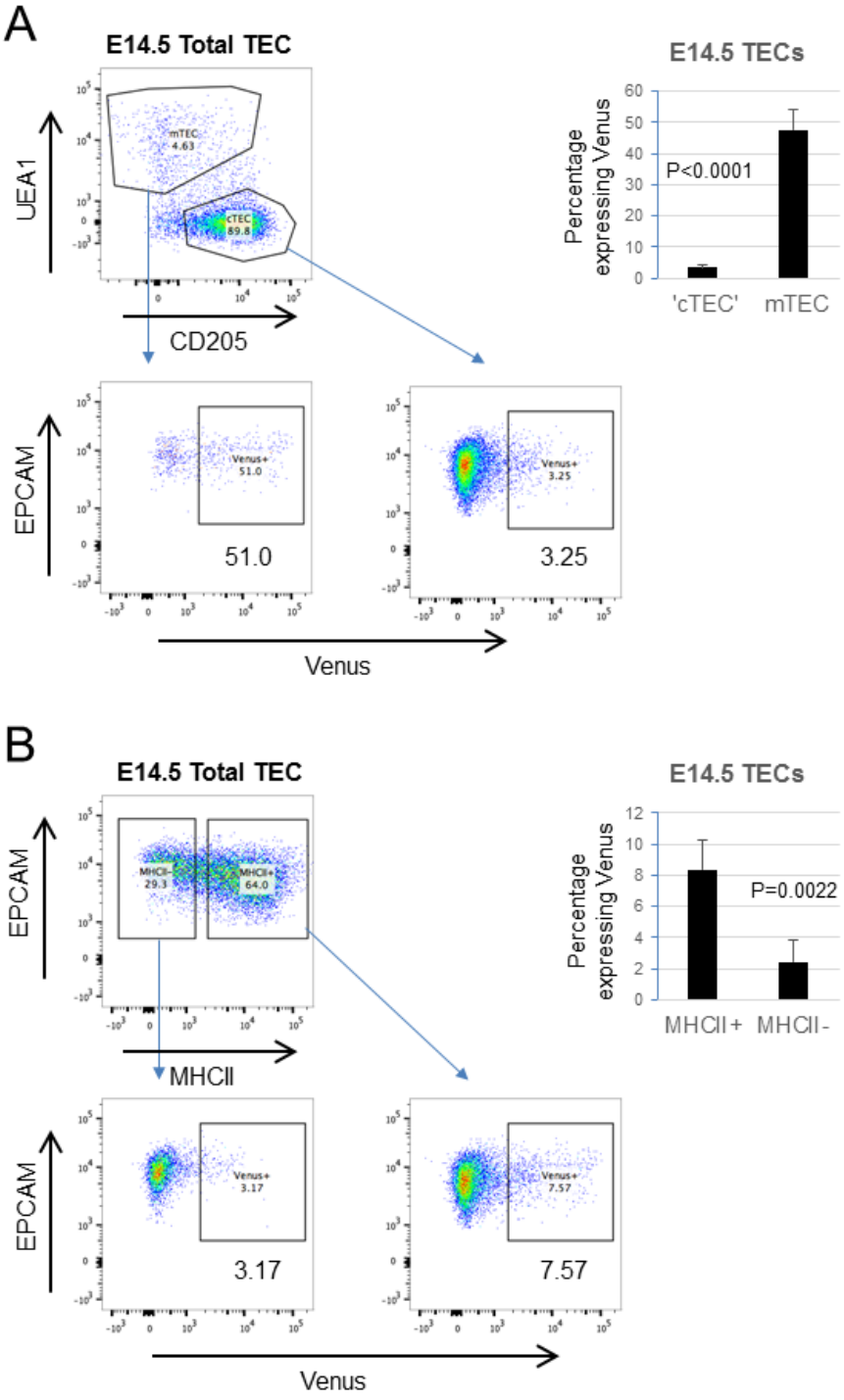

Figure 3.5 Legend on the next page.

Figure 3.5 Enrichment of Notch signalling activity in E14.5 mTECs.

CBF1:H2B-Venus reporter in E14.5 TEC subsets, N=4.

(A) Venus expression in UEA1^{+} CD205^{-} prospective mTEC and UEA1^{-} CD205^{+} prospective cTEC/TEPC ('cTEC') populations.

(B) Venus expression in MHCII^{+} and MHCII^{-} populations.

3.3 Discussion

The earliest mTECs (E14.5) are enriched in the expression of *Notch1*, *Notch2* and the ligand *Jag1* compared to their UEA1$^-$ non-mTEC counterparts. The correlation is present not only in respect with mRNA, but also holds for protein expression. This suggests that emerging mTECs are more receptive to Notch activation, while also capable of propagating Notch signal to neighbouring cells. Single cell RT-qPCR or RNA-seq will be required to establish whether *Jag1* and Notch receptor genes broadly co-express in early mTECs.

Notch3, on the other hand, appeared more robustly transcribed in E12.5 primitive TEPCs, and is downregulated with developmental progress. Interestingly, very little NOTCH3 protein expression was found in E14.5 thymi, indicating that it had ceased to be an important receptor. NOTCH3 molecular structure deviates considerably from NOTCH1 and NOTCH2 (reviewed in Bellavia et al., 2008), and it has been shown to more weakly activate Notch targets in certain circumstances (Beatus et al., 1999). It is currently unclear whether the three Notch receptors drive different levels of signalling in TECs, or indeed what the functional relevance is, but given what is understood regarding Notch signalling, one of a few possibilities is likely. As *Notch3* was associated with earlier progenitors, and *Notch1* and *Notch2* more with mTECs, these receptors may act on separate TEC lineages. If we assume that the signalling strength is increased by switching from NOTCH3 to NOTCH1 and NOTCH2, this shift may indicate higher levels of Notch signalling thresholds in mTECs than TEPCs. Finally, the expression of *Notch1* and *Notch2* are Notch-dependent in E14.5 TECs (Chapter VI), raising the possibility that these receptors may be involved in positive feedback to preserve the competence for extended Notch signalling in mTECs, whereas NOTCH3 may initiate the process in the first place.

As far as the expression of putative Notch targets is concerned, data documented here and previously (Vaidya, unpublished) support the notion that Notch is already active in TEPCs and that the pathway is dynamically regulated. Of note, while Notch reporter CBF1:H2B-Venus revealed that Notch activity is more prevalent in E14.5 mTECs compared to cTEC/TEPCs, the expression of *Hes1* and *Hey1* was not considerably over-represented in UEA1$^+$ TEC population, and *HeyL* only modestly

so. This disagreement may be reconciled by considering the perdurance of the Venus reporter, since it reports cells both actively signalling and having recently done so. *Hes1* and *HeyL*, two Notch-dependent genes confirmed in Chapter VI, both exhibited higher expression at E12.5 and had decreased by E14.5. Taken together, the most congruent hypothesis may be that Notch activity is higher in primitive TEPCs that go on to become mTECs.

Among the list of candidate genes examined, *Hes6* and *Fbxw7*, two potential negative Notch regulators, are downregulated specifically in early mTECs. The significance of this expression pattern is currently unknown, but if these genes indeed act as negative Notch modulators, it would suggest mechanisms that enable the temporary maintenance of Notch signalling in these early mTECs. Furthermore, *Ascl1* was identified as a potential marker of emerging mTECs.

Collectively, these data suggest that Notch signalling is active in TEPCs, and possibly persists in early mTECs. In the following chapters, I characterized the precise function of Notch signalling in TEC development.

Chapter IV Effect of Notch disruption on TEC development

To investigate the functions of Notch in early TEC development, I used a combination of genetic ablation and pharmacological inhibition to eliminate Notch signalling in TECs. The conditional knockout model deletes RBPJκ from cells that have expressed *Foxn1*, hence preventing gene expression changes resulting from Notch. On the other hand, treating fetal thymic explants with a γ-secretase inhibitor (DAPT) in culture inhibits the intracellular cleavage of Notch receptors and the production of NICD. The two complementary approaches target different parts of the pathway, allowing the distinction between Notch-dependent and -independent effects on TEC differentiation.

4.1 A genetic model for Notch perturbation in TECs

To study the consequence of losing Notch signalling in developing TECs, a conditional knockout model was developed by crossing $Foxn1^{Cre}$ (Gordon et al., 2007) and $Rbpj^{FL/FL}$ (Han et al., 2002) mice (Fig 4.1A). In cells expressing *Foxn1*, exons 6 and 7 of the *Rbpj* gene, which encode the DNA binding domain of the protein, are excised by Cre recombinase. Deletion of *Rbpj* renders these cells unresponsive to Notch activation, since the transcriptional complex including NICD can no longer bind DNA. For simplicity, $Foxn1^{Cre}$; $Rbpj^{FL/FL}$ homozygous mutants are referred to as 'conditional knockout' (cKO) hereafter.

The silent GFP (sGFP) mouse model is a faithful reporter of Cre activity, in which a floxed STOP cassette is excised upon Cre recombination, allowing GFP to be expressed and detected (Gilchrist et al., 2003). In mice carrying both $Foxn1^{Cre}$ and sGFP alleles, almost 100% E14.5 TECs were GFP^{+} (Fig 4.1B), hence the $Foxn1^{Cre}$-mediated recombination is highly efficient by three days after *Foxn1* initiation in TECs. In addition, PCR genotyping analysis of FACS sorted cKO TECs from 4-week postnatal thymi showed that while the deleted band was clearly detectable, the floxed band was absent (Fig 4.1C). This suggests that TECs carrying the undeleted

allele do not contribute significantly to adult cKO thymic epithelium. Therefore, deletion of the *Rbpj* locus was specific and efficient in the cKO model.

In addition to TECs, *Foxn1* is also expressed in the epidermis. This leads to a deleterious skin phenotype in the cKO model that becomes apparent between postnatal 4 and 8 weeks (Nicolas et al., 2003). These mice lost hair and showed abnormal excessive growth in facial skin. For this reason, most analyses were carried out with mice no older than 8 weeks.

4.2 Phenotype of the Rbpj conditional knockouts

I quantitatively assessed the TEC phenotype of postnatal day 14 Rbpj cKO mice with flow cytometry using the antibody panel in Table 1.2 in Chapter 1. At this stage, the percentage of mTECs in cKOs was significantly lower than in controls (Male control – 79.7 ± 1.7%, cKO - 67 ± 3.1%; Female: control – 58.2 ± 2.5%, cKO – 43.5 ± 1.4%) (Fig 4.2A). Inspection of cell number revealed that the difference was due to the hypoplasia of mTECs in cKOs rather than cTEC expansion (Fig 4.2B). No difference was observed between Cre^- and heterozygous thymi. Interestingly, the fold reduction of mTEC cellularity in cKOs was more pronounced in males than in females, and while both $mTEC^{hi}$ and $mTEC^{lo}$ cellularity were lower in males, only the $mTEC^{hi}$ subset was significantly reduced in females (Fig 4.2B).

No difference was found in the relative proportions of DN, DP and SP thymocyte populations (Fig 4.2C), indicating that T cell development was not blocked in cKOs. There was also no difference in thymic Tregs and Treg precursor numbers (Fig 4.2D). Therefore, the phenotype appeared restricted to the epithelial compartment.

To elucidate the kinetics of the mTEC hypoplasia phenotype, Rbpj cKO thymi were analyzed at a variety of developmental ages. The reduction of mTEC numbers was observed as early as E14.5 using IHC: two mTEC markers K14 and UEA1 were both less abundant in cKO thymic sections compared to controls (Fig 4.3A). The proportion of mTECs was also lower in cKOs at E18.5 (Fig 4.3B) and postnatal 2-week (Fig 4.2A). However, the mTEC proportion had normalized by 8-week (Fig 4.3C), and this was followed by a secondary loss of mTECs by 16-week (Fig 4.3D).

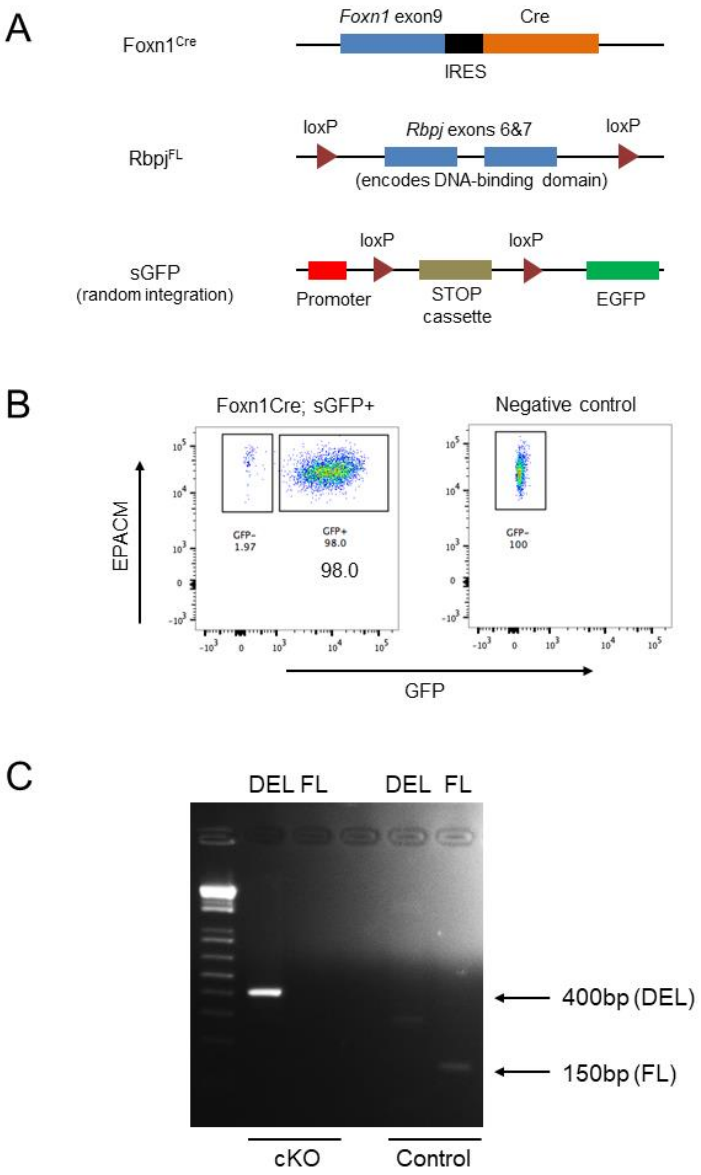

Figure 4.1. Validation of the Foxn1^{Cre}; Rbpj$^{FL/FL}$ conditional knockout (cKO).

(A) Schematics of Foxn1^{Cre}, Rbpj^{FL} and sGFP alleles.

(B) E14.5 silent GFP activation by Foxn1^{Cre}. Cre recombination efficiency in the EPCAM+ TECs was close to 100%.

(C) PCR analysis of genomic DNA in FACS sorted 4-week cKO and control (Foxn1^{WT}; Rbpj$^{+/FL}$) TECs. The deleted allele (DEL) was present while the undeleted floxed allele (FL) was undetectable in cKO TECs.

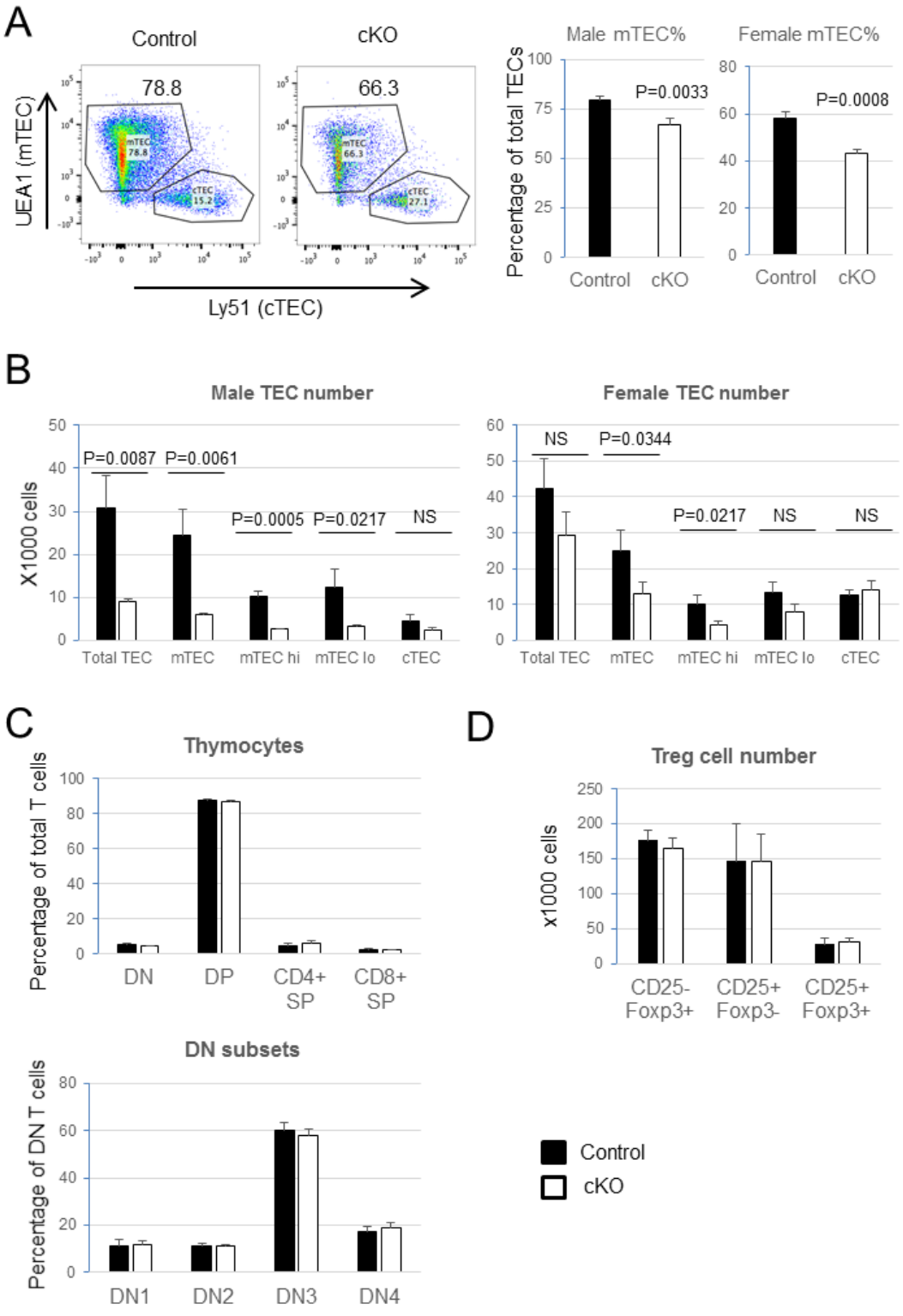

Figure 4.2 Legend on the next page.

Figure 4.2 mTEC hypoplasia in 14-day-old Rbpj cKO.

(A) Plots show representative flow cytometry analysis of total TECs (male). The percentage of mTECs in total EPCAM^{+} TEC population was quantified. N=3 for both male and female statistics.

(B) Absolute cell count of total TEC and subsets at postnatal 14 days. N=3 for both male and female statistics. Gating strategy is shown in Appendix: 'Gating strategy (adult TEC)'.

(C) The proportion of double negative (DN), double positive (DP) and single positive (SP) thymocyte populations in postnatal 14-day female thymi. DN thymocytes were further divided to DN1-4 stages and quantified against total DN. N=3 and all comparisons are non-significant. Gating strategy is shown in Appendix: 'Gating strategy (adult thymocytes)'.

(D) Total number of mature thymic Tregs (CD25^{+} Foxp3^{+}) and two Treg precursor populations (CD25^{+} Foxp3^{-} and CD25^{-} Foxp3^{+}) in postnatal 14-day males. Thymocytes were pre-gated on CD4^{+} TCRβ^{hi} CCR6^{-} population. N=3 and all comparisons are non-significant. Gating strategy is shown in Appendix: 'Gating strategy (adult Tregs)'.

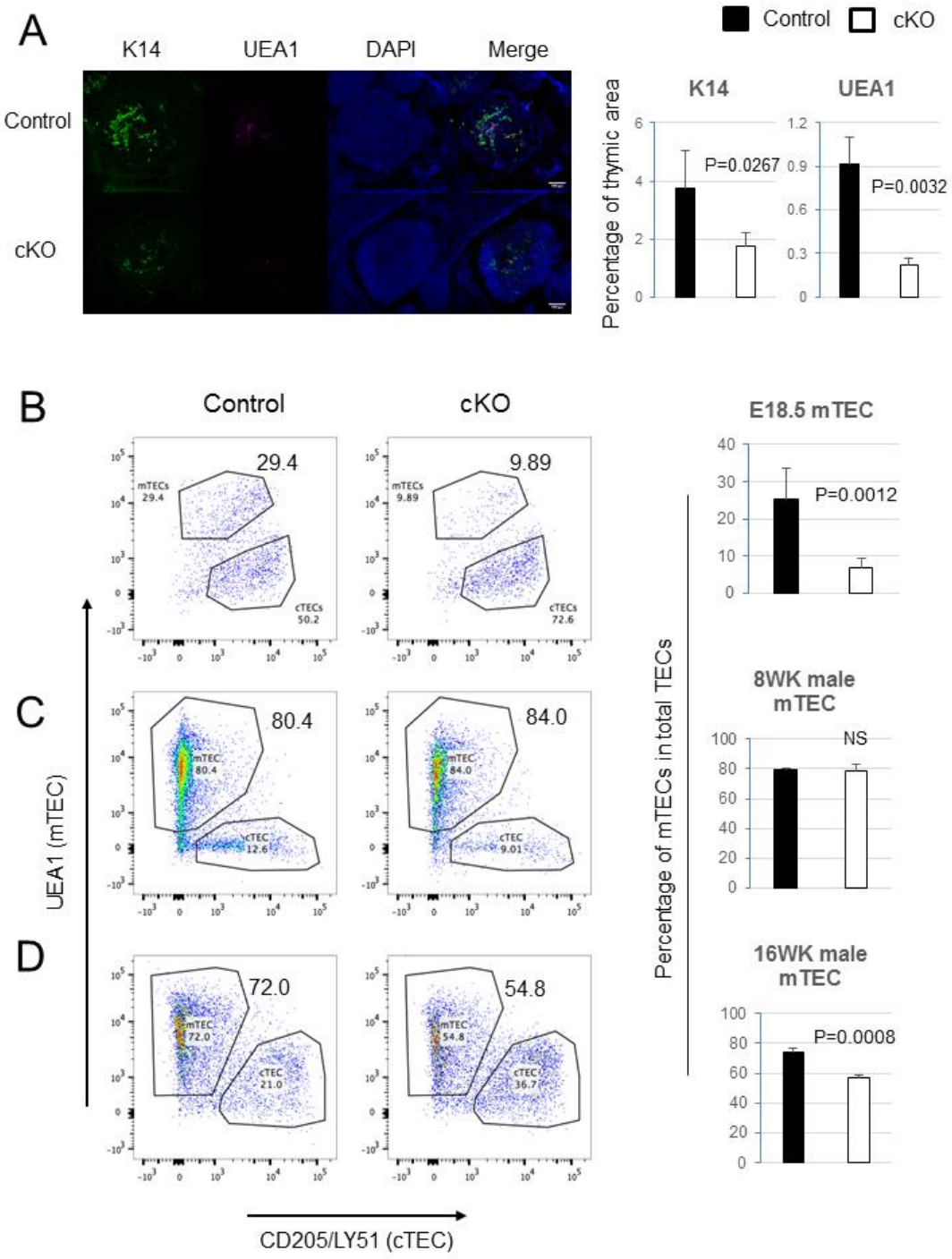

Figure 4.3 Legend on the next page.

Figure 4.3 Kinetics of the mTEC phenotype in Rbpj cKO.

(A) E14.5 cKO and control embryos were serially sectioned and mTEC markers K14 and UEA1 were examined by IHC. Percentage positive for a marker was denoted as area that is above positive threshold divided by total thymic area. Scale bar=100μm. N=4 for K14 and N=3 for UEA1.

(B-D) The proportions of mTECs and cTECs in total TECs for (B) E18.5 (C) postnatal 8-week and (D) postnatal 16-week male thymi. It is standard practice to use CD205 as a fetal cTEC marker, and LY51 for postnatal cTECs. N=3 for cKOs at each age. The 16-week data were collected by Dr. Kathy O'Neill.

4.3 Notch activity in determining mTEC number is temporally restricted

In order to investigate the phenotype further, I set out to determine whether Notch was required constantly, or in a confined time window, for mTEC development.

As TEC-specific Cre drivers that permit temporal control were not available, or not specific enough (Ulyanchenko, unpublished), fetal thymus organ culture (FTOC) was adopted in conjunction with a widely used γ-secretase inhibitor DAPT to antagonize Notch signalling in TEC development from various ages. For older tissue (E15.5 or order), fetal thymi were cultured using an established protocol at the air-liquid surface (Hikosaka et al., 2008). In this protocol thymic explants were incubated on membrane filters over the FTOC medium (Fig 2.1B). Since younger tissue is smaller and more fragile, a separate system was designed where the primordia were submerged and grown on a thin layer of matrigel (Fig 2.1A). Based on previous findings (Popis, Farley and Blackburn, unpublished) that FGF8 and BMP4 elevated *Foxn1* expression in cultured E10.5 3rd pharyngeal pouches (3PPs), these growth factors were added to the N2B27 medium to make up the 'TEPC medium'.

I first validated this culture system. E10.5 3PPs grown in TEPC medium increased marginally in size over time and became more three dimensional (Fig 4.4A). Between E10.5 and E12.5, TECs upregulate *Foxn1*, *Il-7* and downregulate *Tbx1*. After two days in culture, epithelial cells in the explants expressed similar levels of *Foxn1*, *Il-7* and *Tbx1* to E12.5 TECs (Fig 4.4B), indicating that the TEC precursors underwent some degree of maturation in culture. Moreover, E12.5 thymi cultured after 3 days exhibited a higher proportion of UEA1^{+} mTECs and downregulated PLET1 further than E15.5 TECs (Fig 4.4C), suggesting that in this period the culture system promotes faster differentiation than *in vivo*.

When DAPT was added to the medium, at the highest concentration used in this thesis (50μM), there was a slight increase in the number of cells expressing apoptosis marker active caspase 3 compared to DMSO control (Fig 4.5A). However, the proportion of apoptotic TECs was only 3%, indicating that DAPT toxicity was relatively low at the concentrations used here. Moreover, treatment of E12.5 lobes

with DAPT led to lower expression of the Notch target *Hes1* (Fig 4.5B), establishing that the inhibitor was effective in targeting the Notch pathway.

Compared to DMSO-treated controls, E12.5 thymi cultured in the presence of 20μM DAPT displayed medullary hypoplasia similar to fetal Rbpj cKOs (Fig 4.6A). Treatment with DAPT at three different concentrations (1μM, 10μM and 20μM) shows that the reduction of mTEC proportion is dosage-dependent (Fig 4.6A). Furthermore, at 20μM DAPT the significant decrease in cell number was specific to mTECs (Fig 4.6A). Consistent with flow cytometry results, I showed using IHC that $K14^+$ $UEA1^+$ mTEC clusters were readily detectable in control explant (Fig 4.6B). In comparison, mTEC foci in the DAPT treated explants were fewer and smaller, though not altogether absent (Fig 4.6B). Together, these data demonstrate that γ-secretase inhibition on E12.5 thymic explants phenocopied the mTEC deficiency in Rbpj cKOs. Since targeting Notch receptor cleavage and gene expression produced highly similar results, we can deduce with confidence that the mTEC phenotype is due to the loss of Notch activity.

To address whether the requirement for Notch in mTEC development was limited to a time window, E14.5 and E16.5 thymi were subjected to DAPT treatment in FTOC. For E14.5 primordia DAPT was applied at 10μM and 20μM, and for E16.5 the concentration was at 20μM and 50μM. Whereas the mTECs of E14.5 explants were also sensitive to DAPT treatment (20μM data shown), mTECs were not diminished by DAPT treatment in E16.5 explants, even at 50μM (Fig 4.6C). Taken together, these data indicate that Notch is required in a restricted time window to determine mTEC cellularity in thymus organogenesis.

Notably, the E16.5 tissue was cultured at air-liquid interface, which may have undermined exposure to the inhibitor as opposed to E12.5 and E14.5 lobes that were submerged in culture medium. However, since DAPT did have an effect on the mTEC population of E15.5 thymi cultured at medium surface (Chapter VI), which are of a similar size, this lack of response possibly reflects more of the properties of the tissue rather than the different experimental set-ups.

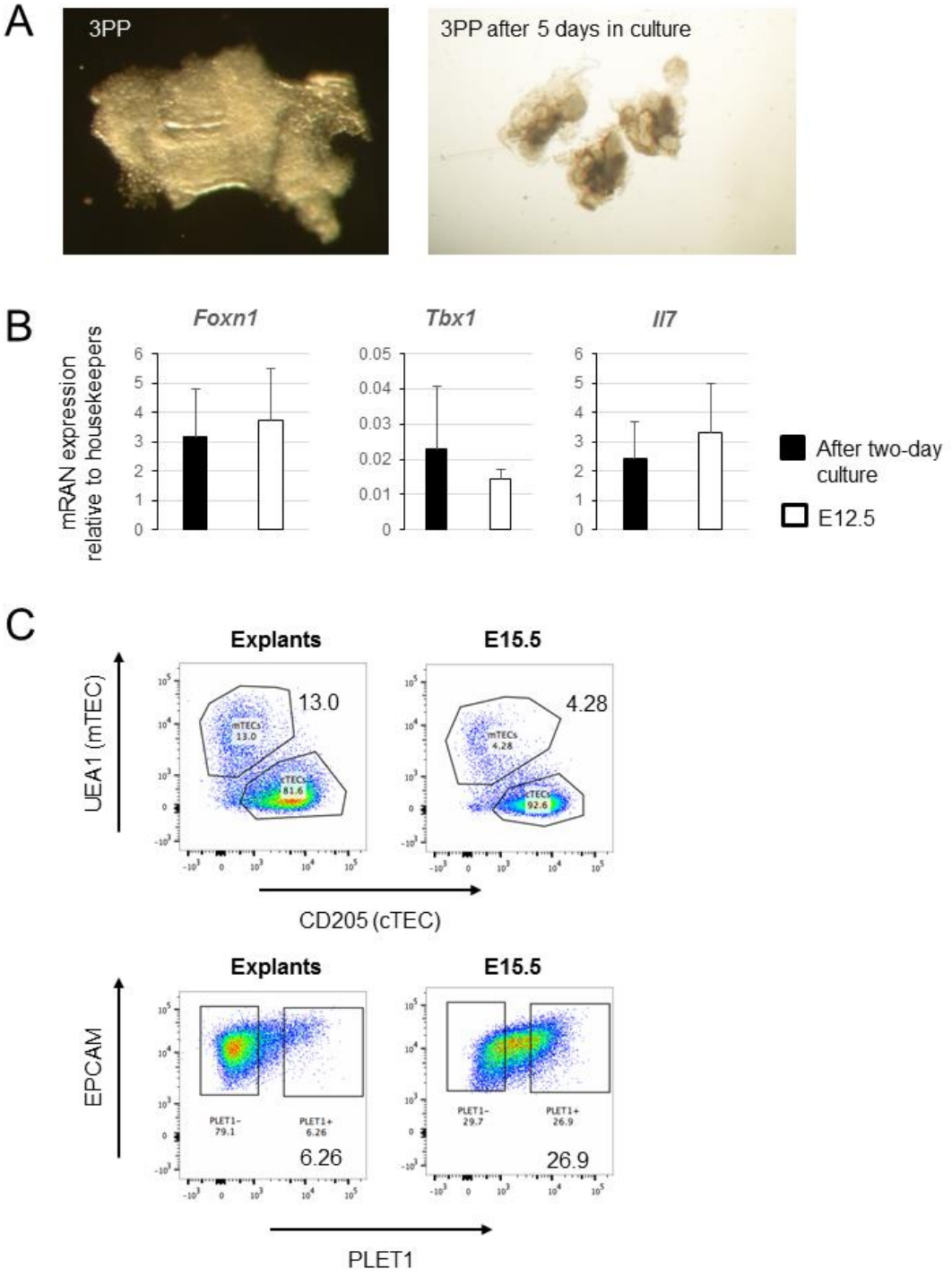

Figure 4.4 Legend on the next page.

Figure 4.4 Validation of the TEPC culture condition

(A) The morphology of a freshly dissected E10.5 third pharyngeal pouch (3PP), and 3PP explants after 5-day culture in the TEPC medium. Images not to scale.

(B) The mRNA expression levels of *Foxn1*, *Tbx1* and *Il-7* in EPCAM^{+} TECs sorted from E10.5 3PPs cultured in TEPC medium for two days, compared with E12.5 TECs. N=2.

(C) The distribution of UEA1, CD205 and PLET1 in E12.5 thymic lobes cultured for three days in TEPC medium ('Explants'), compared to E15.5 TECs.

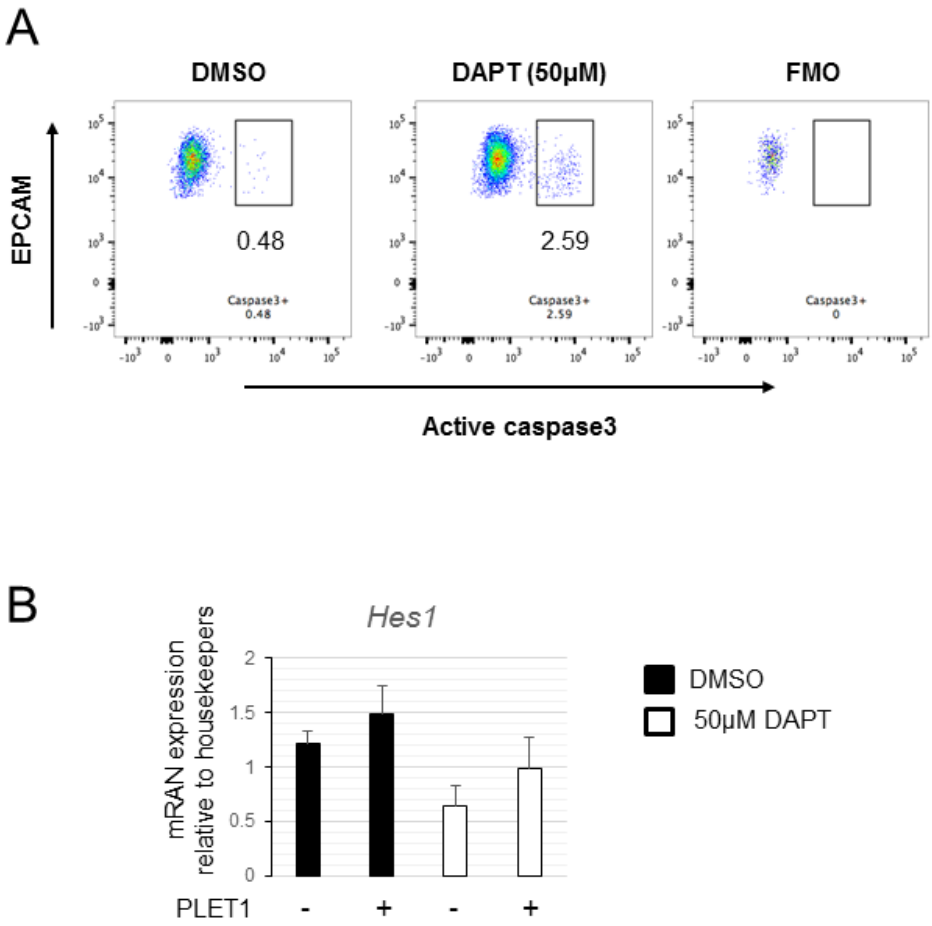

Figure 4.5 Validation of the γ-secretase inhibitor DAPT

(A) Apoptosis rate (caspase3 positive) among TECs following overnight culture of E12.5 lobes with DMSO or 50μM DAPT.

(B) Notch target *Hes1* was less highly expressed in PLET1^{+} and PLET1^{-} TECs from E12.5 lobes treated with 50μM DAPT for two days compared to DMSO controls. N=2.

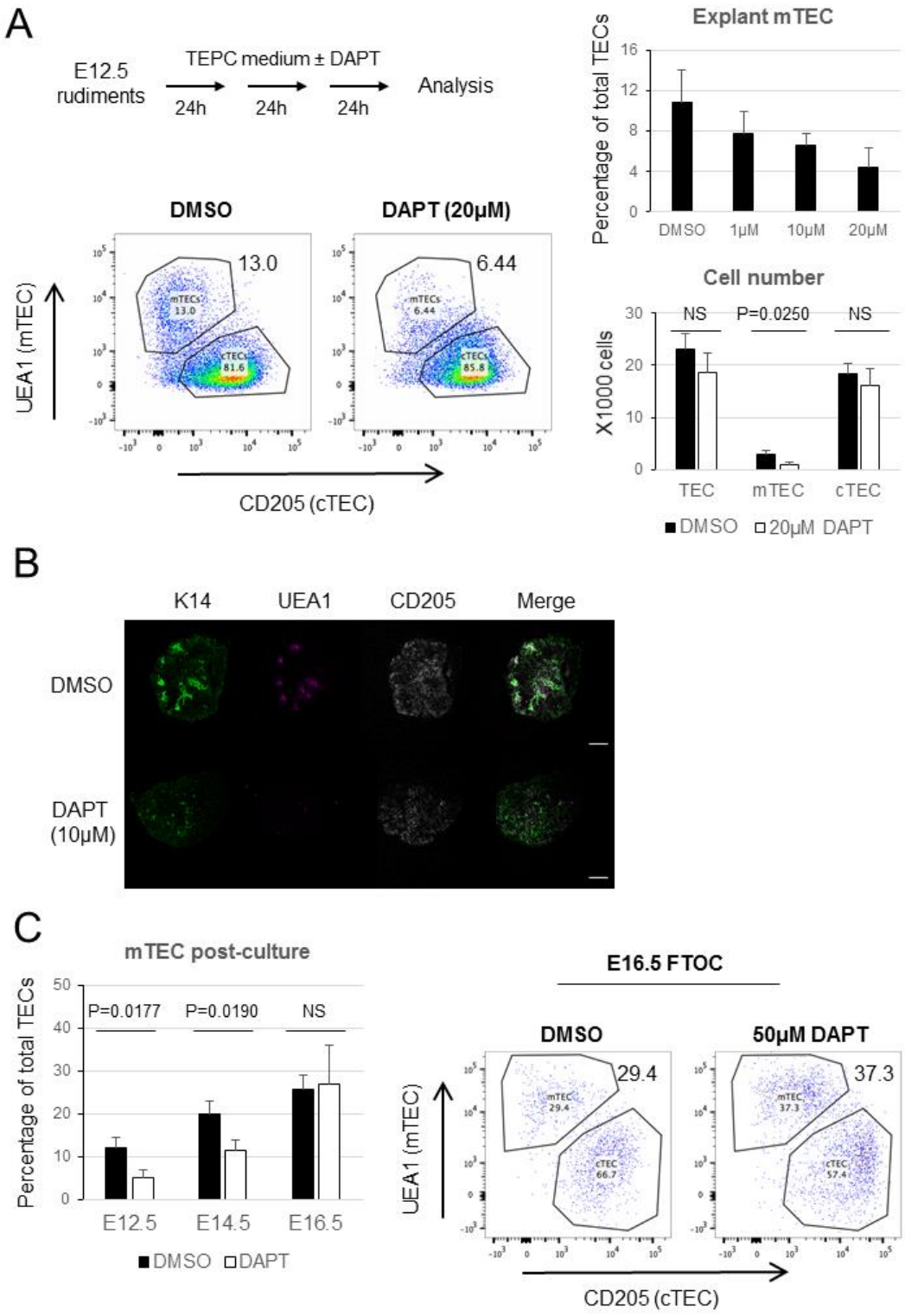

Figure 4.6 Legend on the next page.

Figure 4.6 DAPT treatment phenocopies mTEC reduction in Rbpj cKO

(A) E12.5 thymic lobes were cultured for three days in DMSO control or several DAPT concentrations. N=3. Representative plots for total TECs are shown. The reduction in mTEC percentage is dependent on the concentration of the inhibitor, and the only significant difference in cell number was found in the mTECs. Cell number is the total of 9 explants.

Gating strategy is shown in Appendix: ‘Gating strategy (FTOC)’.

(B) Immunofluorescence staining of mTEC (K14 and UEA1) and cTEC (CD205) markers post culture. Scale bar=100μm.

(C) The percentage of mTECs following three-day FTOC of the age indicated. Data shown are from DMSO controls and the highest concentration of DAPT used, namely 20μM for E12.5 and E14.5, 50μM for E16.5 lobes. N=3. Representative mTEC:cTEC plots of E16.5 culture are shown.

4.4 Notch is required for the initial emergence of mTECs

The results so far point to a role of Notch in the early stage of mTEC differentiation. Paradoxically, although mTECs were less numerous in the Rbpj cKO model, they nonetheless developed and matured. The exact time frame during which the mTEC lineage is specified from bipotent progenitors remains controversial (Hamazaki et al., 2016), and the deletion of *Rbpj* with Foxn1^{Cre} may commence too late to affect the specification of the first mTEC progenitors, considering that functional null state is only reached with sufficient decay of residual wildtype RBPJ proteins.

To address whether Notch regulates mTEC specification, E10.5 3PPs were dissected and cultured in TEPC medium with or without DAPT for 5 days and examined for mTEC development. The E10.5 endoderm of 3PP is a simple epithelium and there has been no evidence that these cells have differentiated towards mTEC or cTEC fate. Moreover, contrary to the delay in the genetic model, the inhibitor should block the signalling immediately in culture. As RANK receptor signalling is known to enhance the proliferation of RANK$^+$ mTEC progenitors present in culture, RANK ligand was added to half of the wells treated either with or without DAPT for the last two days to enhance any difference between DAPT treatment and control samples (Fig 4.7A).

The control explants generated a small but consistent UEA1$^+$ mTEC population, whereas this population was not found after a 5-day culture at 50μM DAPT (Fig 4.7B). Perhaps due to the presence of parathyroid cells which also originate from the 3PP, a considerable fraction of EPCAM$^+$ epithelial cells in both conditions expressed neither UEA1 nor CD205, therefore I elected to quantify the cell number positive for these definitive TEC markers. On average 90 UEA1$^+$ cells per three control explants were detected by the end of culture, and this was reduced to less than 20 per three explants in tissue treated with DAPT (Fig 4.7B). RANK ligand did not increase the mTEC cell count in either condition, suggesting that these mTECs were immature progenitors that did not yet express functional RANK receptor. In comparison, the number of CD205$^+$ cTECs was not altered by DAPT treatment (Fig 4.7B).

In line with the flow cytometry data, IHC analysis showed that both K14$^+$ UEA1$^+$ mTEC and CD205$^+$ cTEC clusters developed in the control condition, but mTEC

development was specifically suppressed by DAPT treatment (Fig 4.7C). In some explants, rare cells expressing mTEC markers were found at the border of what appeared to be the incompletely closed lumen of the 3PP (arrow), reminiscent of the CLDN3/4^{+} cells in the apical side of 3PP that were speculated to be biased towards the mTEC fate (Hamazaki et al., 2007).

Haematopoietic cells have not entered the thymic anlage at E10.5 (Luis et al., 2016), and as a result this culture system was devoid of crosstalk between TECs and T cells. Perhaps for this reason the explants did not grow substantially in size, but initial differentiation into mTEC and cTEC lineages occurred nonetheless. This observation is consistent with previous findings that the initial divergence of cTEC and mTEC sub-lineages is crosstalk-independent (Klug et al., 2002; Nowell et al., 2011). Thus, the tendency to differentiate may be inherent to TEPCs and does not require interaction with T cells.

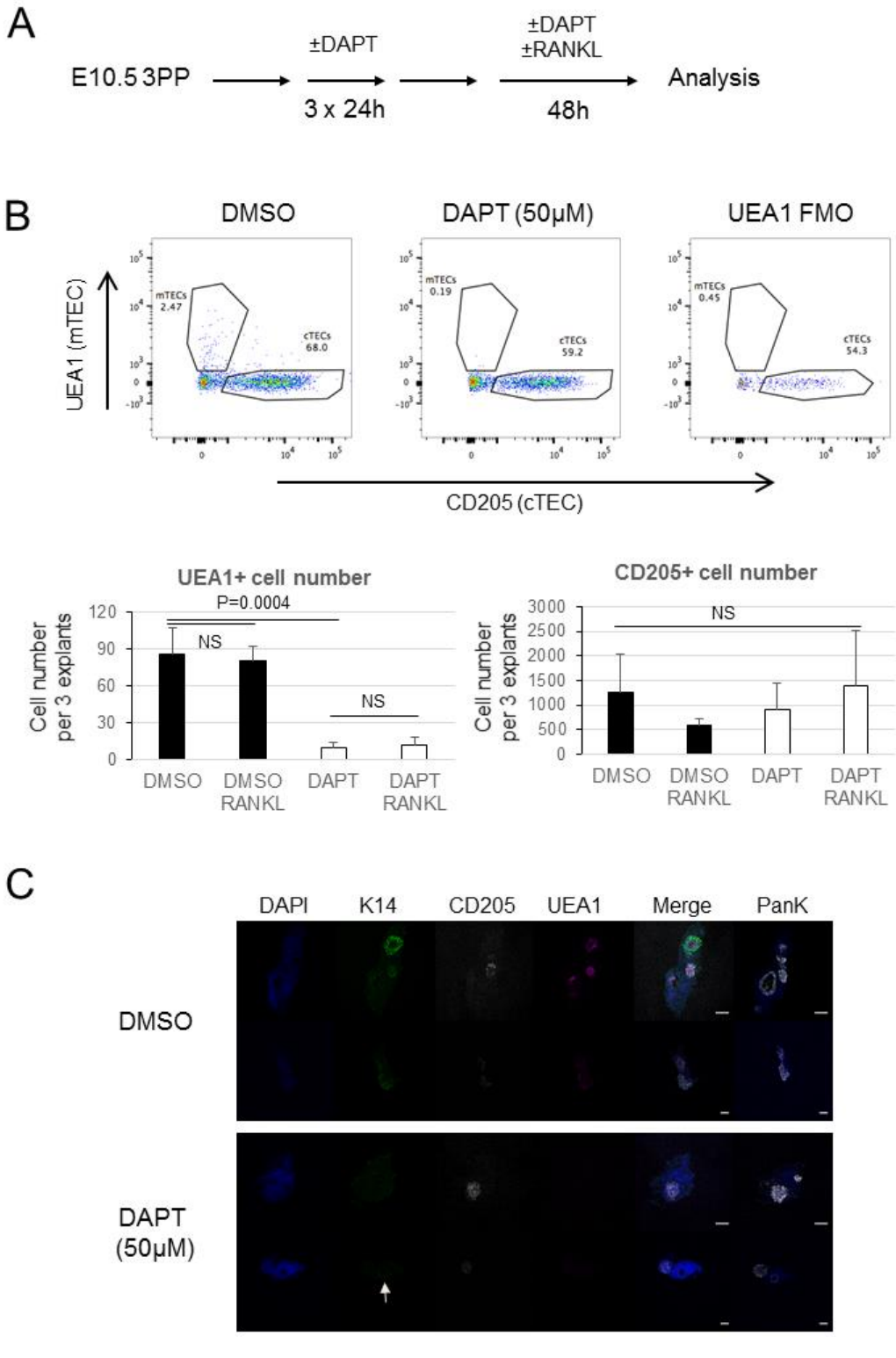

Figure 4.7 Legend on the next page.

Figure 4.7 mTEC emergence is blocked by early Notch inhibition.

(A) Experimental plan of DAPT culture with E10.5 3PP tissue.

(B) Representative mTEC:cTEC plots of explants treated with DMSO and 50μM DAPT throughout are shown. The number of cells (total of three explants) in the ‘mTECs’ and ‘cTECs’ gates were counted and quantified for all four conditions. N=3.

(C) Immunofluorescence of mTEC (K14 and UEA1) and cTEC (CD205) markers on sections of the explants after culture. Pan-keratin (PanK) was stained on the adjacent sections to highlight the extent of the epithelium. Scale bar=100μm.

4.5 Discussion

I have shown here that the primary phenotype of the loss of Notch function in developing TECs is the reduction of mTEC cell number. Both genetic ablation of *Rbpj* and chemical inhibition data support this conclusion. In contrast, cTEC or thymocyte alterations were not observed following Notch perturbation.

Aside from the comparison between control and Rbpj cKO, this study also revealed differences between male and female TECs (Fig 4.2). Given that the sample size is not large (N=3 for each sex), the contribution of variation is difficult to exclude. Nonetheless, it does appear that the proportion of mTECs in total TECs is higher in males, and that TEC cellularity is larger in female thymi. Also, Rbpj cKO seems to induce a higher mTEC cellularity fold change in males (3-fold) than in females (2-fold). 4OH-tamoxifen, a well characterized small molecule targeting the estrogen receptor, can increase mTEC proportion in FTOC (personal observation). It is hence possible that the sex differences may reflect the role of sex steroid signalling in mTEC development. Alternatively, it could be the result of different TEC proliferation rate in males and females (Dumont-Lagacé et al., 2014).

Using the FTOC system, the results presented here also underline that Notch acts in a limited time window (E10.5-16.5) to regulate mTEC development, and that Notch is required for the emergence of the very early mTEC progenitors. That DAPT treatment on later thymi, or what I regard as late *Rbpj* deletion (by $Foxn1^{Cre}$), incompletely abolished the mTEC population suggests that once the mTEC progenitor pool is established, these cells are no longer sensitive to the intensity of Notch signalling they experience.

Indeed, this shift in TEPC behaviour with age is well documented. For instance, fetal mTEPCs identified by Sekai and co exhibit very little reconstitution capacity in adults (Sekai et al., 2014), suggesting that either they no longer express the same markers, or that they are not as regenerative as their fetal counterparts. β5t-expressing fetal TECs can give rise to both mTECs and cTECs, but this behaviour is extinguished postnatally (Ohigashi et al., 2015). Moreover, while all fetal TECs actively proliferate, numerous postnatal TECs only cycle slowly (Dumont-Lagacé et al., 2014; Tan and Nusse, 2017).

In the context of Notch signalling, these results are not in apparent agreement with Goldfarb's conclusion that Notch needs to be suppressed by HDAC3 for mTEC differentiation to proceed normally (Goldfarb et al., 2016). However, upon closer examination, the two studies can be reconciled by considering the stage-specific nature of Notch signalling. Goldfarb et al uncovered the suppression of Notch by analyzing a Notch reporter and the Notch gain-of-function mutant in postnatal and adult TECs, and by these stages the initial wave of Notch activity in mTEC lineage emergence would have already subsided. As is discussed in the next chapter, the adult Notch gain-of-function phenotype may be the product of multiple alterations. The lack of investigation on the initial fetal phenotype may have led to their different and incomplete interpretation.

The Rbpj cKO mice exhibited a period of mTEC normalization between postnatal 2-week and 8-week, before a secondary loss of mTEC number was observed by 16-week. This postnatal kinetics may be explained by the compensatory proliferation of mTECs in cKO thymi that eventually led to mTEC progenitor exhaustion. Further evidence on TEC proliferation rate is required to substantiate this hypothesis.

Chapter V Constitutive Notch activity delays TEC maturation

In the preceding chapter I have shown that the development of the mTEC sub-lineage is impaired in the Notch loss-of-function models. Lessons from other organ systems emphasize that the dosage of Notch a progenitor cell experience may profoundly affect its differentiation outcome (section 1.6). To this end, a gain-of-function approach was adopted to study the effect of sustained high Notch activity on TEC differentiation. By driving the expression of NICD in developing TECs, the main aim of these experiments is to understand whether Notch is instructive or permissive for mTEC commitment.

5.1 TEC-specific Notch gain-of-function model

The results presented in chapter IV suggested that mTEC specification is defective when Notch signalling is disrupted in early fetal TECs. This prompted us to study the effects of constitutive Notch signalling on TEC differentiation. The $Rosa26^{loxP\text{-}STOP\text{-}loxP\text{-}NICD\text{-}IRES\text{-}EGFP}$ model (NICD hereafter) is a Cre-inducible genetic system designed to express NICD from the constitutive promoter of *Rosa26* gene (Murtaugh et al., 2003). Cre mediates the recombination and removal of a loxP-flanked STOP cassette, allowing the transcription of Notch intracellular domain coding sequence and that of EGFP (Fig 5.1A). In order to create a model in which NICD would be activated solely in embryonic TECs, homozygous NICD females were crossed to homozygous $Foxn1^{Cre}$ male mice. The embryos of this mating scheme would harbour one allele of $Foxn1^{Cre}$ and $Rosa26^{NICD}$ each.

The phenotype of postnatal $Foxn1^{Cre}$; NICD thymus was described recently (Goldfarb et al., 2016). However, these thymi exhibited severe hypoplasia, complicating the interpretation of experimental results. Since the γ-secretase inhibitor data presented in section 4.3 point to a temporally restricted role for Notch in fetal mTECs, TECs were isolated from $Foxn1^{Cre}$; NICD embryos at E14.5 and E16.5 for phenotypic profiling.

The NICD construct allows the recombination efficiency to be reported by GFP fluorescence of the cells. 90.6 ± 1.3% of the EPCAM$^+$ TECs in Foxn1^{Cre}; NICD thymi were GFP$^+$ at E14.5, and the percentage did not increase significantly at E16.5 (Fig 5.1B). The mosaicism between the GFP$^+$ and GFP$^-$ TECs described below (Fig 5.2B) suggests that GFP accurately reported NICD levels.

5.2 E14.5 NICD phenotype

Fetal TEC maturation is marked by the gradual downregulation of PLET1 and the increase of MHCII in both the mTEC and cTEC lineages (Nowell et al., 2011). Strikingly, at E14.5, most if not all Foxn1^{Cre}; NICD TECs were PLET1$^+$ (94.6 ± 2.9%), whereas 32 ± 4.0% of control TEC were below the positive threshold (Fig 5.2A Left). Moreover, nearly half of control TECs were MHCII$^+$ (44.7 ± 4.4%) compared to 20% of Foxn1^{Cre}; NICD TECs (20.0 ± 1.2%; Fig 5.2A Middle). These expression profiles suggest that constitutive NICD reduced the progress of TEC differentiation.

At E14.5 UEA1$^+$ mTECs form a small population, comprising about 5% of total TECs. If Notch actively promotes commitment to mTEC fate, the expected outcome of NICD overexpression would be the conversion of the majority of TECs to mTECs. However, at E14.5 the proportion of UEA1$^+$ mTECs in the Foxn1^{Cre}; NICD TECs was not significantly different from that of controls (NICD: 4.9 ± 0.2%; controls: 4.4 ± 0.3%; Fig 5.2A Right). Therefore, it seems that forced NICD expression initially blocked TEPC differentiation, rather than instructed the acquisition of mTEC fate.

Despite limited cell number, I also analyzed the GFP$^-$ TECs in Foxn1^{Cre}; NICD thymi. This revealed remarkably lower expression of PLET1 in GFP$^-$ compared to GFP$^+$ TECs in the same embryos (Fig 5.2B). Indeed, the PLET1 profile of GFP$^-$ TECs resembled that of control TECs, consistent with their having experienced only wildtype levels of NICD. This observation also indicated that the failure to downregulate PLET1 is a primary consequence of NICD overexpression.

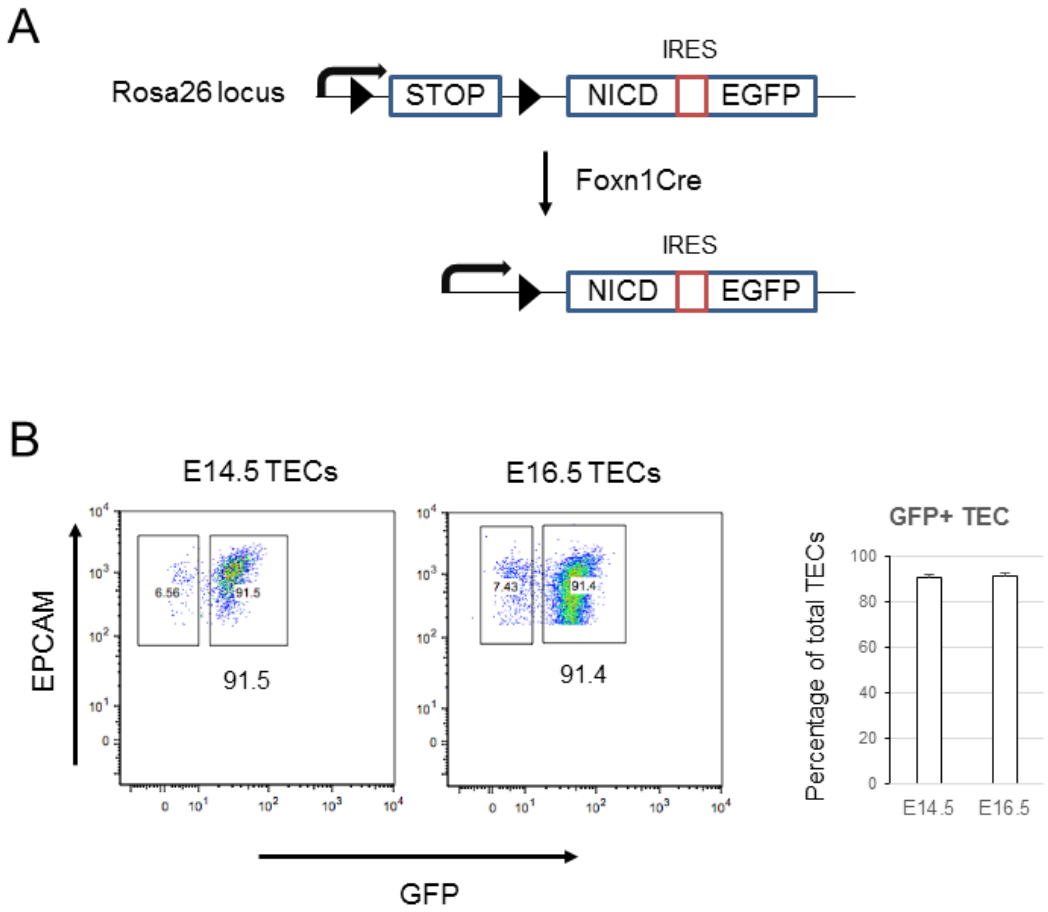

Figure 5.1 Cre-inducible Notch gain-of-function model.

(A) Schematics of the *Rosa26* locus before and after excision of the STOP cassette triggered by Cre. Adapted from Murtaugh et al, 2003.

(B) Percentage of recombined cells in total EPCAM^{+} TECs, indicated by the activation of GFP. N=4 for E14.5 and N=3 for E16.5.

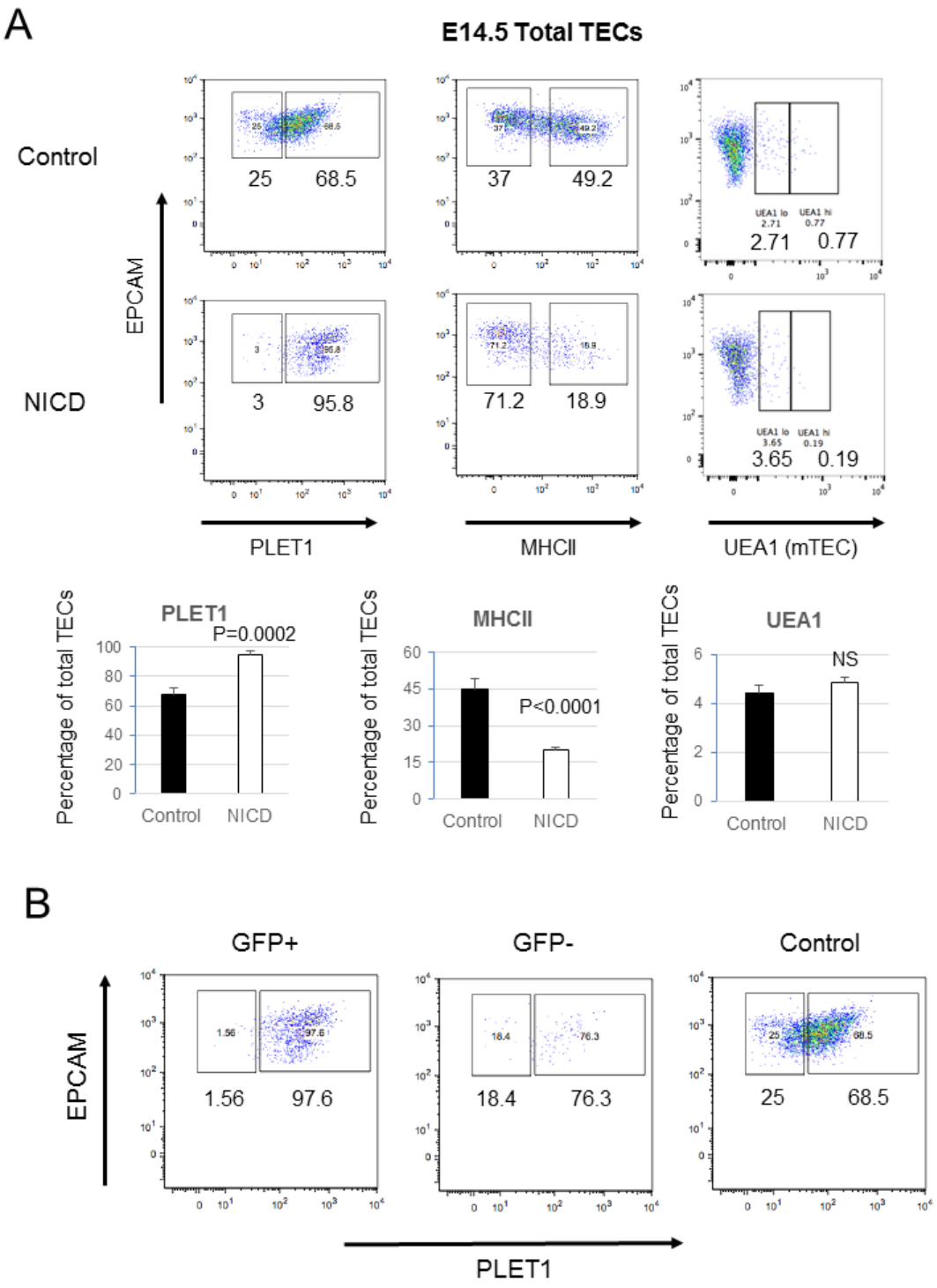

Figure 5.2 Legend on the next page.

Figure 5.2 Inducible NICD results in TEC maturation arrest but no significant conversion to mTECs.

(A) The percentage of cells expressing PLET1, MHCII and UEA1 in total $EPCAM^{+}$ TECs. N=3 for control and N=4 for NICD. $UEA1^{+}$ population was further divided into $UEA1^{lo}$ and $UEA1^{hi}$ subsets in the plots. Total $UEA1^{+}$ was used for statistical analysis.

(B) PLET1 expression mosaicism in the GFP^{+} and GFP^{-} populations of E14.5 NICD TECs.

Gating strategy is shown in Appendix: ‘Gating strategy (NICD)’.

5.3 E16.5 NICD phenotype

As E14.5 TECs undergo further proliferation and differentiation, it was of interest to analyze control and $Foxn1^{Cre}$; NICD thymi at a later stage. E16.5 fetal tissue was first studied with IHC for the expression of various TEC markers (introduced in Table 1.3 in Chapter 1).

Early TEC progenitors are mostly $K5^+$ $K8^+$, and as differentiation proceeds K5 is confined to the medullary region and the CMJ (Klug et al., 2002; Klug et al., 1998). The demarcation between $K5^+$ and $K5^-$ areas was lost in $Foxn1^{Cre}$; NICD thymi and $K5^+$ $K8^+$ co-expression was detected throughout the thymic section (Fig 5.3A). The disruption of the cortico-medullary architecture was also illustrated by the expression pattern of another mTEC marker K14. Instead of the distinctive medulla ($K14^+$ $CD205^-$) and cortex ($K14^-$ $CD205^+$) seen in the control thymi, constitutive NICD led to the extension of K14 expression into the $CD205^+$ presumptive cortical domain (Fig 5.3B). Interestingly, unlike the altered pattern of medulla-associated keratins, the border between $UEA1^+$ and $UEA1^-$ regions in $Foxn1^{Cre}$; NICD thymi corresponded in precisely converse fashion with CD205. Despite the aberrant expression of K5 and K14, AIRE protein expression within the $UEA1^+$ regions was at comparable levels in $Foxn1^{Cre}$; NICD (32.5% of $UEA1^+$ cells) and control tissue (32.9% of $UEA1^+$ cells) (Fig 5.3C), suggesting that mTEC precursors specified under high Notch activity are competent to respond to the activators upstream of AIRE. The expression of PLET1 is also broader in $Foxn1^{Cre}$; NICD thymi (0.225 per thousand μm^2 in control; 0.859 per thousand μm^2 in NICD) (Fig 5.3C).

Similar to the IHC data, flow cytometry revealed that control TECs could be separated into distinct $UEA1^+$ $CD205^-$ mTECs and $UEA1^-$ $CD205^+$ cTECs. However, a substantial proportion of TECs expressed intermediate levels of both markers in the Notch gain-of-function model (Fig 5.4 Left). Notwithstanding the poor separation, the percentage of $UEA1^+$ $CD205^-$ TECs in $Foxn1^{Cre}$; NICD thymi was 35.7 ± 7.6%, a 5-fold increase from 6.6 ± 1.1% in controls, and overall the epithelium expressed higher levels of PLET1 (NICD: 76.3 ± 10.3%; controls: 22.7 ± 5.8%; Fig 5.4 Middle), as was the case for E14.5 samples. Taken together with the E14.5 data, these data suggest that although constitutive Notch activity does not convert all TEC

progenitors into mTECs, the delayed differentiation evident at E14.5 may contribute to a latent increase in the propensity for mTEC differentiation and/or proliferation.

Examined separately, both UEA1^{+} CD205^{-} and UEA1^{-} CD205^{+} populations in Foxn1^{Cre}; NICD embryos exhibited lower MHCII and higher PLET1 expression than those in the age-matched wildtype controls (Fig 5.5), indicative of more primitive differentiation states. However, given that the proportional difference in MHCII expression in mTECs was fairly small (control: 90.4 ± 3.1% positive; NICD: 76.9 ± 4.8% positive) (Fig 5.5A), and that Foxn1^{Cre}; NICD mTEC expressed AIRE normally (Figure 5.3C), these mTECs were arguably similar in differentiation status to their wildtype counterparts. On the contrary, the proportion of MHCII^{+} TECs among the CD205^{+} subset was reduced almost by half (control: 79.2 ± 5.9%; NICD: 48.2 ± 5.3%), suggesting the block in cTEC maturation imposed by NICD was considerably stronger (Fig 5.5B). Since CD205 is expressed by early bipotent TEPCs and cTECs alike (Baik et al., 2013), this phenotype may again demonstrate that the exit from the primitive progenitor state was suppressed by high levels of Notch signalling.

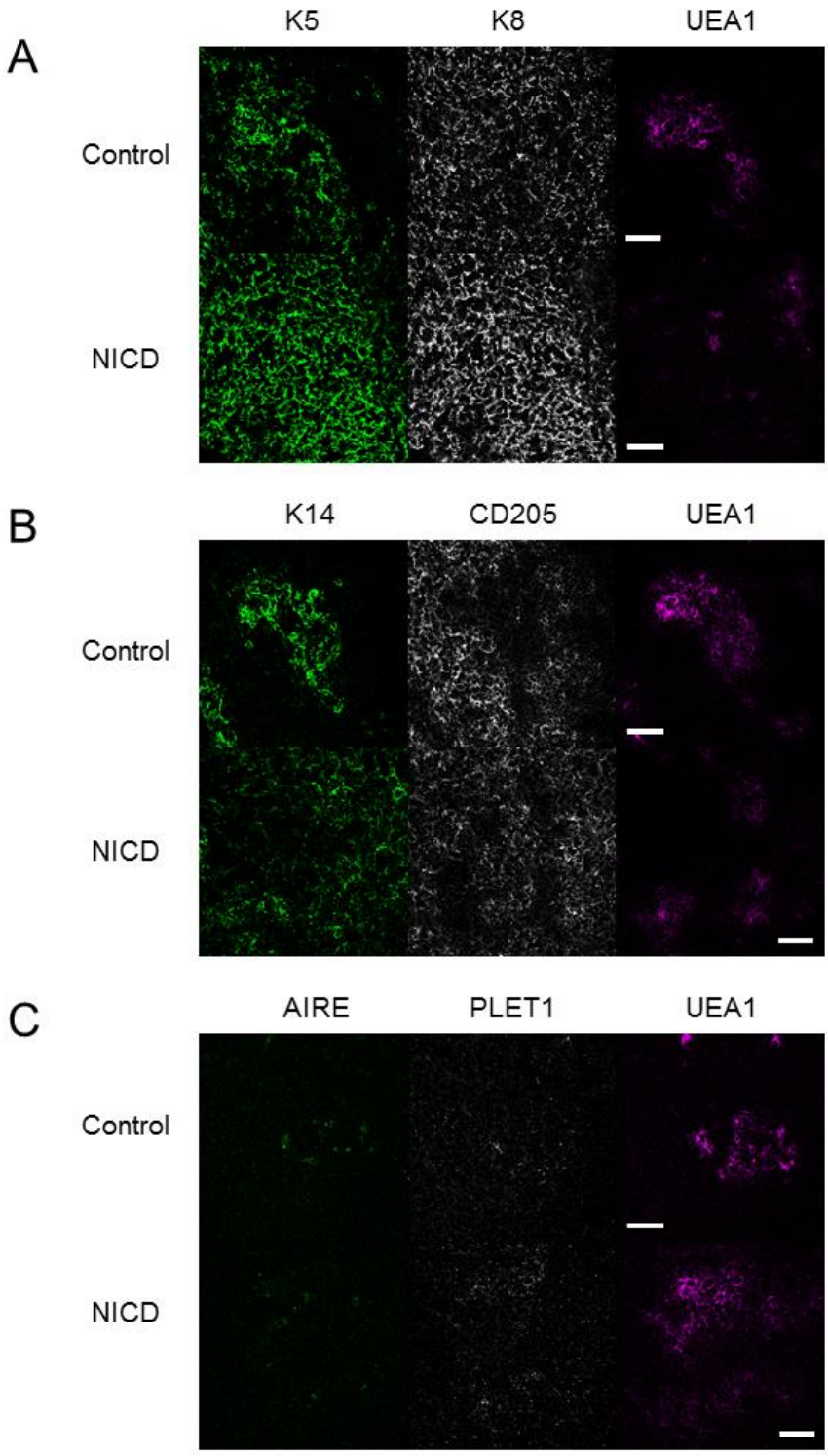

Figure 5.3 IHC profiles of (A) K5, K8 and UEA1 (B) K14, CD205 and UEA1 (C) AIRE, PLET1 and UEA1 expression in E16.5 thymic epithelium. Scale bar=50μm.

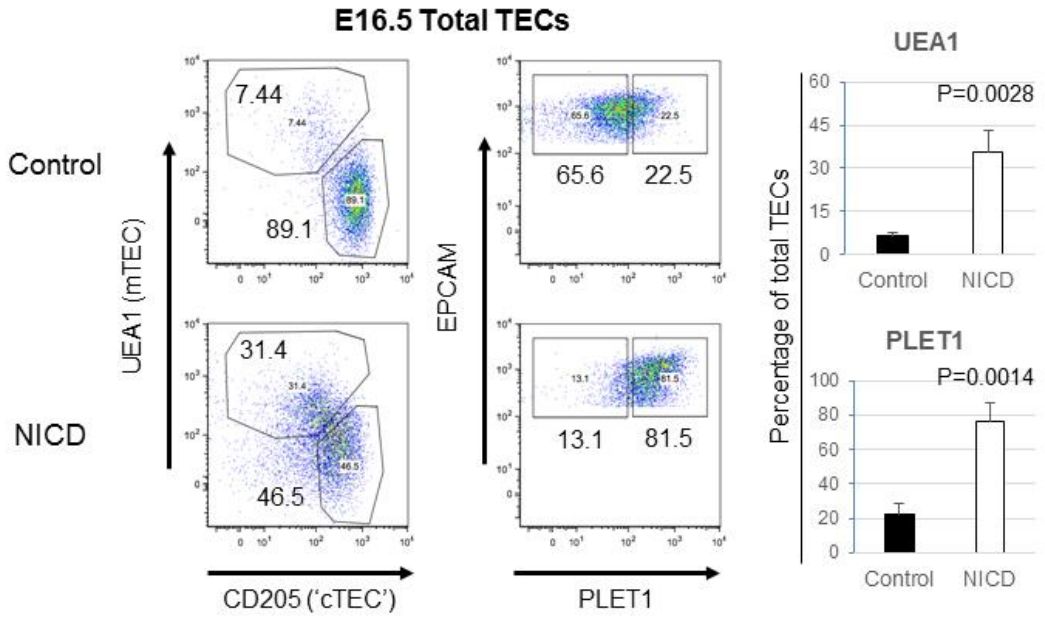

Figure 5.4 E16.5 NICD TECs exhibit poor resolution between mTEC and cTEC populations, high mTEC proportion, and PLET1^{hi} profile.

Left: total TECs were divided based on the expression of mTEC marker UEA1 and cTEC/TEPC marker CD205.

Middle: the PLET1 profile of total E16.5 TECs.

N=3 for both control and NICD.

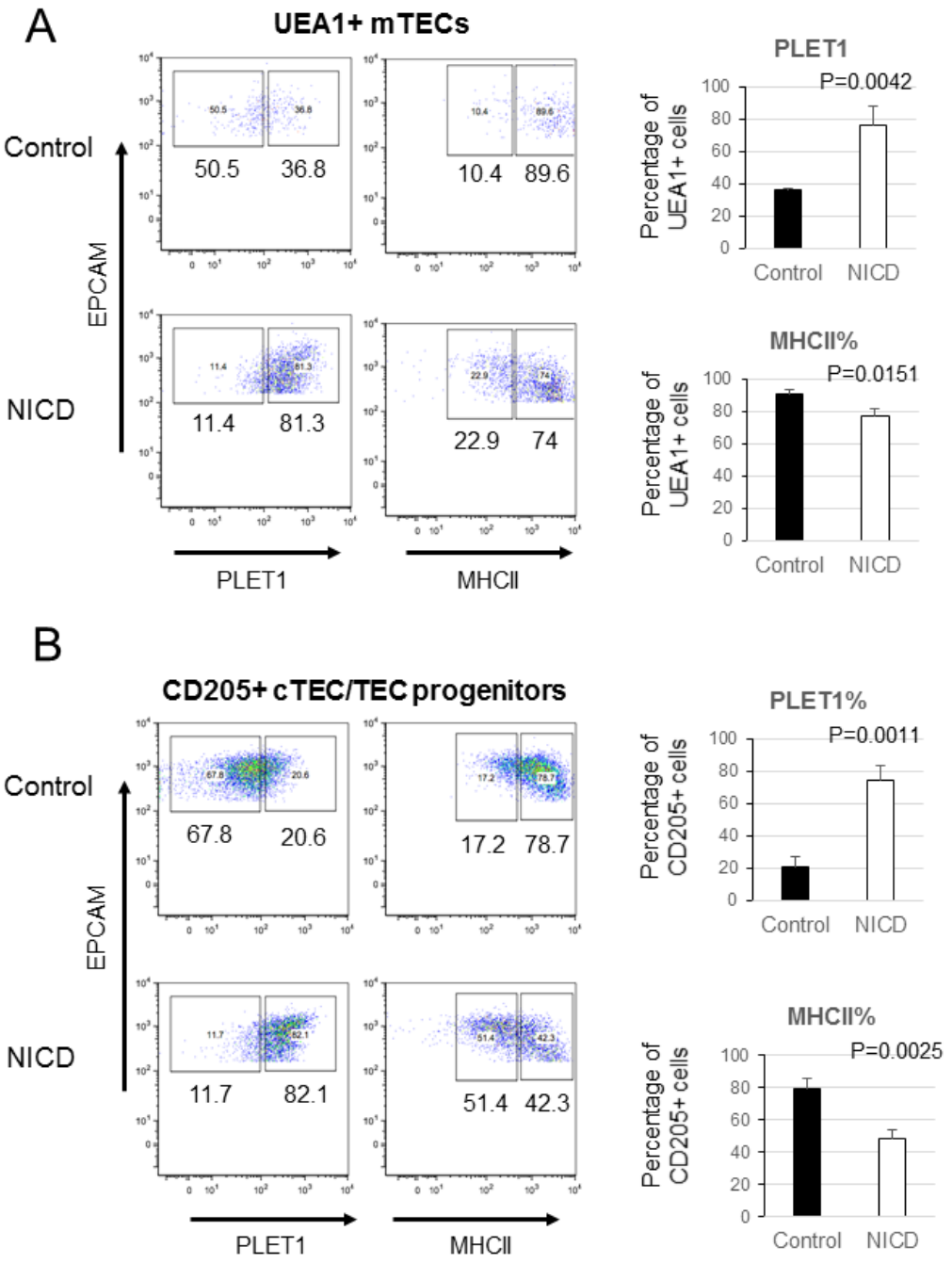

Figure 5.5 Developmental arrest in both sub-lineages of E16.5 NICD TECs.

PLET1 and MHCII expression (A) UEA1^{+} CD205^{-} mTECs and (B) CD205^{+} UEA1^{-} cTEC/TEPCs in E16.5 thymi. The UEA1^{+} and CD205^{+} TECs were gated as shown in Fig 5.4. N=3 for both control and NICD.

5.4 Discussion

The Rbpj cKO and γ-secretase FTOC data supported the hypothesis that Notch signalling acts in a limited time window (E10.5-16.5) to determine the pool size of mTEC progenitors, at least partly via regulating mTEC specification. It was imperative to elucidate whether Notch activity is sufficient to induce mTEC cell fate or is merely necessary for it. The characterization of Notch gain-of-function model provided essential data that allow us to distinguish between the two possible mechanisms.

The two scenarios are depicted in Figure 5.6. In hypothesis A, which I term the 'mTEC commitment model', Notch directly drives the cell fate decision of bipotent TEPCs into the mTEC lineage. In the absence of Notch, mTEC commitment does not occur whereas the cTEC lineage is unaffected. For this model to be correct, we would predict that higher Notch activity will favour mTEC fate, and the constitutive expression of NICD will convert a higher percentage of TECs into the mTEC lineage. Since this model only concerns cell lineage, we would not expect to see alterations in the subsequent maturation of mTECs and cTECs.

On the other hand, hypothesis B (mTEC competence model) posits that Notch regulates TEC differentiation by maintaining the bipotency of TEPCs. This scenario takes into account the theory that cTEC/mTEC lineage specification is asymmetric, as TEPCs resemble cTECs in terms of function and phenotype while mTEC commitment likely requires an additional stimulus (reviewed in Alves et al., 2014). Consequently, mTECs cannot emerge when TEPC bipotency (mTEC competence) is prematurely extinguished in the Notch loss-of-function condition. If this model is correct, we would predict that constitutive Notch activity would arrest TECs at a TEPC-like state, and maturation is completely blocked.

The results presented here show that the primary effect of the constitutive expression of NICD was the retention of immature TEC markers, although an increased mTEC contribution was observed at a later stage. Importantly, even at the later time point (E16.5), the effect of NICD induction was not simply numerical, as both mTEC and cTEC/TEPC populations displayed a primitive marker expression profile. These observations are more consistent with the mTEC competence model than the mTEC

commitment model, but this simple either/or model fails to explain why some degree of TEC differentiation did occur, and additional factors need to be considered.

It is possible that the latent pro-mTEC effect observed at E16.5 resulted from secondary mechanisms that modulated Notch activity above the extent of NICD induction. This could potentially account for different outcomes being favoured by the graded response to Notch. For instance, if mTEC commitment requires a higher threshold than the maintenance of bipotent TEPCs, such a threshold may be achieved through positive feedback. The alternative theory is that mTEC fate is instructed by a yet unidentified signal, and since the TEPC pool is larger in the presence of NICD due to impaired differentiation to the cTEC lineage, more cells would in turn be competent to be instructed into the mTEC lineage.

The dosage of NICD induction is important in the context of this experiment. Following Cre-mediated recombination, one allele of the *Rosa26* locus drives the expression of NICD. Hence the result is similar to homogeneous Notch activation at physiological levels in all recombined cells. If indeed the gain-of-function phenotype is dosage sensitive, similar to the loss-of-function phenotype (Fig 4.6A), we may expect to observe a more severe differentiation arrest upon the induction of multiple copies of NICD.

Of interest, manipulating *Foxn1* expression, either by generating hypomorphic alleles (Nowell et al., 2011) or activating the *Foxn1* repressor TBX1 (Reeh et al., 2014), resulted in the primitive TEC phenotype similar to forced NICD expression – high PLET1 and low MHCII. The reason that NICD-expressing TECs did undergo some degree of differentiation may be that FOXN1 remained switched on and countered the effect of excessive Notch. The relationship between Notch and Foxn1 is further examined in the next chapter.

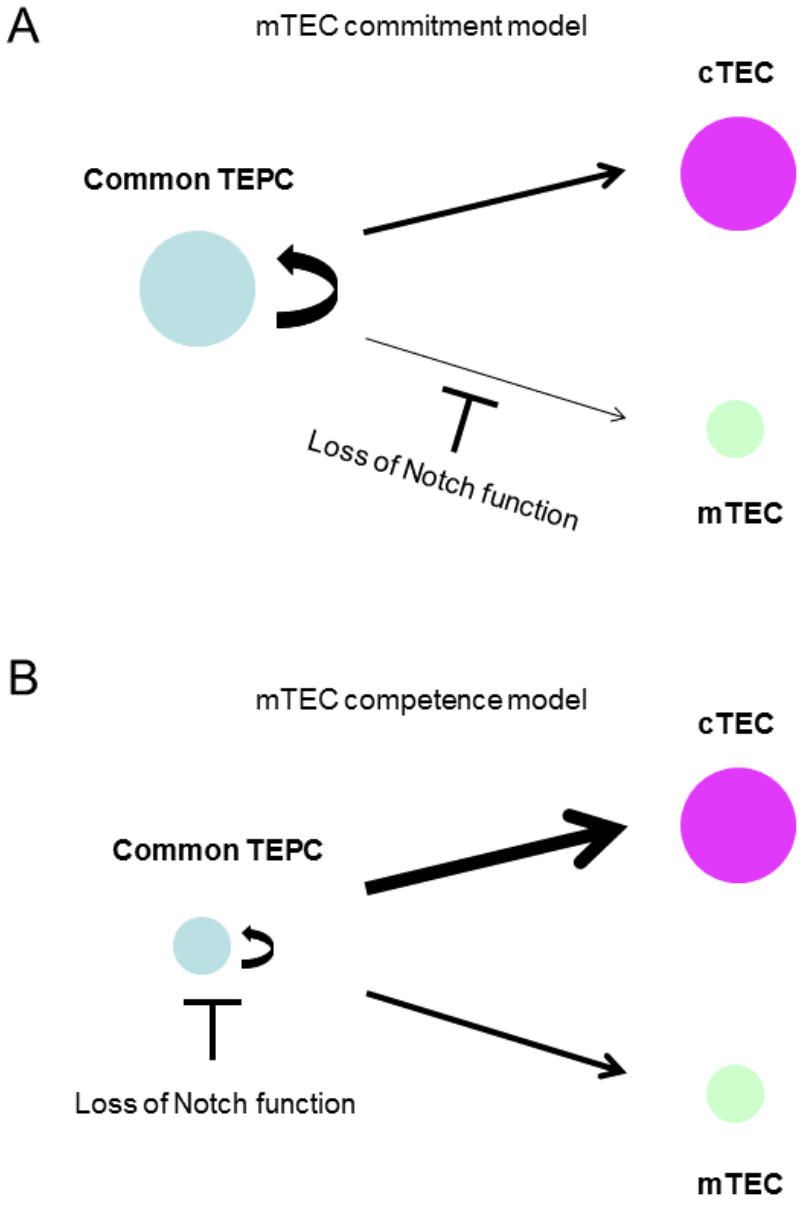

Figure 5.6 Two models for the Notch loss-of-function phenotype.

(A) Notch regulates the commitment of bipotent TEPCs to the mTEC lineage.

(B) Notch regulates the maintenance of bipotent TEPCs (i.e. the competence to become mTECs). In the absence of Notch TEPCs prematurely differentiate into cTECs.

The size of circles indicates cell number. The width of arrows represents the probability of the event to occur.

Chapter VI Mechanistic insights of Notch signalling in TECs

Having investigated the role of Notch in TEC development by studying loss- and gain-of-function mutants, and demonstrated a profound effect on mTEC development, I wish to determine how Notch pathway controls this process. Two candidate targets, RANK signalling (section 1.4.7) and ASCL1, were examined. To identify novel targets, RNA-seq was also carried out to discover transcriptional changes brought about by altering Notch activity.

6.1 Potential synergy between Notch and RANK signalling

Several tumour necrosis factor superfamily (TNFSF) ligands are secreted by thymocytes and serve as agents in thymic crosstalk to enhance the proliferation and maturation of mTECs, partly through activating the canonical and non-canonical NFκB pathways. Of these factors, RANK ligand (RANKL) uniquely induces both the expansion of mTECs and the acquisition of AIRE expression (Bichele et al., 2016; Hikosaka et al., 2008). To study the potential interaction between Notch and NFκB pathways, the FTOC protocol in which E15.5 lobes are cultured at air-liquid interface over medium containing deoxyguanosine (dGuo) and RANKL was adopted. The purpose of dGuo treatment was to deplete T cells and thus to block intrinsic crosstalk between thymocytes and TECs. Simultaneously, the provision of RANKL readily facilitated the increase in mTEC frequency and in this regard compensated the lack of T cells (Fig 6.1A), concordant with published reports.

I first addressed whether inhibiting Notch signalling would abolish the effect of RANK stimulation. To this end, three separate culture conditions were established. All three conditions contained dGuo, the first dGuo alone, the second supplemented with RANKL, and the third with both RANKL and DAPT to impose Notch signalling inhibition. After three days, low DAPT concentration had no impact on RANK stimulation, however at 50μM an effect was observed. The co-treatment of RANKL and DAPT elicited increased mTEC frequency from baseline dGuo levels, but the rise was attenuated compared to RANKL treatment alone (Fig 6.1).

Since DAPT toxicity is minor at the concentration used here (Fig 4.5A), the apparent synergy between Notch and RANK in driving mTEC development may have arisen via two possible mechanisms. Notch may directly interact with components of the pathway activated by RANKL, and hence DAPT treatment may have reduced the efficiency of RANK signalling. Alternatively, Notch and RANK may regulate separate checkpoints in the mTEC lineage without physical crosstalk. In such a scenario, Notch inhibition does not hamper the efficiency of RANK stimulation, but rather constrains the number of cells capable of responding to RANKL. To distinguish between these two hypotheses, E15.5 thymi from Rbpj cKO and control littermates were interrogated using the same FTOC set-up. Since the genotype of embryos was unknown at the start of culture, half of the embryos were incubated in the dGuo only condition, and half in dGuo with RANKL.

In terms of mTEC frequency, the influence of the two pathways appeared to be additive. Control explants treated with RANKL yielded the highest proportion of mTECs, whereas Rbpj cKO thymi cultured without RANK signalling input contained a barely detectable mTEC population (Fig 6.2A). The absence of either Notch (through *Rbpj* deletion) or RANK signalling (through dGuo treatment and the lack of RANKL) decreased the mTEC frequency to a similar level, and there were significantly more mTECs in the cKO tissue co-treated with RANKL than cKO lobes in dGuo alone (Figure 6.2A, B). Thus, mTECs residing in the Rbpj cKO thymi could respond to RANKL.

Furthermore, in control explants, RANKL also raised the proportion of $MHCII^+$ mTECs (Fig 6.2C), of which $AIRE^+$ mTECs are a subset. Notably, RANK-stimulated mTECs in cKO explants showed a similar percentage of $MHCII^+$ cells to RANK-stimulated controls, and significantly higher than the few mTECs in unstimulated cKO tissue (Figure 6.2C). This finding suggests that the efficiency of RANK treatment was comparable in control and Rbpj cKO explants. In contrast, explants cultured in all four conditions contained similar proportions of $MHCII^+$ cTECs (Figure 6.2D), an expected finding as RANKL does not act on cTECs. Overall, these results, and the 3PP culture experiments in Chapter IV, illustrated that Notch and RANK regulate distinct events in mTEC development. Although the timing of the two checkpoints seems to overlap, placing Notch temporally upstream of RANK, the

functional data do not necessarily require direct genetic or biochemical interactions between those pathways for explanation.

6.2 Notch does not facilitate mTEC development through ASCL1

The bHLH transcription factor ASCL1 is preferentially expressed in adult mTECs over cTECs (Goldfarb et al., 2016). In development, the appearance of *Ascl1* mRNA expression was found to correlate with the emergence of mTECs in the fetal thymus (Fig 6.3A). Moreover, its expression in E14.5 Rbpj cKO TECs was reduced by 3-fold in both $PLET1^{+}$ and $PLET1^{-}$ populations compared to control (Fig 6.3B). These results led me to speculate that *Ascl1* may be a factor downstream of Notch in TEC differentiation. Alternatively, it may simply be a marker of early mTECs.

To address this issue, mice heterozygous for an *Ascl1* null allele were crossed to generate homozygous $Ascl1^{-/-}$ null mutants (Guillemot et al., 1993). Thymi were dissected from E17.5 fetuses, cryo-sectioned and analyzed with IHC. No differences were detected with regard to the expression of mTEC markers K14, CLDN3 and UEA1, or cTEC marker CD205 between wildtype and *Ascl1* null thymi (Figure 6.3C). Therefore, the significance of ASCL1 appears not to be in the establishment of the mTEC lineage. The reduced *Ascl1* expression in Rbpj cKO was likely due to the fact that fewer mTECs were produced under low Notch activity.

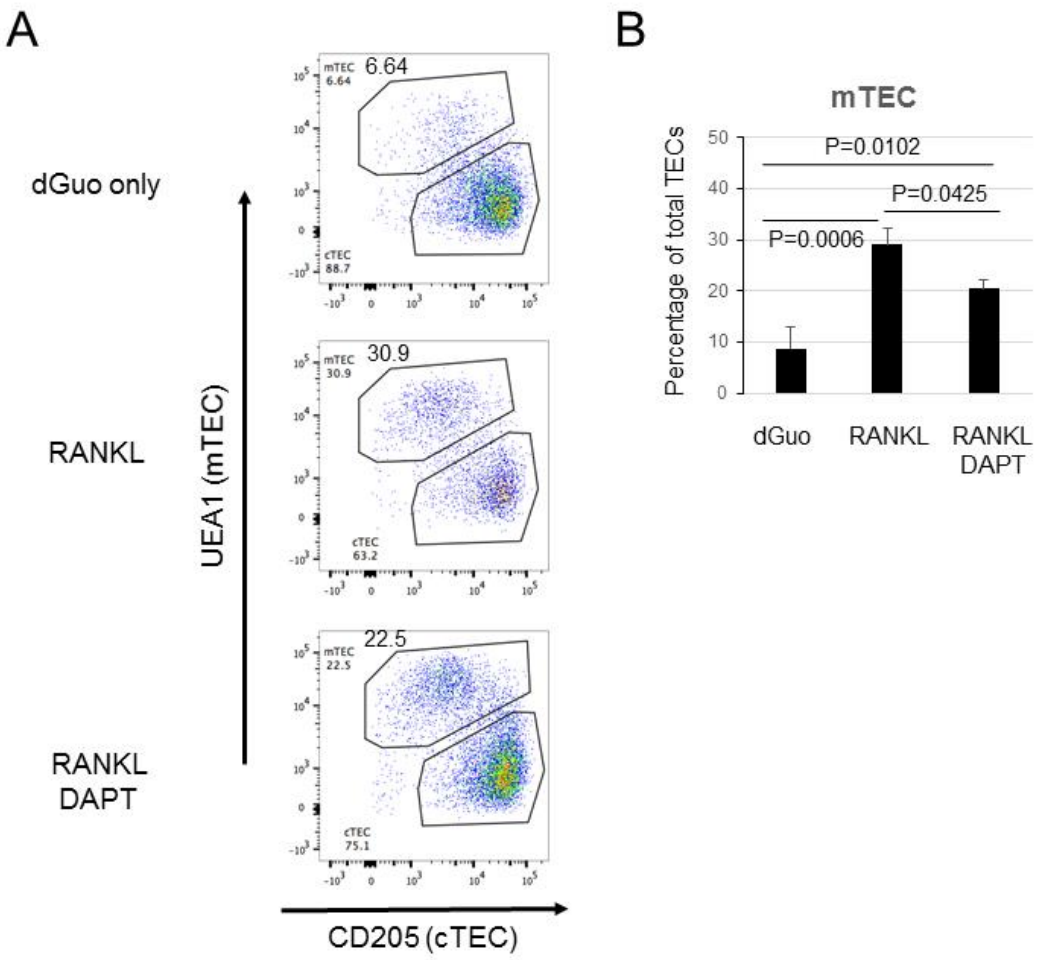

Figure 6.1 Notch inhibition by DAPT attenuated mTEC expansion elicited by RANK ligand treatment.

Wildtype E15.5 thymic lobes were dissected and cultured for three days.

(A) The proportions of UEA1^{+} mTECs and CD205^{+} cTECs in total TECs after culture.

(B) Quantitation of the mTEC frequencies after culture. N=3.

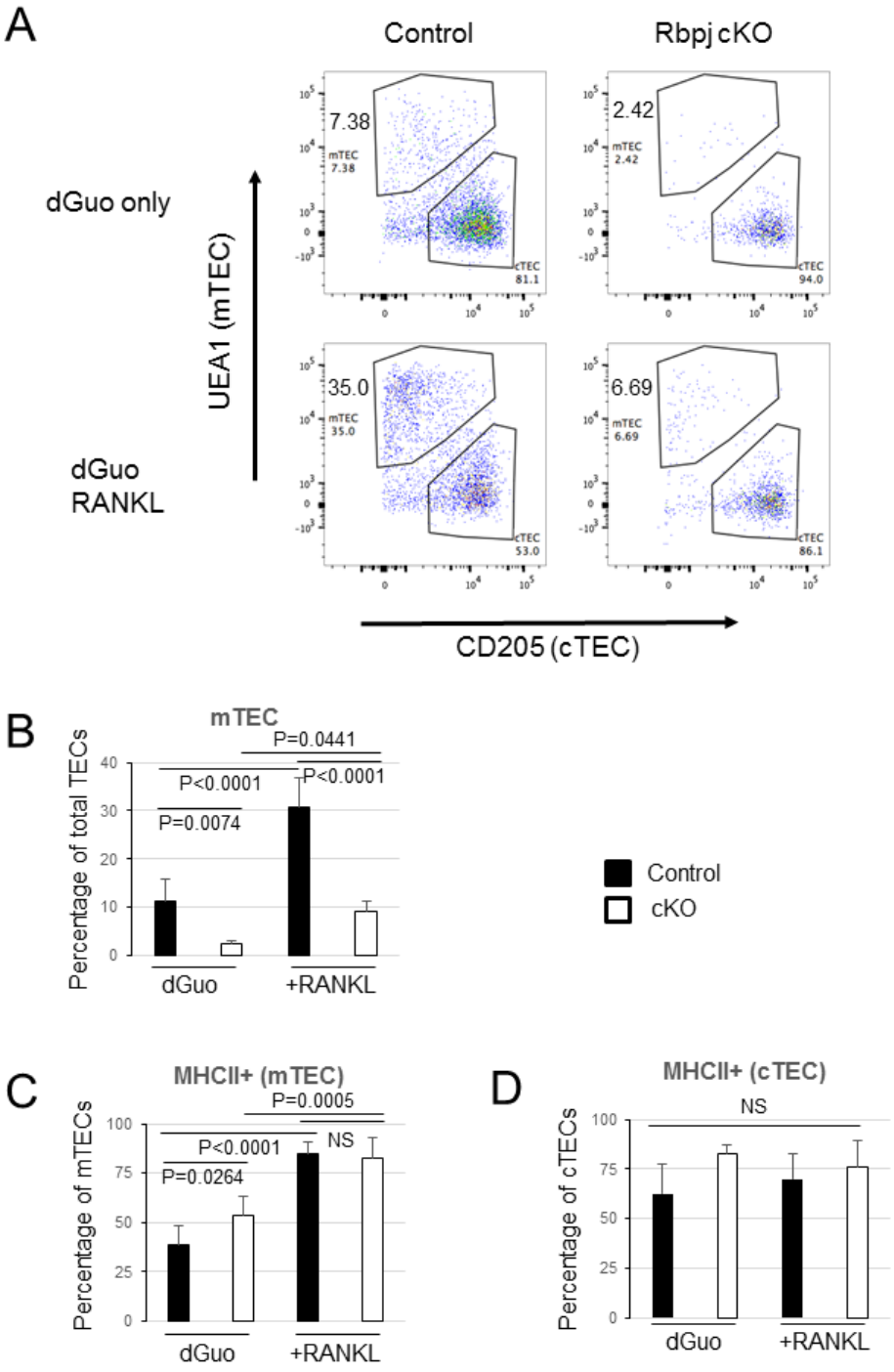

Figure 6.2 Legend on the next page.

Figure 6.2 The effect of RANK ligand treatment on E15.5 control and Rbpj cKO thymi. Thymi lobes from Rbpj cKO and control littermates were cultured for three days in individual 24-well plate wells.

(A) The proportions of $UEA1^+$ mTECs and $CD205^+$ cTECs in total TECs after culture. The four samples presented were of the same litter.

(B-D) Quantitation of (B) the mTEC frequencies in total TECs, (C) proportions of $MHCII^+$ cells in mTECs, and (D) proportions of $MHCII^+$ cells in cTECs after culture.

N=6 for dGuo only controls. N=5 for dGuo only cKO thymi. N=5 for RANKL treated controls. N=4 for RANKL treated cKO thymi.

Gating strategy is shown in Appendix: ‘Gating strategy (FTOC)’.

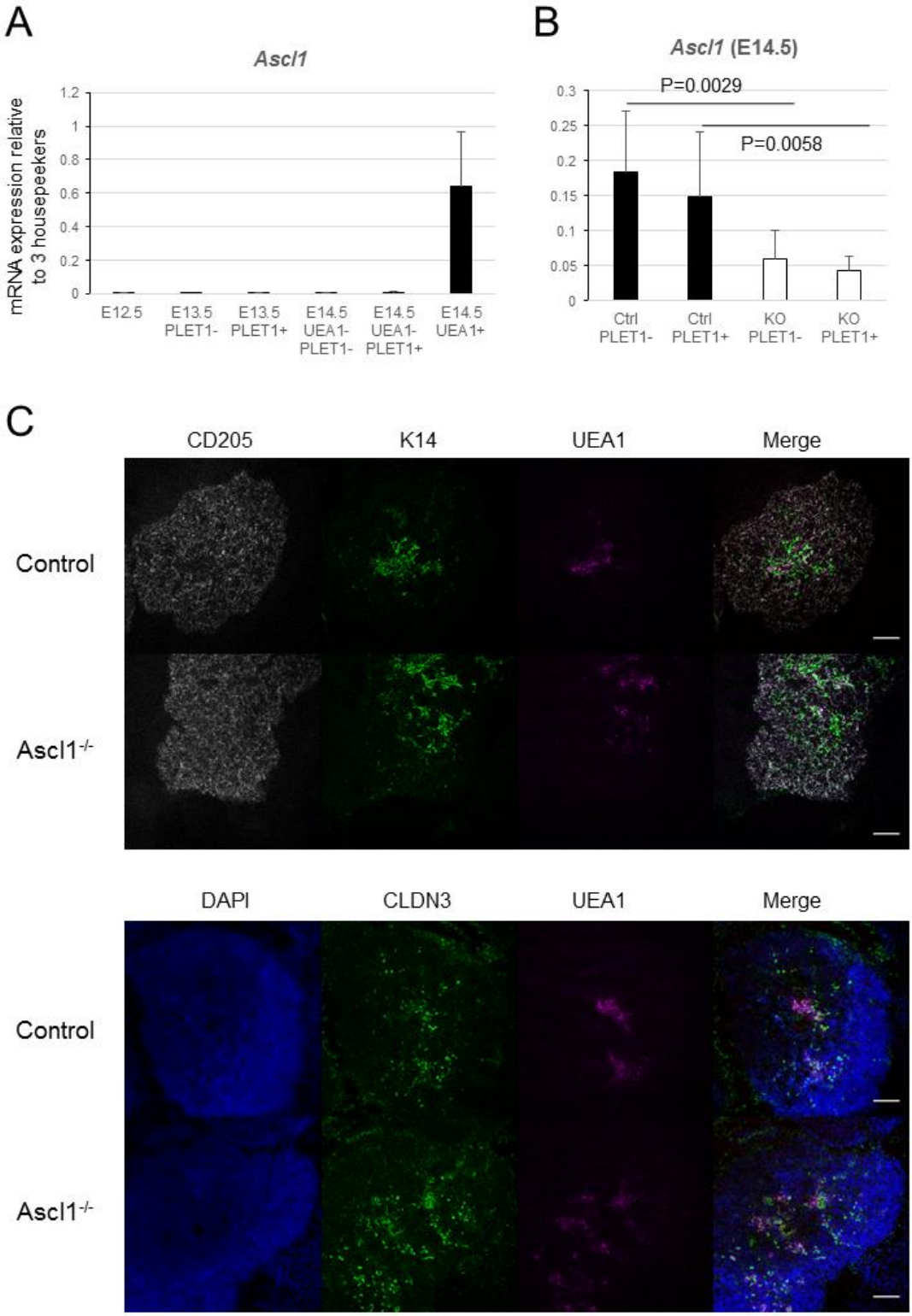

Figure 6.3 Legend on the next page.

Figure 6.3 ASCL1 does not account for the function of Notch in TEC development.

(A) The expression of *Ascl1* mRNA in early TEC populations. N=6 for E12.5 and E13.5 populations, and N=3 for E14.5 populations.

(B) *Ascl1* mRNA expression in the PLET1^{+} and PLET1^{-} E14.5 TEC populations of Rbpj cKO ('KO') and control littermate thymi ('Ctrl'). 200 cells per embryo were isolated and N=7.

(C) IHC analysis of mTEC and cTEC markers on E17.5 Ascl1$^{-/-}$ null mutant and control (homozygous wildtype) thymic sections. Scale bar = 100μm.

6.3 Positive autoregulation of the Notch pathway

To shed light on how Notch signalling controls TEC cell fate, I studied the transcriptomes of Rbpj cKO and Foxn1^{Cre}; NICD fetal TECs. As mTEC number is influenced by Notch, I reasoned that epithelial cells in early primordia should be subdivided according to PLET1 expression, which is less sensitive to *Rbpj* deletion, rather than mTEC and cTEC markers. The proportion of mTECs expressing PLET1 is higher than cTEC/TEPCs throughout fetal thymic organogenesis (Sheridan, unpublished), therefore in control samples a slight mTEC enrichment can be expected in the PLET1$^+$ subset.

To validate this approach, RT-qPCR was performed on FACS-sorted E14.5 control and Rbpj cKO TECs in order to assess the expression of Notch pathway genes and canonical targets. This set of expression patterns (Fig. 6.4) provided several insights. Firstly, as expected, the levels of conventional Notch targets *Hes1* and *Heyl* were reduced in cKO PLET1$^+$ and PLET1$^-$ TECs (Fig 6.4E, F). Secondly, as opposed to *Hes1* and *Heyl* whose expression was similar in the PLET1$^+$ and PLET1$^-$ populations, the levels of *Notch1*, *Notch3* and *Jag1* in controls were higher in the PLET1$^+$ compartment (Fig 6.4A, C, D). Considering their enrichment in E14.5 mTECs (Chapter III), these results reinforced the notion that PLET1$^+$ population contains more mTECs. Next, the expression of *Notch1*, *Notch2*, *Notch3* and *Jag1* in both populations was significantly lower in cKO thymi compared to controls (Fig 6.4A-D), suggesting that one outcome of Notch activation seems to be the upregulation of Notch receptors and JAG1 ligand. One can envisage that this positive feedback loop may lead to sharpened responsiveness to further Notch signalling, and in the case of JAG1, lateral propagation to extend the domain of cells experiencing Notch. Finally, the expression of *Foxn1* was unchanged in Rbpj cKOs (Fig 6.4G), ruling out the possibility that Notch is a major regulator of *Foxn1* at this stage.

To conduct a more unbiased transcriptomic analysis, I then collected TECs for RNA sequencing. To this end, 100 cells were collected for each of the following populations: E12.5 PLET1$^+$ total TECs from control and cKO rudiments; E14.5 PLET1$^+$ and PLET1$^-$ TECs from control and cKO thymi; E14.5 constitutive NICD PLET1$^+$ TECs. NICD TECs at E14.5 were nearly completely PLET1$^+$ (Figure 5.2A),

therefore only this population was collected. Bioinformatics analysis was performed by Anastasia Kousa, and the results were interpreted by Anastasia Kousa and me.

Principal component analysis (PCA) using the 500 most differentially expressed genes in all datasets revealed that the transcriptomes broadly separated into three groups on the two most influential components (Fig. 6.5A). The E14.5 Foxn1^{Cre}; NICD gain-of-function samples formed a tightly clustered group (Group 1). Although of the same biological age, E14.5 control and Rbpj cKO samples clustered together (Group 2) at some distance from the NICD TECs. Moreover, a third group (Group 3) was found to consist of E12.5 control and cKO samples. Varying the number of genes used to plot PCA had little effect on the overall cluster composition. If we consider the linear route on the PCA plot between Group 3 and Group 2 to be developmental progression, it may be argued that persistent NICD delayed TEC maturation. However, Group 1 also deviated substantially from this linear axis, indicating a cell state not present in normal development, or the expansion of a rare cell population in the gain-of-function samples.

The transcriptomes of E12.5 Rbpj cKO and E12.5 control TECs were highly similar, possibly due to the insufficient decay of residual wildtype RBPJ proteins. In comparison, when all E14.5 control and cKO TECs (Group 2 of Fig. 6.5A) were plotted separately, the control PLET1^{+} and PLET1^{-} populations, representing mTEC and cTEC enriched subsets respectively, were distinguishable on PC2, whereas such distinction was much smaller between the corresponding cKO subsets (Fig 6.5B). Overall, these data highlight that the deletion of *Rbpj* begins to exert transcriptional changes between E12.5 and E14.5.

To identify genes and pathways regulated by Notch, a Gene Set Enrichment Analysis (GSEA) was carried out comparing the transcriptomes of E14.5 PLET1^{+} NICD against E14.5 PLET1^{+} controls. 35 pathways were found to be statistically upregulated, and 2 downregulated, in NICD samples. Only three of these substantially altered pathways, all of which were upregulated, concern cell signalling (Table 6.1).

Consistent with the positive autoregulation shown by RT-qPCR comparing loss-of-function to control TECs (Fig 6.4), a strong Notch pathway signature was found in

the NICD transcriptome under 'Notch1ICD regulates transcription' (Table 6.2A). Beside the conventional bHLH targets and *Notch1*, two *Mastermind-like* genes, *Maml2* and *Maml3*, were also found to be elevated. MAML factors form the transcriptional complex with RBPJ and NICD to promote Notch-dependent gene expression (Petcherski and Kimble, 2000; Wu et al., 2002). By producing more MAML2 and MAML3, it is plausible that TECs may become more efficient in transducing the signal and more readily responsive to Notch activation.

Notch aside, two more gene sets of interest were uncovered by the analysis. Despite including only four significantly upregulated genes, the list 'Inflammatory response pathway' contains some of the most highly induced genes in the entire dataset (Table 6.2B). The top three genes identified encode collagen molecules *Col3a1*, *Col1a1* and *Col1a2*. The role of collagen on TEC differentiation is not clear but the remodelling of extracellular matrix (ECM) may be a mechanism through which Notch maintains the potency of TEPC. As an example, muscle satellite cell quiescence requires Notch signalling and the integrity of the basal lamina (Mourikis and Tajbakhsh, 2014). Many ECM proteins (integrins, collagens and other adhesion molecules) are Notch targets in satellite cells (Brohl et al., 2012), hinting at a role of the pathway to aid the construction of stem cell niche.

We have also found increased expression of genes ascribed to EGFR signalling under 'Signalling by constitutively active EGFR' (Table 6.2C). Apart from *Egfr* itself, several genes coding for cytoplasmic components of the pathway such as *Kras*, *Pik3ca* and *Pik3r1* were identified. The EGFR-STAT3 axis has been shown to regulate mTEC cellularity (Satoh et al., 2016), raising the possibility that Notch creates a microenvironment primed for mTEC expansion.

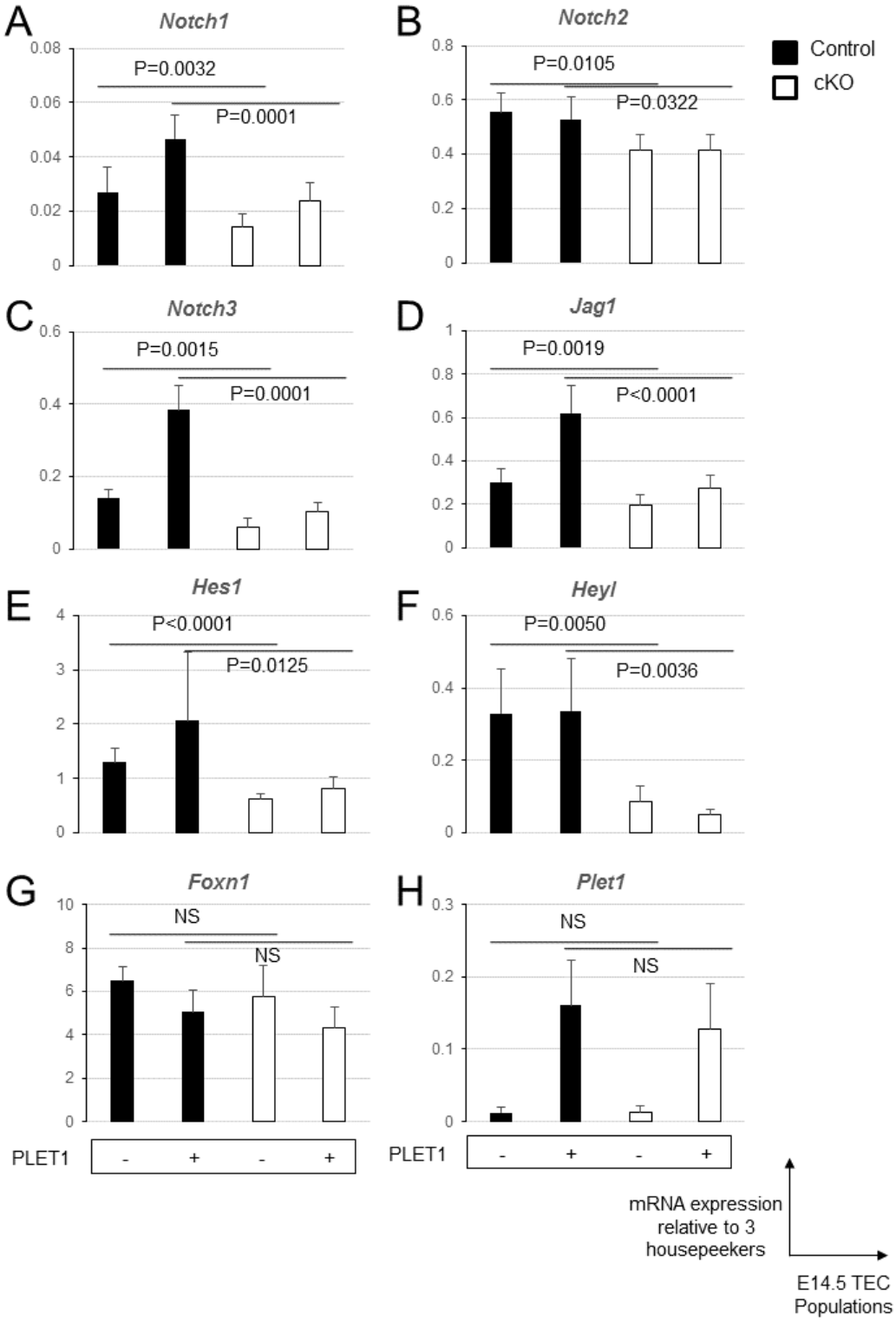

Figure 6.4 Legend on the next page.

Figure 6.4 Candidate genes downregulated in Rbpj cKO TECs.

200 PLET1^{+} and PLET1^{-} TECs per E14.5 Rbpj cKO and control littermate thymi were sorted, and their mRNA examined by RT-qPCR. Two tailed T test was conducted for both populations between controls and cKOs.

N=7 for *Notch1, Jag1, Hes1*. N=6 for *Foxn1, Plet1*. N=4 for *Notch2, Notch3, HeyL*.

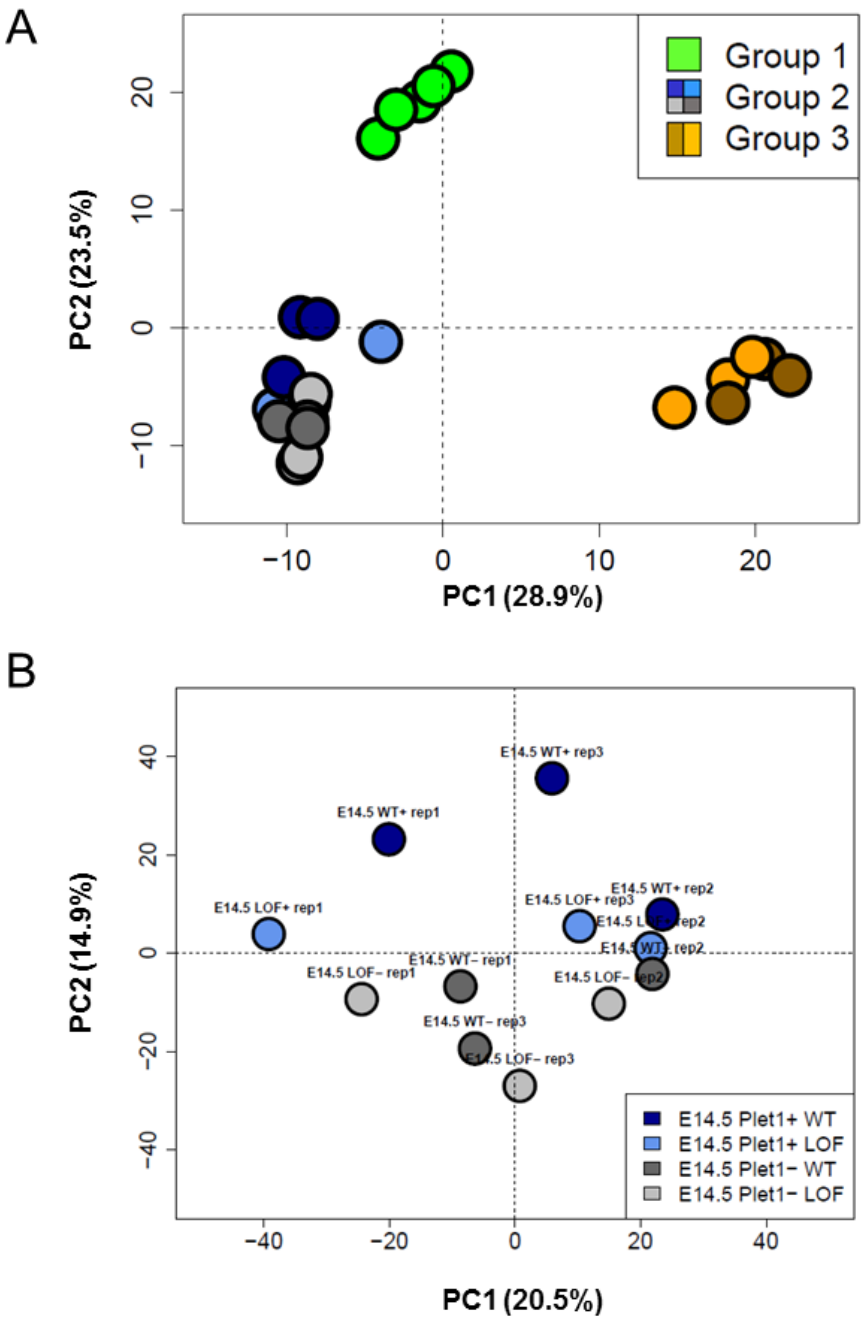

Figure 6.5 Legend on the next page.

Figure 6.5 Principal component analysis (PCA) of RNA-seq datasets, by Anastasia Kousa.

(A) PCA with top 500 differentially expressed genes in all samples.

Group 1: E14.5 NICD (gain-of-function, 'GOF').

Group 2: E14.5 control ('WT') and Rbpj cKO (loss-of-function, 'LOF'). Colour code labels: Top left – control, PLET1^{+}; Top right – cKO, PLET1^{+}; Bottom left – control, PLET1^{-}; Bottom right – cKO, PLET1^{-}.

Group 3: E12.5 control and Rbpj cKO. Colour code labels: Left – control; Right – cKO.

(B) PCA of E14.5 control ('WT') and Rbpj cKO ('LOF') only. Plotted with top 2000 most variable genes in the populations indicated.

	Size	ES	NES	Nom. p-value	FDR q-value	FWER p-value
Inflammatory response pathway	**16**	**0.54**	**1.71**	**0.017**	**0.053**	**0.384**
NOTCH1 ICD regulates transcription	**37**	**0.44**	**1.66**	**0**	**0.067**	**0.472**
Signalling by constitutively active EGFR	**18**	**0.43**	**1.39**	**0.054**	**0.232**	**0.959**

Table 6.1 Statistically upregulated signalling pathways in transgenic NICD E14.5 PLET1$^+$ TECs compared to control E14.5 PLET1$^+$ TECs. The genes in these lists with significantly enhanced expression are shown in Table 6.2. Gene Set Enrichment Analysis (GSEA) was performed by Anastasia Kousa.

A

'Notch1ICD regulates transcription'

Gene name	Fold change (log2)
Heyl	2.43
Hes1	2.039
Hey2	1.832
Maml3	1.349
Gm10093	1.347
Notch1	1.338
Ubb	0.943
Tle1	0.94
Hdac10	0.887
Ncor1	0.791
Maml2	0.788
Hey1	0.728
Gm8430	0.673
Rbx1	0.668
Cdk8	0.667

B

'Inflammatory response pathway'

Gene name	Fold change (log2)
Col3a1	9.29
Col1a1	5.338
Col1a2	2.616
Il4ra	2.572

C

'Signalling by constitutively active EGFR'

Gene name	Fold change (log2)
Egfr	1.312
Hsp90aa1	1.155
Pik3ca	1.123
Ubb	0.943
Gm8430	0.673
Cbl	0.561
Uba52	0.414
Kras	0.319
Gab1	0.307
Ubc	0.288
Pik3r1	0.236

Table 6.2 Legend on the next page.

Table 6.2 Significantly upregulated genes that contributed to gene sets in Table 6.1, and fold enrichment in E14.5 NICD PLET1^{+} TECs against E14.5 control PLET1^{+} TECs. Note not all genes in the Table 6.1 gene sets (column 'Size') were statistically significant. Statistical tests were conducted by Anastasia Kousa.

6.4 Interplay between Notch and FOXN1

To make sense of how Notch specifically regulates TEC lineage decision and potency, a panel of markers was selected to reflect the maturation of TECs as well as the differentiation towards either mTEC or cTEC sub-lineage among the RNA-seq samples (Fig 6.6). Unsupervised clustering split the samples into three groups in agreement with PCA in Fig 6.5A. Interestingly, there was also a sub-cluster in the E14.5 control and Rbpj cKO group that included only the PLET1^{+} controls (W5+, W7+ and W17+), indicating a similar pattern to that revealed in Fig 6.5B. As for gene clusters, three broad groups were separated, of which the second one could be further divided based on the overall pattern (purple and cyan).

Here I attempt to summarize the patterns of the four gene clusters (in top-down order in Fig 6.6). The green cluster genes were expressed at variable levels at E12.5, and at E14.5 were more highly expressed in PLET1^{+} than PLET1^{-} populations. In Foxn1^{Cre}; NICD thymi where only PLET1^{+} population was present, these genes were uniformly highly expressed. This cluster includes mTEC associated *Krt5* (encodes cytokeratin 5), *Cldn3*, *Cldn4* and generic TEC marker *Epcam*. The pattern of *Plet1* expression verified the purity of samples.

The purple and cyan genes, collectively forming the second cluster, were uniformly upregulated from E12.5 to E14.5 in both control and Rbpj cKO TECs. The purple subgroup genes, to which *Foxn1* and its targets *Dll4, CtsL, Psmb11* (encodes β5t) belong (Zuklys et al., 2016), failed to be upregulated in the Foxn1^{Cre}; NICD TECs. On the contrary, genes in the cyan subgroup were upregulated relatively normally despite constitutive Notch activity. Two classes of genes were found in the cyan cohort, either associated with mTEC development (*Ltbr, Krt14, Tnfrsf11a* [encodes RANK] and *Cd40*), or involved in antigen presentation (*Ciita, H2-Aa, H2-Ab1* and *H2-Eb1*). Notably, the relatively normal expression of *Ltbr*, *Rank* and *Cd40* in loss- and gain-of-function datasets illustrates the weak dependence of NFκB signalling on Notch, in concordance with functional characterization (section 6.1).

Finally, the yellow cluster genes were expressed at variable levels in E12.5 and E14.5 control and loss-of-function samples, but were uniformly repressed in the presence of NICD. Genes in this cluster do not seem to share a clear category. *Pax9*

is important for TEC development (Hetzer-Egger et al., 2002). *Kitl* is a Foxn1 target and together with *Il-7* instructs early thymocyte development in the cortex (Godfrey et al., 1992; Morrissey et al., 1994). *Fgfr2* has been implicated in the growth of early thymic epithelium (Revest et al., 2001). What is more, *Ly75* (encodes CD205) is expressed both in TEPCs and cTECs.

Several conclusions can be drawn from this panel. First, while the mTEC program (*Cldn3, Cldn4, Krt5, Krt14, Ltbr, Rank* and *Cd40*) appears compatible with enforced Notch signalling, the expression of cTEC markers (*Krt8, Ctsl, Psmb11* and *Ly75*) was severely reduced. Therefore, the effect of ubiquitous Notch activity was primarily manifested in the TEPC/cTEC lineage. Secondly, many of the cTEC-related genes significantly lowered in the NICD datasets were FOXN1 targets, suggesting that Notch-induced blockade of cTEC progression may be mediated through repressing the expression and/or activity of FOXN1. Thirdly, the yellow cluster genes were specifically repressed in the NICD samples. This may have contributed to a transcriptomic state that is not normally present during thymic organogenesis, reflected in the deviation from the temporal advance in Fig 6.5A.

We further explored the relationship between Notch and FOXN1 with the Rosa26$^{CAG\text{-}FL\text{-}STOP\text{-}FL\text{-}Foxn1\text{-}IRES\text{-}GFP}$ 'iFoxn1' transgenic mice, an inducible Foxn1 overexpression model controlled by Cre (Bredenkamp et al., 2014b). Dr. Kathy O'Neill curated these results (Fig 6.7).

Mating between male Foxn1^{Cre} and female iFoxn1 mice produced double transgenic progeny that continuously overexpress Foxn1 in TECs, referred to here as TgFoxn1. Very few mTECs were present in E17.5 TgFoxn1 thymi, a strongly similar phenotype to the Rbpj cKO Notch loss-of-function model (Fig 6.7A, B). The overall number of CD205^{+} cTECs were not significantly different littermate controls, but a substantial proportion of cTECs did not express MHCII (Fig 6.7B). Gene expression analysis using RT-qPCR confirmed a threefold increase in *Foxn1* expression and a twofold reduction in the mTEC expression of *Notch1* and *Notch3* (Fig 6.7C). Thus, the phenotypic similarities between Notch loss-of-function and FOXN1 gain-of-function appear to be supported by molecular interactions. A possible mechanism is that FOXN1 represses Notch through its direct target *Fbwx7*. FBXW7 is known to

promote the turnover rate of NICD (Carrieri and Dale, 2016), limiting Notch target gene expression. Future experiments are required to verify this hypothesis.

To sum up, our RNA-seq and *Foxn1* overexpression experiments revealed cross repressive interactions between Notch and FOXN1. Based on the functional characterization of Notch and published literature on FOXN1 (Nowell et al., 2011), it seems plausible that there is a competition between the two factors, with Notch favouring the TEPC state and FOXN1 promoting differentiation. It is notable that in this model mTEC development is highly connected to the maintenance of TEPCs. As remarked in the last chapter, that Notch is instructive in the entry into the mTEC lineage is not the only theory compatible with our results. Alternatively, by safeguarding the bipotency of TEPCs, the pre-requisite for mTEC commitment, Notch may allow the time window for mTEC specification to extend beyond the initial phase of development.

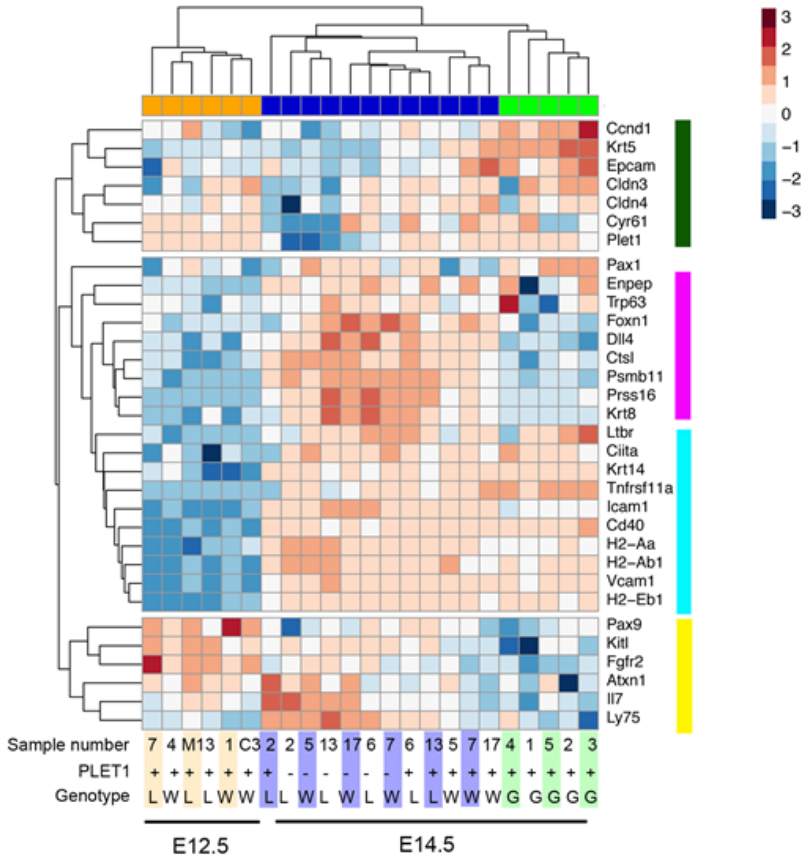

Figure 6.6 Expression of selected lineage markers in all RNA-seq datasets. Heatmap courtesy of Anastasia Kousa.

Clustering of samples is consistent with PCA (Fig 6.5):

Group 1: E14.5 Foxn1^{Cre}; NICD ('G')

Group 2: E14.5 control (W) and Rbpj cKO (L)

Group 3: E12.5 control (W) and Rbpj cKO (L).

Four broad groups (green, purple, cyan and yellow) were produced based on unsupervised clustering of their expression pattern.

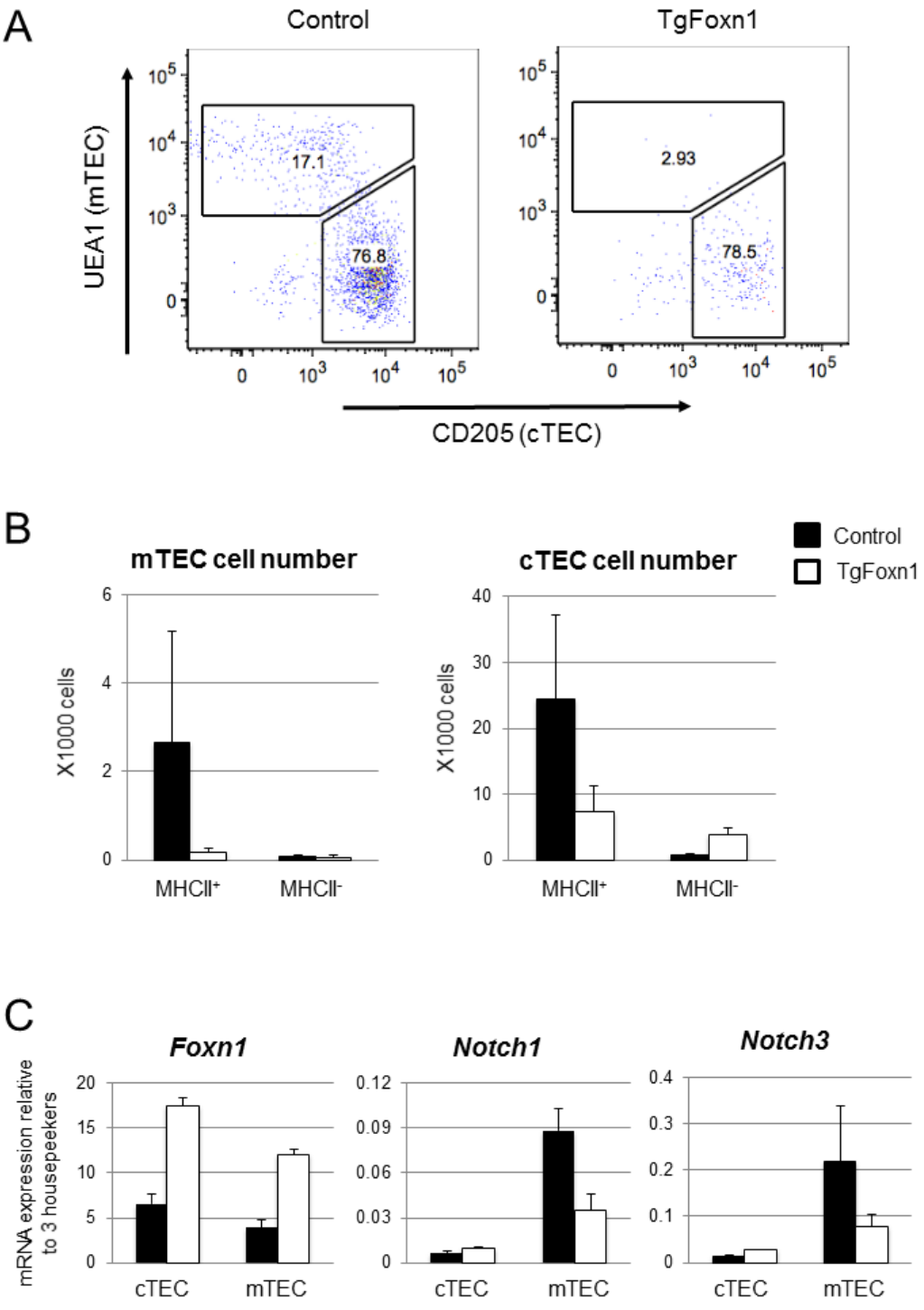

Figure 6.7 Legend on the next page.

Figure 6.7 *Foxn1* overexpression phenotype resembles Rbpj cKO.

(A) Representative plots showing the percentage of $UEA1^{+}$ mTEC and $CD205^{+}$ cTEC populations in E17.5 control and $Foxn1^{Cre}$; iFoxn1 ('TgFoxn1') thymi.

(B) Absolute cell numbers of mTECs and cTECs in E17.5 control and TgFoxn1 thymi, divided by the presence or absence of MHCII marker. Error bars show standard deviation. N=3.

(C) The mRNA expression of *Foxn1*, *Notch1* and *Notch3* in mTECs and cTECs isolated from control and TgFoxn1 thymi. Relative expression values were normalized against housekeepers. N=3.

6.5 Discussion

This chapter addresses the mechanisms through which the Notch pathway may regulate the differentiation of TEPCs.

Since the NFκB pathway is also known to be a potent inducer of mTEC development, I first characterized the relationship between Notch and NFκB using FTOC. Notch inhibition reduced the extent of mTEC expansion resulting from RANK stimulation, indicating that the two pathways are synergistic in generating normal mTEC cellularity. Moreover, RANK remains effective in expanding the mTEC population even in the absence of RBPJ and hence canonical Notch signalling. This suggests that the two pathways are likely to be independent, although we cannot categorically rule out the possibility that these mTECs have escaped *Rbpj* deletion by Cre. Nevertheless, taking into account results in preceding chapters which show that Notch regulates mTEC emergence by acting at the level of TEPCs, and that RANK is only effective in stimulating maturing mTEC precursors (Akiyama et al., 2016; Baik et al., 2016), an argument could be made that temporally, rather than biochemically, Notch is upstream of RANK. One limitation of this culture approach is the simplification of the NFκB pathway down to a single ligand, RANKL, given the involvement of other ligands, for instance lymphotoxin (Boehm et al., 2003). Further experiments are required to elucidate whether the relationship between Notch and RANK also holds for Notch and LTβR.

To unveil targets and mechanisms underlying the Notch phenotype, RNA-seq was conducted to investigate the transcriptomic changes in Notch loss- and gain-of-function models. We detected no difference between E12.5 control and Rbpj cKO transcriptomes, suggesting that the effective Notch loss-of-function is delayed compared to Cre initiation, possibly due to the slow degradation of wildtype RBPJ proteins. To our surprise, the differences between E14.5 control and Rbpj cKO transcriptomes are also modest. This might be partly due to which TEC populations were collected. To minimize the effect of defective mTEC development, I chose to collect the PLET1^{+} and PLET1^{-} subsets as the cellularity of these populations is less affected by Rbpj cKO. This decision may have contributed to the modest differences because only a minority of E14.5 PLET1^{+} and PLET1^{-} TECs are mTECs, thus the

single-cell level changes are diluted by cells whose gene expression is unaffected by Notch. The main difference between E14.5 control and Rbpj cKO expression is the reduction of Notch pathway genes, including *Notch1*, *Notch3*, *Jagged1*, *Hes1* and *HeyL*.

In comparison, analysis of the Notch gain-of-function transcriptomes revealed more profound changes. The induction of NICD raised the expression of Notch pathway components and targets in E14.5 TECs, again reinforcing the idea that the pathway exhibits positive feedback in early fetal TECs. Cells actively transducing Notch signalling may perpetuate the activity through the upregulation of some key targets – the receptor *Notch1* and transcriptional co-activators *Maml2* and *Maml3*. Moreover, we also discovered that some of the most highly upregulated genes in the presence of constitutive NICD are collagen genes *Col3a1*, *Col1a1* and *Col1a2*. Exactly how the extracellular matrix influences the development of TEPCs is unclear, but this finding provides clues for future tissue engineering attempts aiming to devise optimal conditions for controlling TEC differentiation. A third pathway downstream of Notch appears to be the EGFR pathway, through which mature mTECs undergo expansion (Satoh et al., 2016).

In line with phenotypic profiling, our RNA-seq data showed that in the Notch gain-of-function model, the expression of many cTEC enriched genes fails to be upregulated at E14.5, and many of these genes are *Foxn1* and its targets. This finding prompted us to study how Notch influences, and is influenced by, FOXN1, so far considered to be unimportant in TEC lineage decision (Nowell et al., 2011). Constitutively high expression of FOXN1 led to a reduced mTEC population, phenocopying the effect of Notch loss-of-function. Gene expression analysis revealed that FOXN1 induction diminished the expression of Notch receptors, suggesting a direct link between excessive FOXN1 and the suppression of Notch activity.

As alluded to in Chapter V, TECs in the Notch gain-of-function model display similar maturation arrest to cells in FOXN1 hypomorphs. It may be helpful to think of both Notch and FOXN1 as TEC maturation or TEPC differentiation factors. With Notch antagonizing differentiation and FOXN1 driving maturation, there exists a

state of cross-repressive interaction between the two factors. Since the TEPC phenotype appears to be intrinsically linked to mTEC differentiation potential, the precocious maturation of TEPCs, caused either by the loss Notch or by prolonged FOXN1 overexpression, would extinguish TEPC bipotency and result in reduced mTEC cellularity. This regulatory node also helps to explain why, despite the early TEPC-like marker expression in constitutive NICD thymi, TECs eventually undergo some degree of differentiation (Chapter V). High Notch activity did not prevent these cells from expressing FOXN1 entirely, hence allowing them to eventually overcome the TEPC state and differentiate.

Chapter VII Concluding Remarks

7.1 Summary of experimental results

This thesis set out to examine the role of Notch signalling in regulating the early lineage divergence of TEC progenitors.

In chapter III, I studied the expression of Notch pathway components in thymus organogenesis. The expression of Notch ligands DLL4 and JAG1, and Notch receptors NOTCH1, NOTCH2 and NOTCH3 were found in E12.5-14.5 TECs, as well as the canonical Notch targets.

The functional relevance of Notch signalling in TEC development was investigated in chapter IV through Notch perturbation in TECs. Both genetic disruption and pharmacological inhibition showed that in the absence of Notch signalling, the development of the mTEC lineage is specifically affected. Using thymic tissue organ culture (FTOC), the significance of Notch activity in mTEC development was mapped precisely to between E10.5 and E16.5. The lack of Notch signalling in the very early primordium (E10.5 3PP) led to a drastic suppression of mTEC development, suggesting that Notch is required for the initial emergence of mTECs.

These results raised the question as to whether mTEC specification per se is regulated by Notch, or the competence to become mTECs, which I addressed in chapter V with Notch gain-of-function analysis. Constitutive Notch activity primarily dictated an immature TEPC-like phenotype ($K5^{+}$ $K8^{+}$ $PLET1^{hi}$ $MHCII^{low}$). Cortico-medullary architecture was found to be disrupted, and persistent Notch activity resulted in a profound arrest of cTEC maturation, contradicting with an mTEC-restricted role of Notch. Crucially, I found that constitutively active Notch signalling is permissive rather than instructive for mTEC development. Overall, these data suggest that Notch determines mTEC progenitor pool by controlling TEPC differentiation.

In chapter VI, several targeted and unbiased approaches were taken to identify functional Notch targets and mechanisms underpinning the cellular behaviours in Notch loss- and gain-of-function models. While mTEC development is dependent on

both Notch and RANK signalling, the proliferation of specified mTECs mediated by RANK could occur despite the attempts to eliminate Notch. Their different temporal requirements indicate that the two pathways regulate independent checkpoints in mTEC development, and that Notch is temporally upstream of RANK. Furthermore, we studied the transcriptomes of Notch loss-of-function and gain-of-function TECs by RNA-seq. Bioinformatic analysis revealed that Notch exhibits a positive feedback loop to enhance its own activity. We have also identified a number of collagen genes and the EGFR pathway as potential functional targets downstream of Notch. Finally, we noted that the overexpression of FOXN1 in developing TECs produced a similar phenotype to the ablation of Notch. Gene expression data suggest a cross repressive relationship between Notch and FOXN1 in TEC differentiation.

7.2 Conclusion

Notch signalling is active in early fetal TECs. Abolishing or overexpressing Notch in TECs both resulted in aberrant TEC differentiation. The impact of Notch on mTEC development is limited to the earlier phase of TEC differentiation, and is distinct from RANK-facilitated mTEC proliferation and maturation. Transcriptomic analysis shed light on several potential mechanisms through which Notch may control TEC differentiation. Based on these data, an updated model of early TEC lineage regulation is proposed (Fig. 7):

Notch activity in TEC progenitors appears to determine whether the bipotency of TEPCs is maintained or extinguished, with cTEC the preferred fate in premature differentiation. As the two sub-lineages emerge, Notch signalling is downregulated in cTECs but continues to be active in early mTECs, possibly as the result of positive feedback. Moreover, whilst Notch favours preserving primitive TEPCs, FOXN1 promotes the differentiation of TECs in both mTEC and cTEC lineages. These two potent factors seem to antagonize each other, and their combined influence orchestrates the outcome of TEC differentiation. On the other hand, the emergence of mTECs can occur only in the presence of Notch, after which mTEC progenitors expand and mature through crosstalk with TNFSF ligands, including RANKL.

This updated model of TEC differentiation clarifies some previous uncertainties around the formation of cTEC and mTEC lineages. Although there is evidence for bipotent and unipotent TEC progenitors, their progenitor-progeny relationship was not well understood. Based on lineage tracing and developmental progression, it was proposed that bipotent TEPCs express mature cTEC markers β5t and CD205. From this an inference was made that TEPCs are phenotypically more closely related to the cTEC lineage, while mTEC specification probably requires input from additional signals (Alves et al., 2014). However, the cue for mTEC specification and the duration of TEPC bipotency were unclear.

Our data suggest that Notch is required for the mTEC lineage, but it is unlikely to be the missing "specifier" that commits bipotent TEPCs to the mTEC fate. In fact, the results highlight the dependence of mTEC emergence on the maintenance of immature TEPCs. Precocious extinguishing of bipotency, brought about by Notch ablation or FOXN1 overexpression, appears to lead to the irreversible differentiation to the cTEC lineage, thereby exhausting cells with mTEC potential. Notwithstanding the caveats of the FTOC system, I have shown that this window of Notch sensitivity is limited to between E10.5 and E16.5, and this phase may reflect the approximate duration of TEPC bipotency in thymus development. The end stage of this estimate is earlier than that deduced from β5t lineage tracing (Mayer et al., 2015; Ohigashi et al., 2015), but the discrepancy may be due to the NFκB pathway (and mTEC expansion) increasingly outweighing the importance of Notch (and progenitor potency) on mTEC cellularity in late fetal stages. Nonetheless, given that Notch signalling is actively repressed in adult mTECs (Goldfarb et al., 2016), it makes sense for its role in fetal TEC lineage determination to be a temporally limited one.

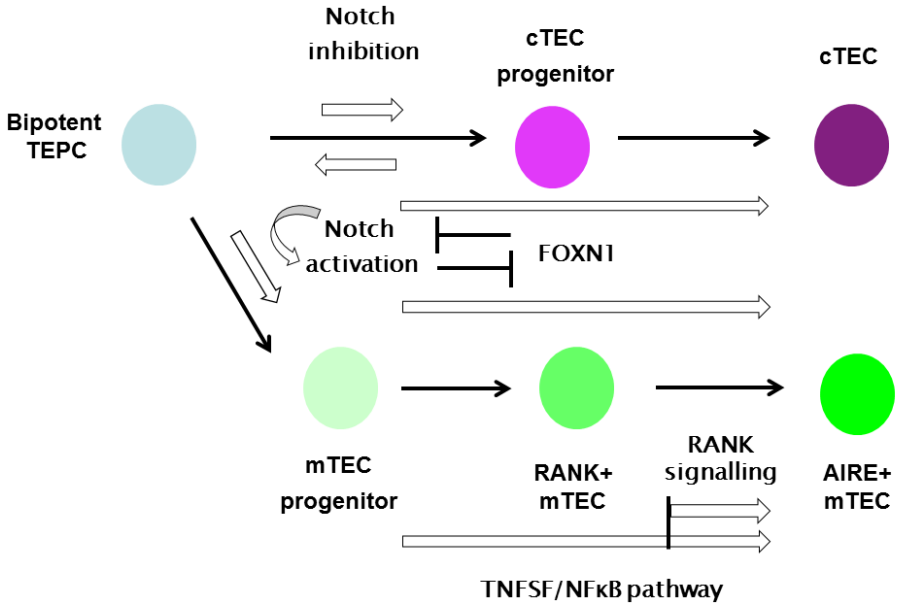

Figure 7 An updated model of TEC lineage regulation.

7.3 Future work

Notch signalling is the result of ligand-receptor binding between adjacent cells. Experiments in this thesis focused on the effect of Notch activity levels on TEC differentiation. These approaches have been informative but were not conducive to uncover the source of Notch ligands activating TEC receptors. Enforced DLL1 on B cells or T cells enhances the number and organization of mTECs in a reaggregate culture system, pointing to DLL1 as a possible ligand. It is also noticeable that Notch signalling in TECs induces *Jag1* expression, prompting a hypothesis where Notch can act in a lateral induction fashion among developing TECs, similar to the scenario regarding sensory cell development in the inner ear (Hartman et al., 2010).

Our data and that of others indicate that Notch signalling is deployed differently in the early primordium and adult thymic epithelium. Goldfarb and colleagues have attempted to study the role of Notch in postnatal TECs with the NICD induction model used in this thesis (Goldfarb et al., 2016), but their interpretation was confounded by the absence of initial fetal phenotype analysis. A definitive investigation would require transgenic mice that enable the inducible manipulation of Notch activity. I am also intrigued by how the capacity for Notch signalling was modulated in fetal and adult thymi. One possibility is that the competence to receive Notch signal is regulated at the chromatin level. The invention of ATAC-seq (Buenrostro et al., 2013) has greatly reduced the number of cells required to generate a map of open chromatin. Comparing the chromatin states of adult TECs with fetal TECs would be informative in elucidating differential regulatory landscape at these developmental stages.

In order to culture the thymic rudiments from younger embryos, an adapted FTOC system was developed in the thesis (Chapter IV). As this culture system can accommodate the growth of early primordia, it allows the interrogation of the signalling requirements of TEPCs. The behaviour of primitive TEPCs is the product of a multitude of signalling inputs. By utilizing this culture system, further work may reveal a more integrated picture of signals in the early thymic environment, and the precise effect of individual factors on the potency, proliferation and differentiation of various TEC progenitors.

This study focused on the TEC population-level responses to signalling stimuli. It would be of interest to tease out the effect of signalling at the single cell level. This is becoming more feasible thanks to rapid technological advances (reviewed in Hoppe et al., 2014). Many aspects related to TEC development may benefit from the transition from population to single cell analysis. It would facilitate the discovery of regulators that contribute to differential cellular behaviour and aid the identification of cell states hitherto indistinguishable by current characterization methods. Specifically, bipotent TEPCs and definitive cTECs share a number of markers, which rendered the interpretation of some data in this thesis difficult. Single cell analysis may uncover novel markers that allow the identification and tracking of the two cell states during organogenesis, and hence alter the assumptions made to reach conclusions in studies like this. It may also shed light on the missing mTEC "specifier" whose identity has thus far been elusive.

Parallel to single cell transcriptomics, initial attempts to screen scaffold biomaterials suitable for supporting the growth and differentiation of TEPCs have been carried out in this laboratory. To date, rather than forming organoids, fetal TECs in culture tend to lose TEC-specific markers and degenerate, precluding the imaging of single TECs in a physiologically relevant context. Although several TEC cells lines have been established, their resemblance to *in vivo* TECs are not widely accepted. The development of complex culture systems that support thymic organoids will greatly benefit *in vitro* studies that can unveil dynamic cellular responses to microenvironmental changes, including to Notch. A particular interest to me is the role of collagen in modulating TEPC differentiation. Collagen genes are significantly upregulated in response to sustained Notch activity in TECs (Chapter VI). If the immature TEC phenotype we observed in the $Foxn1^{Cre}$; $Rosa26^{NICD}$ model is partly down to increased presence of collagen in the thymus, we would expect to find evidence of delayed differentiation in organoids cultured in a collagen-rich scaffold.

A long-term objective of this laboratory is to engineer thymic tissue that can reconstitute the adaptive immune system in immunodeficient or immunosenescent individuals (Bredenkamp et al., 2015). Realizing this goal would require a high degree of control in generating distinct subtype of stromal cells, or better, TEPCs capable of self-renewal. Despite the existing protocols to differentiate TECs from

pluripotent stem cells (Parent et al., 2013; Sun et al., 2013), or by direct conversion from fibroblasts (Bredenkamp et al., 2014b), cells generated from these procedures are highly variable, perhaps reflecting that the conditions in which these cells were produced are sub-optimal. The immediate potential of this study is therefore to improve, by manipulating Notch signalling, the efficiency of obtaining pure cortical, medullary or progenitor TEC populations. Furthermore, we have found potential mechanisms that may operate in tandem or against Notch in TEC development (Chapter VI). If confirmed experimentally, these mechanisms would further improve current strategies to obtain TECs that are of a higher purity.

Chapter VIII Appendices

8.1 Gating strategies for flow cytometry

8.1.1 Gating strategy (fetal TEC)

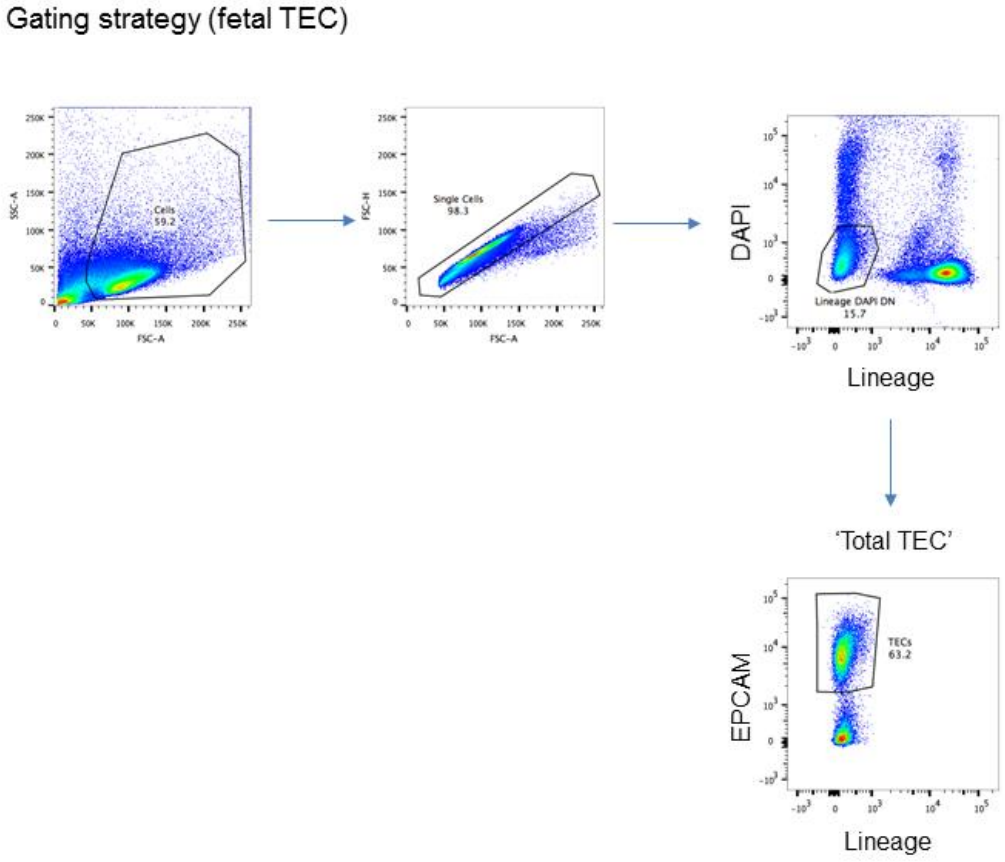

8.1.2 Gating strategy (adult TEC)

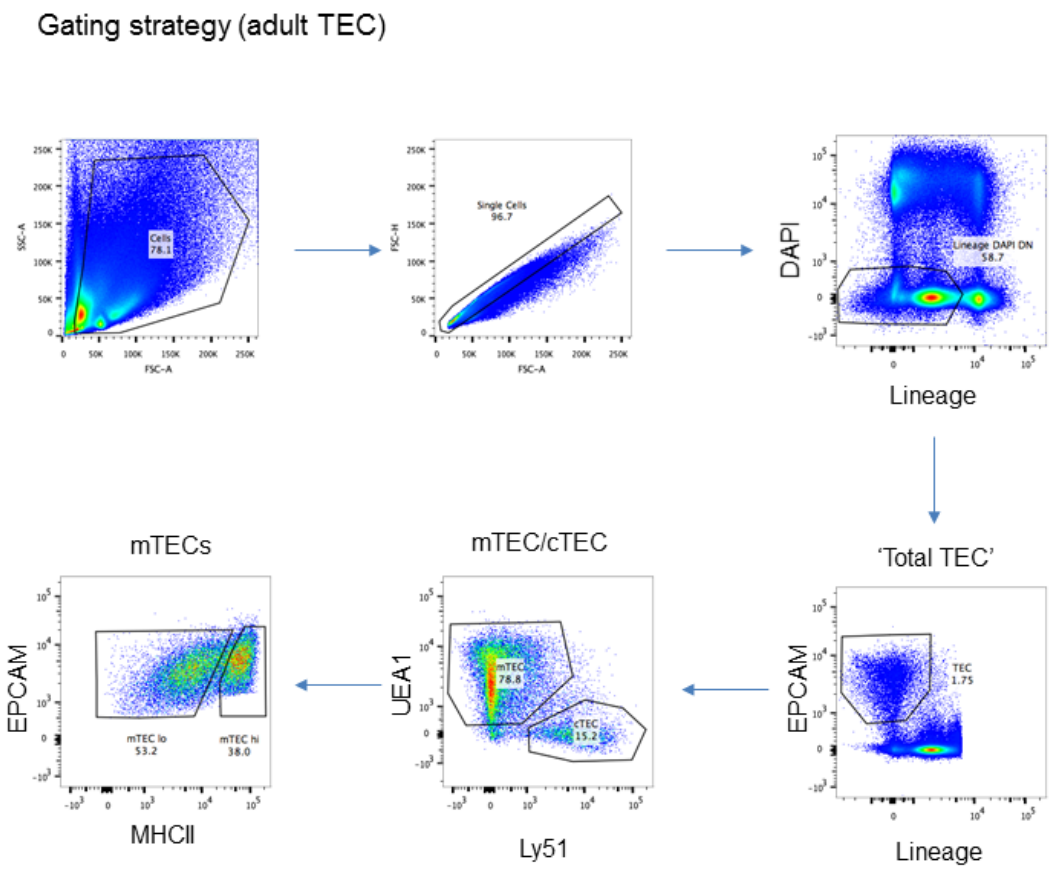

8.1.3 Gating strategy (adult thymocytes)

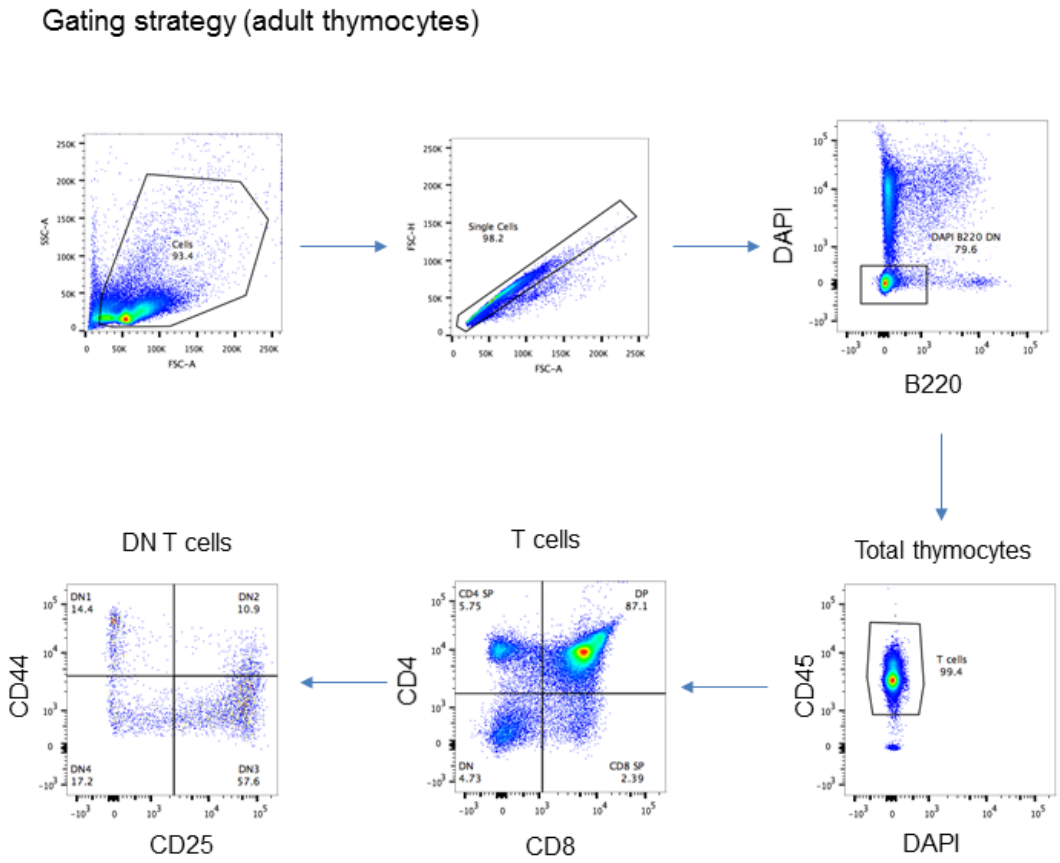

8.1.4 Gating strategy (adult Tregs)

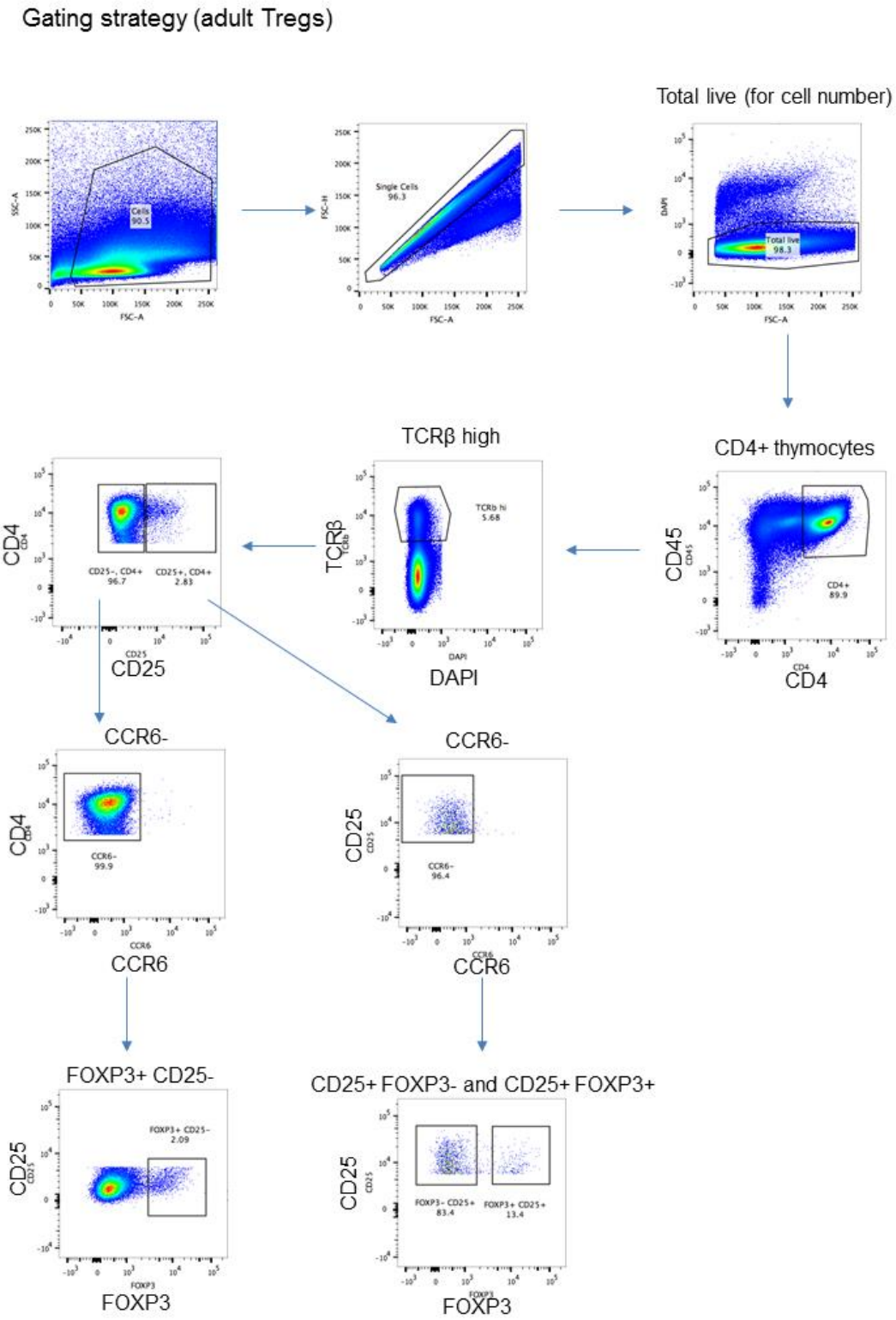

8.1.5 Gating strategy (NICD)

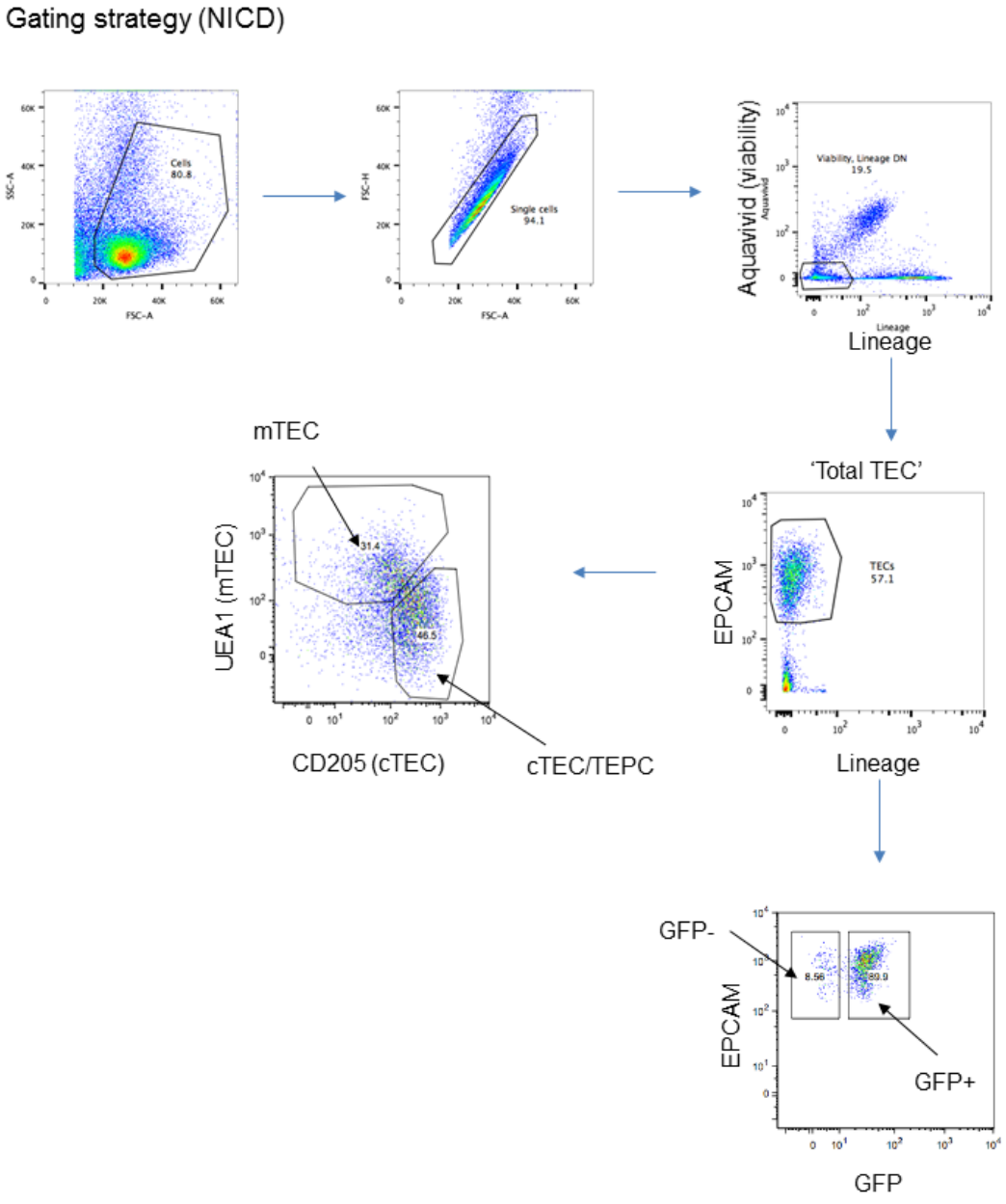

8.1.6 Gating strategy (FTOC)

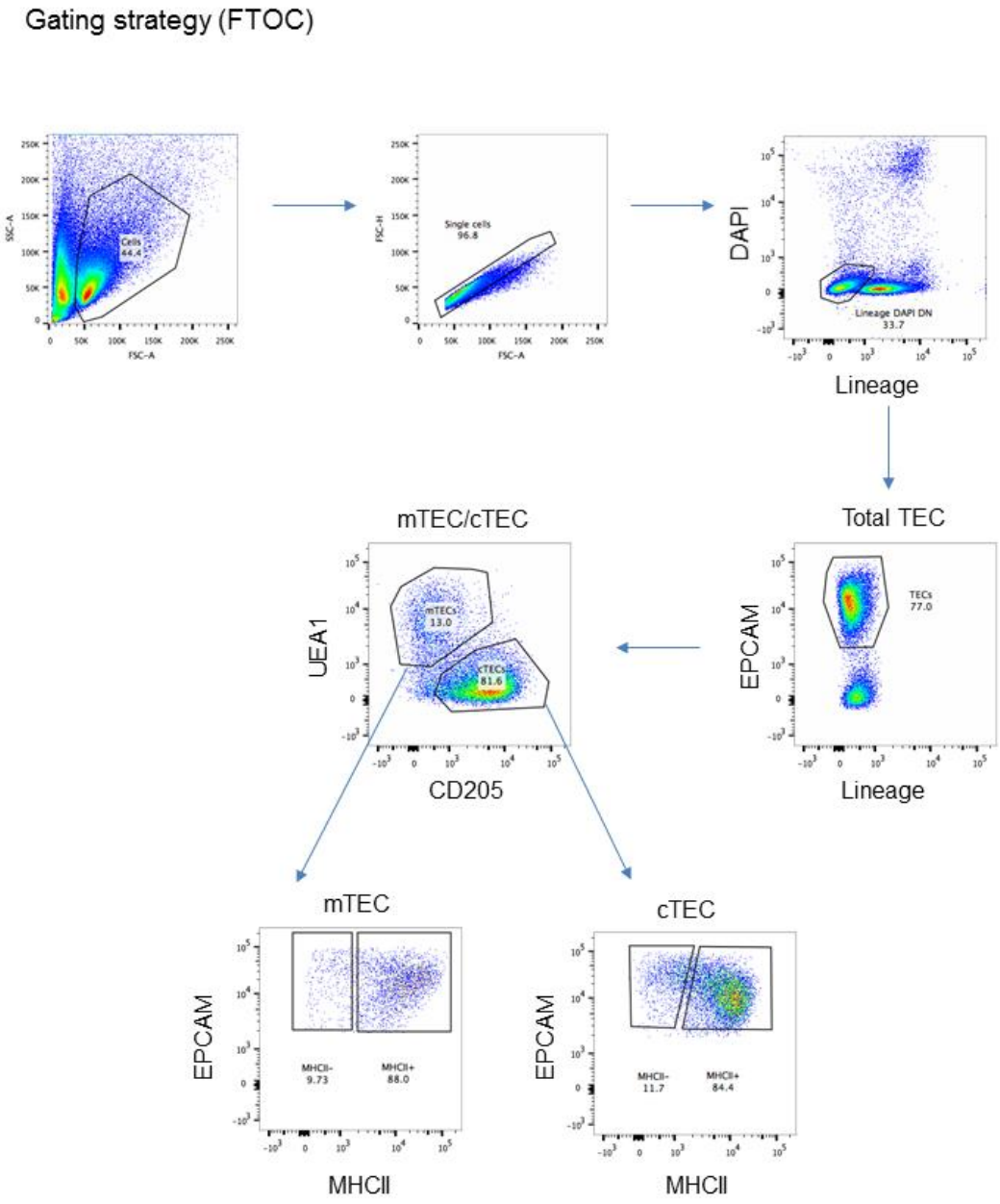

8.2 Data used for quantification in the thesis

Figure 3.2-3.3 RT-qPCR results: normalized expression values

Notch1	E12.5	E13.5 PLET1^{low}	E13.5 PLET1^{hi}	E14.5 UEA1^{-} PLET1^{-}	E14.5 UEA1^{-} PLET1^{+}	E14.5 UEA1^{+}
Run1	0.03667933	0.018241059	0.048324174	0.019370433	0.053536501	0.153183 6
Run2	0.031058051	0.02006898	0.051712851	0.020985775	0.039738099	0.086303 1
Run3	0.023249336	0.015104384	0.054787858	0.013068363	0.035402621	0.139017
Run4	0.023053204	0.025324308	0.048324174			
Run5	0.028403691	0.036651092	0.046355646			
Run6	0.024898838	0.037478895	0.054872314			

Notch2	E12.5	E13.5 PLET1^{low}	E13.5 PLET1^{hi}	E14.5 UEA1^{-} PLET1^{-}	E14.5 UEA1^{-} PLET1^{+}	E14.5 UEA1^{+}
Run1	0.502702852	0.52123288	0.432934964	0.319377223	0.285190929	0.771996 7
Run2	0.350570809	0.415939166	0.407065634	0.245799784	0.257028457	0.642702 2
Run3	0.340721919	0.413066064	0.432268616	0.274628938	0.245421464	0.582366 8
Run4	0.261018184	0.390483457	0.351652462			
Run5	0.275264199	0.352465891	0.316195532			

Notch3	E12.5	E13.5 PLET1^{low}	E13.5 PLET1^{hi}	E14.5 UEA1^{-} PLET1^{-}	E14.5 UEA1^{-} PLET1^{+}	E14.5 UEA1^{+}
Run1	0.535886731	0.181606644	0.415298977	0.070805243	0.209254903	0.300756 3
Run2	0.459385676	0.161544104	0.353553391	0.10503113	0.245989163	0.176640 6
Run3	0.407065634	0.100288092	0.550952558	0.051197679	0.156402267	0.272312 2

Jag1	E12.5	E13.5 PLET1^{low}	E13.5 PLET1^{hi}	E14.5 UEA1^{-} PLET1^{-}	E14.5 UEA1^{-} PLET1^{+}	E14.5 UEA1^{+}
Run1	0.692554734	0.339673888	0.568627413	0.155321918	0.391386708	0.725308 5
Run2	0.582815484	0.28783887	0.629960525	0.155921188	0.347078363	0.513661 2
Run3	0.455861244	0.208129815	0.775572381	0.175015616	0.267943366	0.659754

Dll4	E12.5	E13.5 PLET1^{low}	E13.5 PLET1^{hi}	E14.5 UEA1^{-} PLET1^{-}	E14.5 UEA1^{-} PLET1^{+}	E14.5 UEA1^{+}
Run1	0.543367431	0.938799442	0.498462043	1.427344254	0.995389679	0.197510 3
Run2	0.599200657	0.970410231	0.460093825	1.73976071	1.242575344	0.287617 3
Run3	0.795536484	1.015522513	0.185565446	1.571587091	1.066832243	0.274206 2

Foxn1	E12.5	E13.5 PLET1^{low}	E13.5 PLET1^{hi}	E14.5 UEA1^{-} PLET1^{-}	E14.5 UEA1^{-} PLET1^{+}	E14.5 UEA1^{+}
Run1	4.662523869	4.25748073	3.914665097	5.278031643	4.009252647	3.732132
Run2	4.431446751	3.558109996	3.045473744	5.48524308	4.055837919	3.8341025
Run3	4.428035126	4.300321268	3.340351678	6.214143493	4.489848193	3.2640579
Run4	3.993843435	4.046477761	3.544434711			
Run5	4.080904329	4.267328972	3.407913905			
Run6	4.414414872	4.185951382	3.834102454			

Hes1	E12.5	E13.5 PLET1^{low}	E13.5 PLET1^{hi}	E14.5 UEA1^{-} PLET1^{-}	E14.5 UEA1^{-} PLET1^{+}	E14.5 UEA1^{+}
Run1	2.539323929	2.138599997	2.946268452	0.652176035	0.878633452	0.8970954
Run2	3.090366144	2.04359755	1.900878955	0.650169998	0.689361834	0.8023047
Run3	2.313376368	1.475405083	3.301984466	0.789433085	0.872564288	1.0993621
Run4	1.637064439	0.868541486	1.28243783			
Run5	1.943812265	1.047294123	1.039259226			
Run6	2.026357732	1.116426976	1.111279889			

Hey1	E12.5	E13.5 PLET1^{low}	E13.5 PLET1^{hi}	E14.5 UEA1^{-} PLET1^{-}	E14.5 UEA1^{-} PLET1^{+}	E14.5 UEA1^{+}
Run1	2.545197797	2.982798801	3.694951828	2.099433367	2.308037504	1.713168
Run2	2.419056465	2.830606315	2.848100391	1.961860175	2.445280555	1.575222 4
Run3	2.406050072	2.890083371	3.160165247	2.35472006	2.428389769	1.887748 6
Run4	1.79557317	1.866065983	2.186902481			
Run5	2.290330116	2.356534278	2.624826787			
Run6	2.454715039	2.238018904	2.269260483			

HeyL	E12.5	E13.5 PLET1^{low}	E13.5 PLET1^{hi}	E14.5 UEA1^{-} PLET1^{-}	E14.5 UEA1^{-} PLET1^{+}	E14.5 UEA1^{+}
Run1	0.747424624	0.255056521	0.401152369	0.153183555	0.079109787	0.286511 8
Run2	0.770808531	0.356836064	0.366868091	0.201971302	0.106579361	0.214972 2
Run3	0.634342247	0.218982713	0.38778619	0.161793126	0.095391201	0.295248 2

Hes6	E12.5	E13.5 PLET1^{low}	E13.5 PLET1^{hi}	E14.5 UEA1^{-} PLET1^{-}	E14.5 UEA1^{-} PLET1^{+}	E14.5 UEA1^{+}
Run1	0.071683147	0.043888902	0.042853462	0.066216443	0.054535268	0.018624 3
Run2	0.078442416	0.030772336	0.040014499	0.056154893	0.045018652	0.013250 8
Run3	0.077124516	0.047184095	0.045227164	0.044880178	0.035158078	0.010476 7
Run4	0.082532784	0.071793647	0.071904318			

Run5	0.08033777	0.089415371	0.055767003			
Run6	0.079967387	0.103346079	0.07091439			

Fbxw7	E12.5	E13.5 PLET1^{low}	E13.5 PLET1^{hi}	E14.5 UEA1^{-} PLET1^{-}	E14.5 UEA1^{-} PLET1^{+}	E14.5 UEA1^{+}
Run1	0.633365905	0.569065517	0.448202382	0.338368381	0.148994743	0.0726278
Run2	0.492357376	0.516835752	0.41754396	0.361538758	0.13933858	0.0816477
Run3	0.559935802	0.661789563	0.402390086	0.428952228	0.185994689	0.085773
Run4	0.473393273	0.537126324	0.358212823			
Run5	0.499615066	0.529731547	0.369989326			
Run6	0.5184304	0.54672562	0.434940178			

Ascl1	E12.5	E13.5 PLET1^{low}	E13.5 PLET1^{hi}	E14.5 UEA1^{-} PLET1^{-}	E14.5 UEA1^{-} PLET1^{+}	E14.5 UEA1^{+}
Run1	0.000975059	0.190342109	0.002897228	0.005614345	0.005473452	0.561231
Run2	0.011133964	0.002099766	0.005095125	0.011455802	0.018753885	0.9992301
Run3	0.001466575	0.00485755	0.007139308	0.004535746	0.009775142	0.3568361
Run4	0.003364119	0.00209815	0.017769607			
Run5	0.001924753	0.002360541	0.005848256			
Run6	0	0.004599063	0.005056035			

Id1	E12.5	E13.5 PLET1^{low}	E13.5 PLET1^{hi}	E14.5 UEA1^{-} PLET1^{-}	E14.5 UEA1^{-} PLET1^{+}	E14.5 UEA1^{+}
Run1	1.924447674	1.138131035	1.024951437	0.556068043	0.795536484	0.6001243
Run2	2.454715039	1.057018041	1.145165058	0.412430297	0.557354318	0.6010494
Run3	2.774489267	1.339989989	1.62700899	0.846093431	0.79922115	0.5690655

Plet1	E12.5	E13.5 PLET1^{low}	E13.5 PLET1^{hi}	E14.5 UEA1^{-} PLET1^{-}	E14.5 UEA1^{-} PLET1^{+}	E14.5 UEA1^{+}
Run1	0.143476751	0.025796754	0.150958325	0.005280902	0.102001811	0.0778406
Run2	0.084526971	0.016733568	0.184567728	0.003062422	0.093644192	0.0863031

Figure 3.4 Percentage of E13.5 TECs expressing NOTCH1

	UEA1^{+}	UEA1^{-}
Experiment 1	48.5	14.4
Experiment 2	61	35.2
Experiment 3	45	24.4

Figure 3.5 Percentage of E14.5 TECs expressing Venus

	CD205^{+}	UEA1^{+}	MHCII^{+}	MHCII^{-}
Sample 1	3.22	49.8	7.38	3.04
Sample 2	4.97	53	10.8	4.08
Sample 3	2.51	37.9	6.53	0.99
Sample 4	2.83	50.2	8.72	1.54

Figure 4.2 Postnatal 14-day thymus

(A) Percentage of mTECs in total TECs

Male	Control	cKO
Sample 1	78.8	63.8
Sample 2	81.6	69.9
Sample 3	78.6	67.3

Female	Control	cKO
Sample 1	55.9	42.7
Sample 2	60.8	45.1
Sample 3	58	42.7

(B) Absolute cell number of TEC populations

Male	Total TEC	mTEC	mTEC ^{hi}	mTEC ^{low}	cTEC
Control 1	39585.92	31198.7498	11687.63046	16979.86	5997.958
Control 2	27323.42	22307.53736	9849.245851	10785.46	3424.454
Control 3	25098	19738.91884	9275.164907	8770.536	3834.068
cKO 1	9673.732	6169.184015	2260.298785	3454.222	2917.998
cKO 2	9051.195	6296.552868	2617.829858	3210.682	2072.982
cKO 3	8335.514	5613.950723	2587.925535	2656.488	2001.081

Female	Total TEC	mTEC	mTEC ^{hi}	mTEC ^{low}	cTEC
Control 1	37955.88342	21220.07214	8385.721	11444.79	11589.85
Control 2	51836.80138	31513.10974	12936.42	16840.4	14244
Control 3	37653.90984	21825.35132	8766.791	11826.27	11791.74
cKO 1	23519.52269	10034.0077	3028.142	6458.122	11820.75
cKO 2	36264.06184	16360.83609	5467.659	10105.69	16842.81
cKO 3	28118.46138	12004.60917	3769.733	7576.929	13369.67

(C) Percentage of total thymocytes

Female	DN	DP	$CD4^+$ SP	$CD8^+$ SP
Control 1	5.21	87	5.62	2.15
Control 2	5.98	88.3	2.82	2.88
Control 3	4.73	87.1	5.75	2.39
cKO 1	4.45	86	7.14	2.45
cKO 2	4.97	88	4.68	2.38
cKO 3	4.36	87.1	6.22	2.28

Percentage of total DN thymocytes

Female	DN1	DN2	DN3	DN4
Control 1	10.8	9.9	59.8	19.5
Control 2	8.52	12.2	63.8	15.5
Control 3	14.4	10.9	57.6	17.2
cKO1	11.8	10.9	57.3	19.7
cKO2	10.3	12	61	16.7
cKO3	13.5	9.98	56	20.6

(D) Treg cell number

Male	$CD25^-$ $Foxp3^+$	$CD25^+$ $Foxp3^-$	$CD25^+$ $Foxp3^+$
Control 1	164830.9	88840.13198	16717.97196
Control 2	192749.9	192247.4739	34999.75788
Control 3	170403.4	158298.862	31142.68629
cKO 1	166069.1	188148.5966	30122.70071
cKO 2	150220.6	110452.0649	26705.88691
cKO 3	178073.5	138124.9048	37147.78656

Figure 4.3

(A) E14.5 K14 and UEA1 IHC

Percentage of thymic sections positive for marker:

$K14^+$	Control	cKO
Sample 1	3.042215106	1.099275019
Sample 2	5.716159645	2.120426332
Sample 3	3.157568253	1.994872252
Sample 4	3.125845985	1.760695401

$UEA1^+$	Control	cKO
Sample 1	0.762605376	0.178710457
Sample 2	1.122594969	0.205559173
Sample 3	0.867674665	0.271534197

(B) E18.5: percentage of TECs expressing UEA1

$UEA1^+$	Control	cKO
Sample 1	10.9	4.8
Sample 2	15.7	9.9
Sample 3	13.7	5.74
Sample 4	15.3	
Sample 5	16.4	
Sample 6	15.7	
Sample 7	19.8	
Sample 8	23	
Sample 9	20.9	
Sample 10	29.4	
Sample 11	33.4	
Sample 12	28.9	
Sample 13	25.8	
Sample 14	30.2	
Sample 15	29.7	
Sample 16	31.4	

Sample 17	29.7	
Sample 18	31.9	
Sample 19	29.8	
Sample 20	41.1	
Sample 21	36.3	

(C) Postnatal 8-week: percentage of TECs expressing UEA1

$UEA1^+$	Control	cKO
Sample 1	80.4	75.8
Sample 2	79.2	75
Sample 3	77.3	84

(D) Postnatal 16-week: percentage of TECs expressing UEA1

$UEA1^+$	Control	cKO
Sample 1	72	56.9
Sample 2	76.8	59
Sample 3	72.3	55.9

Figure 4.4 RT-qPCR results normalized expression values

	Foxn1		*Tbx1*		*Il7*	
	Explant	E12.5	Explant	E12.5	Explant	E12.5
Experiment 1	2.004626	2.496661	0.035485	0.016289	1.558329	2.133664
Experiment 2	4.313589	4.985637	0.010325	0.012382	3.307075	4.482938

Figure 4.5 RT-qPCR results normalized expression values

Hes1	Control $PLET1^-$	Control $PLET1^+$	DAPT $PLET1^-$	DAPT $PLET1^+$
Experiment 1	1.139007919	1.670175839	0.507761256	1.191040294
Experiment 2	1.296340262	1.302344488	0.772591536	0.771402409

Figure 4.6

(A) Percentage of mTECs in total TECs

UEA1$^+$	DMSO	1µm	10µM	20µM
Experiment 1	12.8	7.2	6	6.1
Experiment 2	14.1	10.2	7.9	6.1
Experiment 3	9.3	5.9	N/A	2.7

Cell number after FTOC of E12.5 lobes (total of 9 explants)

	Total TEC number		mTEC number		cTEC number	
	DMSO	20µM	DMSO	20µM	DMSO	20µM
Experiment 1	20050	15830	2566.4	965.63	16340.75	13582.14
Experiment 2	26038	22783	3671.358	1389.763	20283.6	19843.99
Experiment 3	22985	16925	2137.605	456.975	18365.02	14995.55

(C) Percentage of mTECs in total TECs

	UEA1$^+$	E12.5	E14.5	E16.5
DMSO	Experiment 1	12.8	23.1	29.4
	Experiment 2	14.1	19.6	23.8
	Experiment 3	9.27	17	23.7
DAPT	Experiment 1	6.08	11.8	37.3
	Experiment 2	6.05	13.6	22.1
	Experiment 3	2.68	9.01	21

Figure 4.7

Number of UEA1$^+$ cells (total of 3 explants)

UEA1$^+$ cell number	Experiment 1	Experiment 2	Experiment 3
DMSO	68	110	80
DMSO RANKL	70	93	78
DAPT	14	10	5
DAPT RANKL	12	18	4

Number of CD205$^+$ cells (total of 3 explants)

CD205$^+$ cell number	Experiment 1	Experiment 2	Experiment 3
DMSO	843	770	2148
DMSO RANKL	608	453	724
DAPT	591	627	1526
DAPT RANKL	128	2171	1908

Figure 5.1

Percentage of GFP$^+$ cells in total TECs

E14.5	%GFP$^+$
Sample 1	89.2
Sample 2	91.5
Sample 3	89.9
Sample 4	91.9

E16.5	%GFP$^+$
Sample 1	92.5
Sample 2	91.1
Sample 3	91.4

Figure 5.2

Percentage of PLET1$^+$ cells in total E14.5 TECs

PLET1$^+$	Control	NICD
Sample 1	71.7	95.8
Sample 2	63.8	90.3
Sample 3	68.5	97
Sample 4		95.2

Percentage of MHCII$^+$ cells in total E14.5 TECs

MHCII$^+$	Control	NICD
Sample 1	40.4	18.9
Sample 2	44.4	19.1
Sample 3	49.2	21.1
Sample 4		21

Percentage of UEA1$^+$ cells in total E14.5 TECs

UEA1$^+$	Control	NICD
Sample 1	4.58	4.67
Sample 2	4.04	4.73
Sample 3	4.66	5.14
Sample 4		4.87

Figure 5.3C

Control – 25 AIRE$^+$ in 76 UEA1$^+$ cells. 38.04 μm^2 PLET1 positive staining in total area of 169 μm^2.

NICD – 25 AIRE$^+$ in 77 UEA1$^+$ cells. 145.13 μm^2 PLET1 positive staining in total area of 169 μm^2.

Figure 5.4

Percentage of UEA1$^+$ cells in total E16.5 TECs

UEA1$^+$	Control	NICD
Sample 1	7.44	31.2
Sample 2	5.34	44.5
Sample 3	7.14	31.4

Percentage of PLET1$^+$ cells in total E16.5 TECs

PLET1$^+$	Control	NICD
Sample 1	22.5	64.4

Sample 2	28.5	81.5
Sample 3	17	83

Figure 5.5

(A) Percentage of PLET1^{+} cells in E16.5 mTECs

PLET1^{+}	Control	NICD
Sample 1	36.3	62.5
Sample 2	36.8	84
Sample 3	35.5	81.3

Percentage of MHCII^{+} cells in E16.5 mTECs

MHCII^{+}	Control	NICD
Sample 1	87.8	82.5
Sample 2	89.6	74.3
Sample 3	93.8	74

(B) Percentage of PLET1^{+} cells in E16.5 cTEC/TEC progenitors

PLET1^{+}	Control	NICD
Sample 1	20.6	64.1
Sample 2	27.1	77.4
Sample 3	15	82.1

Percentage of MHCII^{+} cells in E16.5 cTEC/TEC progenitors

MHCII^{+}	Control	NICD
Sample 1	78.7	49.6
Sample 2	73.6	52.7
Sample 3	85.4	42.3

Figure 6.1

Percentage of mTECs in total TECs

UEA1$^+$	dGuo	RANKL	RANKL+50μM DAPT
Experiment 1	6.7	30.9	22.5
Experiment 2	13.6	25.3	19.7
Experiment 3	5.73	30.8	19.3

Figure 6.2

Percentage of mTECs in total TECs

UEA1$^+$	dGuo control	dGuo cKO	RANK control	RANK cKO
Sample 1	17.8	2.32	26.3	9.12
Sample 2	10.1	3.21	39.7	7.31
Sample 3	13.5	1.74	34.3	12.1
Sample 4	13.4	2.6	26.8	8.69
Sample 5	6.39	2	26	
Sample 6	6.23			

Percentage of MHCII$^+$ cells in mTECs

MHCII$^+$	dGuo control	dGuo cKO	RANK control	RANK cKO
Sample 1	25.4	44.1	83.7	78.6
Sample 2	40.7	65	76.9	70.7
Sample 3	50.9	60	87.5	88.5
Sample 4	43.2	43.3	83.1	93.2
Sample 5	41.7	55.6	93.5	
Sample 6	29.9			

Percentage of MHCII$^+$ cells in cTECs

MHCII$^+$	dGuo control	dGuo cKO	RANK control	RANK cKO
Sample 1	80.1	82.9	85.6	87.2
Sample 2	70.7	75.9	71.3	55.6
Sample 3	42.3	85.6	50.6	80.3

Sample 4	46.3	87.5	69	80.2
Sample 5	68.8	83.5	73.4	
Sample 6	67.9			

Figure 6.3

(A) Normalized *Ascl1* expression (developmental pattern)

Ascl1	E12.5	E13.5 PLET1$^-$	E13.5 PLET1$^+$	E14.5 UEA1$^-$ PLET1$^-$	E14.5 UEA1- PLET1$^+$	E14.5 UEA1$^+$
Run1	0.000975059	0.190342109	0.002897228	0.005614345	0.005473452	0.561231
Run2	0.011133964	0.002099766	0.005095125	0.011455802	0.018753885	0.9992301
Run3	0.001466575	0.00485755	0.007139308	0.004535746	0.009775142	0.3568361
Run4	0.003364119	0.00209815	0.017769607			
Run5	0.001924753	0.002360541	0.005848256			
Run6	0	0.004599063	0.005056035			

(B) Normalized *Ascl1* expression (Rbpj cKO)

Ascl1	Control PLET1$^-$	Control PLET1$^+$	cKO PLET1$^-$	cKO PLET1$^+$
Sample 1	0.281698195	0.289617809	0.07577038	0.02121327
Sample 2	0.202750556	0.152947784	0.05615489	0.06672839
Sample 3	0.216467482	0.200885375	0.1411749	0.02087294
Sample 4	0.129408115	0.046070913	0.03910057	0.03280365
Sample 5	0.112396317	0.020459134	0.05949404	0.05390888
Sample 6	0.288504688	0.183858358	0.03227737	0.06918805
Sample 7	0.053536501	0.154249031	0.01911847	0.04091827

Figure 6.4 RT-qPCR results: normalized expression values

Notch1	Control PLET1$^-$	Control PLET1$^+$	cKO PLET1$^-$	cKO PLET1$^+$
Sample 1	0.014942	0.030867	0.012072	0.021312
Sample 2	0.024937	0.050338	0.01322	0.02767
Sample 3	0.028142	0.055853	0.019808	0.031346
Sample 4	0.039464	0.050883	0.021295	0.02977
Sample 5	0.021099	0.048773	0.01277	0.026278
Sample 6	0.038119	0.038741	0.012575	0.016326
Sample 7	0.021944	0.050532	0.009065	0.014433

Notch2	Control PLET1$^-$	Control PLET1$^+$	cKO PLET1$^-$	cKO PLET1$^+$
Sample 1	0.619377	0.534238	0.453061	0.433602
Sample 2	0.494638	0.538784	0.379513	0.465798
Sample 3	0.61085	0.617471	0.473758	0.423699
Sample 4	0.496546	0.41851	0.347078	0.326088

Notch3	Control PLET1$^-$	Control PLET1$^+$	cKO PLET1$^-$	cKO PLET1$^+$
Sample 1	0.121021	0.284533	0.043485	0.067764
Sample 2	0.14492	0.41626	0.050785	0.110338
Sample 3	0.173139	0.430276	0.095612	0.119631
Sample 4	0.125869	0.405189	0.0542	0.118166

Jag1	Control PLET1$^-$	Control PLET1$^+$	cKO PLET1$^-$	cKO PLET1$^+$
Sample 1	0.273995	0.490465	0.194941	0.243914
Sample 2	0.23129	0.577454	0.149916	0.230224
Sample 3	0.249231	0.611791	0.253295	0.362096
Sample 4	0.273573	0.445449	0.14492	0.218141
Sample 5	0.33294	0.682494	0.174612	0.245989
Sample 6	0.399611	0.819794	0.268563	0.343885
Sample 7	0.356013	0.700602	0.189173	0.280399

Hes1	Control PLET1^{-}	Control PLET1^{+}	cKO PLET1^{-}	cKO PLET1^{+}
Sample 1	1.013179	0.967425	0.616046	0.506199
Sample 2	1.048101	1.240663	0.501929	0.600587
Sample 3	1.273579	1.314436	0.750308	0.916651
Sample 4	1.081725	0.915945	0.573024	0.712025
Sample 5	1.407694	2.506294	0.680919	1.079228
Sample 6	1.693491	3.613341	0.735433	0.922316
Sample 7	1.558329	3.89062	0.502703	0.978666

HeyL	Control PLET1^{-}	Control PLET1^{+}	cKO PLET1^{-}	cKO PLET1^{+}
Sample 1	0.160799	0.125289	0.040386	0.034674
Sample 2	0.429283	0.425989	0.106006	0.065607
Sample 3	0.41466	0.420448	0.137738	0.057645
Sample 4	0.31498	0.376312	0.066883	0.046786

Foxn1	Control PLET1^{-}	Control PLET1^{+}	cKO PLET1^{-}	cKO PLET1^{+}
Sample 1	6.660154	5.933523	6.443202	4.451972
Sample 2	5.806939	3.813488	5.906167	5.031927
Sample 3	5.718178	4.535027	3.307075	2.545198
Sample 4	6.581121	4.14106	5.098243	4.189176
Sample 5	7.568461	6.156977	7.271345	4.552524
Sample 6	6.528116	5.762387	6.634556	5.181369

Plet1	Control PLET1^{-}	Control PLET1^{+}	cKO PLET1^{-}	cKO PLET1^{+}
Sample 1	0.000908	0.076004	0.004948	0.076651
Sample 2	0.007693	0.131924	0.003374	0.075596
Sample 3	0.009611	0.149454	0.011832	0.113265
Sample 4	0.020953	0.187722	0.011255	0.095612
Sample 5	0.019415	0.263442	0.029678	0.219151
Sample 6	0.017257	0.156764	0.012958	0.191666

8.3 RT-PCR products

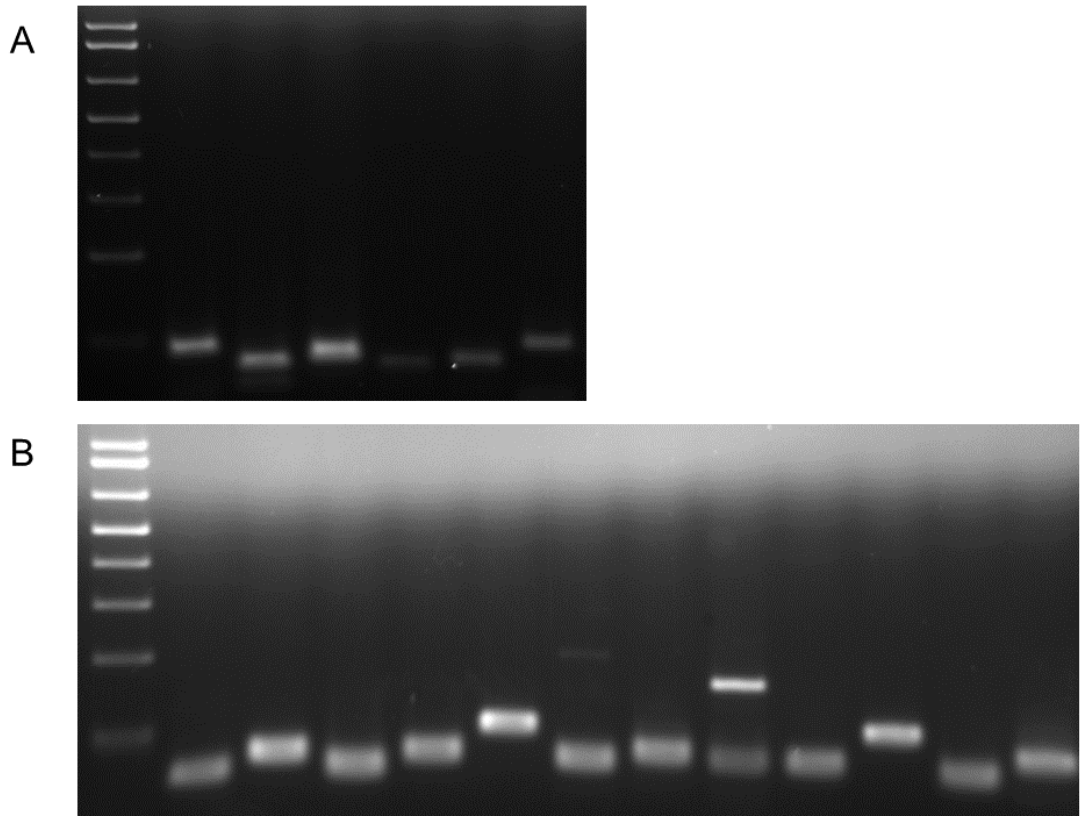

Figure 8.3 Agarose gel electrophoresis of RT-PCR products

(A) Left to right: *Hprt, Hmbs, Ywhaz, Foxn1, Tbx1, Il-7*.

(B) Left to right: *Notch1, Notch2, Notch3, Jag1, Plet1, Hes1, Heyl, Hes6, Ascl1, Fbxw7, Dll4, Rank*.

References

Abu-Issa, R., Smyth, G., Smoak, I., Yamamura, K. and Meyers, E. N. (2002). Fgf8 is required for pharyngeal arch and cardiovascular development in the mouse. *Development* **129**, 4613-4625.

Akiyama, N., Shinzawa, M., Miyauchi, M., Yanai, H., Tateishi, R., Shimo, Y., Ohshima, D., Matsuo, K., Sasaki, I., Hoshino, K., et al. (2014). Limitation of immune tolerance-inducing thymic epithelial cell development by Spi-B-mediated negative feedback regulation. *J Exp Med* **211**, 2425-2438.

Akiyama, N., Takizawa, N., Miyauchi, M., Yanai, H., Tateishi, R., Shinzawa, M., Yoshinaga, R., Kurihara, M., Demizu, Y., Yasuda, H., et al. (2016). Identification of embryonic precursor cells that differentiate into thymic epithelial cells expressing autoimmune regulator. *J Exp Med* **213**, 1441-1458.

Akiyama, T., Maeda, S., Yamane, S., Ogino, K., Kasai, M., Kajiura, F., Matsumoto, M. and Inoue, J. (2005). Dependence of self-tolerance on TRAF6-directed development of thymic stroma. *Science* **308**, 248-251.

Akiyama, T., Shimo, Y., Yanai, H., Qin, J., Ohshima, D., Maruyama, Y., Asaumi, Y., Kitazawa, J., Takayanagi, H., Penninger, J. M., et al. (2008). The tumor necrosis factor family receptors RANK and CD40 cooperatively establish the thymic medullary microenvironment and self-tolerance. *Immunity* **29**, 423-437.

Alpdogan, O., Hubbard, V. M., Smith, O. M., Patel, N., Lu, S., Goldberg, G. L., Gray, D. H., Feinman, J., Kochman, A. A., Eng, J. M., et al. (2006). Keratinocyte growth factor (KGF) is required for postnatal thymic regeneration. *Blood* **107**, 2453-2460.

Alves, N. L., Takahama, Y., Ohigashi, I., Ribeiro, A. R., Baik, S., Anderson, G. and Jenkinson, W. E. (2014). Serial progression of cortical and medullary thymic epithelial microenvironments. pp. 16-22.

Anderson, M. S. and Su, M. A. (2016). AIRE expands: new roles in immune tolerance and beyond. *Nat Rev Immunol* **16**, 247-258.

Andersson, E., Sandberg, R. and Lendahl, U. (2011). Notch signaling: simplicity in design, versatility in function. In *Development*, pp. 3593-3612.

Apelqvist, A., Li, H., Sommer, L., Beatus, P., Anderson, D. J., Honjo, T., Hrabe de Angelis, M., Lendahl, U. and Edlund, H. (1999). Notch signalling controls pancreatic cell differentiation. *Nature* **400**, 877-881.

Arnold, J. S., Werling, U., Braunstein, E. M., Liao, J., Nowotschin, S., Edelmann, W., Hebert, J. M. and Morrow, B. E. (2006). Inactivation of Tbx1 in the pharyngeal endoderm results in 22q11DS malformations. *Development* **133**, 977-987.

Auerbach, R. (1960). Morphogenetic interactions in the development of the mouse thymus gland. *Dev Biol* **2**, 271-284.

Axelson, H. (2004). The Notch signaling cascade in neuroblastoma: role of the basic helix-loop-helix proteins HASH-1 and HES-1. *Cancer Lett* **204**, 171-178.

Bai, G., Sheng, N., Xie, Z., Bian, W., Yokota, Y., Benezra, R., Kageyama, R., Guillemot, F. and Jing, N. (2007). Id sustains Hes1 expression to inhibit precocious neurogenesis by releasing negative autoregulation of Hes1. *Dev Cell* **13**, 283-297.

Baik, S., Jenkinson, E., Lane, P., Anderson, G. and Jenkinson, W. (2013). Generation of both cortical and Aire(+) medullary thymic epithelial compartments from CD205(+) progenitors. *Eur. J. Immunol.* **43**, 589-594.

Baik, S., Sekai, M., Hamazaki, Y., Jenkinson, W. E. and Anderson, G. (2016). Relb acts downstream of medullary thymic epithelial stem cells and is essential for the emergence of RANK(+) medullary epithelial progenitors. *Eur J Immunol* **46**, 857-862.

Bain, V. E., Gordon, J., O'Neil, J. D., Ramos, I., Richie, E. R. and Manley, N. R. (2016). Tissue-specific roles for sonic hedgehog signaling in establishing thymus and parathyroid organ fate. *Development* **143**, 4027-4037.

Bajoghli, B., Aghaallaei, N., Hess, I., Rode, I., Netuschil, N., Tay, B. H., Venkatesh, B., Yu, J. K., Kaltenbach, S. L., Holland, N. D., et al. (2009). Evolution of genetic networks underlying the emergence of thymopoiesis in vertebrates. *Cell* **138**, 186-197.

Balciunaite, G., Keller, M. P., Balciunaite, E., Piali, L., Zuklys, S., Mathieu, Y. D., Gill, J., Boyd, R., Sussman, D. J. and Hollander, G. A. (2002). Wnt glycoproteins regulate the expression of FoxN1, the gene defective in nude mice. *Nat Immunol* **3**, 1102-1108.

Barbarulo, A., Lau, C. I., Mengrelis, K., Ross, S., Solanki, A., Saldana, J. I. and Crompton, T. (2016). Hedgehog Signalling in the Embryonic Mouse Thymus. *J Dev Biol* **4**, 22.

Beatus, P., Lundkvist, J., Oberg, C. and Lendahl, U. (1999). The notch 3 intracellular domain represses notch 1-mediated activation through Hairy/Enhancer of split (HES) promoters. *Development* **126**, 3925-3935.

Bellavia, D., Checquolo, S., Campese, A. F., Felli, M. P., Gulino, A. and Screpanti, I. (2008). Notch3: from subtle structural differences to functional diversity. *Oncogene* **27**, 5092-5098.

Bennett, A. R., Farley, A., Blair, N. F., Gordon, J., Sharp, L. and Blackburn, C. C. (2002). Identification and Characterization of Thymic Epithelial Progenitor Cells. *Immunity* **16**, 803-814.

Bichele, R., Kisand, K., Peterson, P. and Laan, M. (2016). TNF superfamily members play distinct roles in shaping the thymic stromal microenvironment. *Mol Immunol* **72**, 92-102.

Blackburn, C. C., Augustine, C. L., Li, R., Harvey, R. P., Malin, M. A., Boyd, R. L. and Morahan, G. (1996). The nu Gene Acts Cell-Autonomously and is Required for Differentiation of Thymic Epithelial Progenitors. *Proceedings of the National Academy of Sciences of the United States of America* **93**, 5742-5746.

Blackburn, C. C. and Manley, N. R. (2004). Developing a new paradigm for thymus organogenesis. *Nat Rev Immunol* **4**, 278-289.

Blake, J. A. and Ziman, M. R. (2014). Pax genes: regulators of lineage specification and progenitor cell maintenance. *Development* **141**, 737-751.

Bleul, C. and Boehm, T. (2005). BMP signaling is required for normal thymus development. *Journal Of Immunology* **175**, 5213-5221.

Bleul, C., Corbeaux, T., Reuter, A., Fisch, P., Monting, J. and Boehm, T. (2006). Formation of a functional thymus initiated by a postnatal epithelial progenitor cell. *Nature* **441**, 992-996.

Boehm, T., Scheu, S., Pfeffer, K. and Bleul, C. C. (2003). Thymic medullary epithelial cell differentiation, thymocyte emigration, and the control of autoimmunity require lympho-epithelial cross talk via LTbetaR. *The Journal of experimental medicine* **198**, 757.

Boehm, T. and Swann, J. B. (2013). Thymus involution and regeneration: two sides of the same coin? *Nat Rev Immunol* **13**, 831-838.

Boehm, T. and Swann, J. B. (2014). Origin and evolution of adaptive immunity. *Annu Rev Anim Biosci* **2**, 259-283.

Bredenkamp, N., Jin, X., Liu, D., O'Neill, K. E., Manley, N. R. and Blackburn, C. C. (2015). Construction of a functional thymic microenvironment from pluripotent stem cells for the induction of central tolerance. *Regen Med* **10**, 317-329.

Bredenkamp, N., Nowell, C. S. and Blackburn, C. C. (2014a). Regeneration of the aged thymus by a single transcription factor. *Development* **141**, 1627-1637.

Bredenkamp, N., Ulyanchenko, S., Neill, K., Manley, N., Vaidya, H. and Blackburn, C. (2014b). An organized and functional thymus generated from FOXN1-reprogrammed fibroblasts. *Nat. Cell Biol.* **16**, 902-908.

Brohl, D., Vasyutina, E., Czajkowski, M. T., Griger, J., Rassek, C., Rahn, H. P., Purfurst, B., Wende, H. and Birchmeier, C. (2012). Colonization of the satellite cell niche by skeletal muscle progenitor cells depends on Notch signals. *Dev Cell* **23**, 469-481.

Brunk, F., Augustin, I., Meister, M., Boutros, M. and Kyewski, B. (2015). Thymic Epithelial Cells Are a Nonredundant Source of Wnt Ligands for Thymus Development. *J Immunol*.

Bryson, J. L., Griffith, A. V., Hughes Iii, B., Saito, F., Takahama, Y., Richie, E. R., Manley, N. R. and Milstone, D. S. (2013). Cell-Autonomous Defects in Thymic Epithelial Cells Disrupt Endothelial-Perivascular Cell Interactions in the Mouse Thymus. *PLoS ONE* **8**.

Buenrostro, J. D., Giresi, P. G., Zaba, L. C., Chang, H. Y. and Greenleaf, W. J. (2013). Transposition of native chromatin for fast and sensitive epigenomic profiling of open chromatin, DNA-binding proteins and nucleosome position. *Nat Methods* **10**, 1213-1218.

Burkly, L., Hession, C., Ogata, L., Reilly, C., Marconi, L., Olson, D., Tizard, R., Cate, R. and Lo, D. (1995). EXPRESSION OF RELB IS REQUIRED FOR THE DEVELOPMENT OF THYMIC MEDULLA AND DENDRITIC CELLS. *Nature* **373**, 531-536.

Calderon, L. and Boehm, T. (2012). Synergistic, context-dependent, and hierarchical functions of epithelial components in thymic microenvironments. *Cell* **149**, 159-172.

Carrieri, F. A. and Dale, J. K. (2016). Turn It Down a Notch. *Front Cell Dev Biol* **4**, 151.

Celli, G., LaRochelle, W. J., Mackem, S., Sharp, R. and Merlino, G. (1998). Soluble dominant-negative receptor uncovers essential roles for fibroblast growth factors in multi-organ induction and patterning. *Embo j* **17**, 1642-1655.

Chaudhry, M. S., Velardi, E., Dudakov, J. A. and van den Brink, M. R. (2016). Thymus: the next (re)generation. *Immunol Rev* **271**, 56-71.

Chen, L., Xiao, S. and Manley, N. R. (2009). Foxn1 is required to maintain the postnatal thymic microenvironment in a dosage-sensitive manner. *Blood* **113**, 567-574.

Chinn, I. K., Blackburn, C. C., Manley, N. R. and Sempowski, G. D. (2012). Changes in primary lymphoid organs with aging. *Semin Immunol* **24**, 309-320.

Chisaka, O. and Capecchi, M. R. (1991). Regionally restricted developmental defects resulting from targeted disruption of the mouse homeobox gene hox-1.5. *Nature* **350**, 473-479.

Choe, C. P. and Crump, J. G. (2014). Tbx1 controls the morphogenesis of pharyngeal pouch epithelia through mesodermal Wnt11r and Fgf8a. *Development (Cambridge, England)* **141**, 3583-3593.

Chojnowski, J. L., Masuda, K., Trau, H. A., Thomas, K., Capecchi, M. and Manley, N. R. (2014). Multiple roles for HOXA3 in regulating thymus and parathyroid differentiation and morphogenesis in mouse. *Development* **141**, 3697-3708.

Cordier, A. C. and Haumont, S. M. (1980). Development of thymus, parathyroids, and ultimo-branchial bodies in NMRI and nude mice. *Am J Anat* **157**, 227-263.

Cosway, E. J., Lucas, B., James, K. D., Parnell, S. M., Carvalho-Gaspar, M., White, A. J., Tumanov, A. V., Jenkinson, W. E. and Anderson, G. (2017). Redefining thymus medulla specialization for central tolerance. *J Exp Med* **214**, 3183-3195.

Cowan, J. E., McCarthy, N. I. and Anderson, G. (2016). CCR7 Controls Thymus Recirculation, but Not Production and Emigration, of Foxp3(+) T Cells. *Cell Rep* **14**, 1041-1048.

Cowan, J. E., Parnell, S. M., Nakamura, K., Caamano, J. H., Lane, P. J., Jenkinson, E. J., Jenkinson, W. E. and Anderson, G. (2013). The thymic medulla is required for Foxp3+ regulatory but not conventional CD4+ thymocyte development. *J Exp Med* **210**, 675-681.

Crossley, P. H. and Martin, G. R. (1995). The mouse Fgf8 gene encodes a family of polypeptides and is expressed in regions that direct outgrowth and patterning in the developing embryo. *Development* **121**, 439-451.

Dejardin, E. (2006). The alternative NF-kappaB pathway from biochemistry to biology: pitfalls and promises for future drug development. *Biochem Pharmacol* **72**, 1161-1179.

del Alamo, D., Rouault, H. and Schweisguth, F. (2011). Mechanism and significance of cis-inhibition in Notch signalling. *Curr Biol* **21**, R40-47.

Depreter, M. G. L., Blair, N. F., Gaskell, T. L., Nowell, C. S., Davern, K., Pagliocca, A., Stenhouse, F. H., Farley, A. M., Fraser, A., Vrana, J., et al. (2008). Identification of Plet-1 as a Specific Marker of Early Thymic Epithelial Progenitor Cells. *Proceedings of the National Academy of Sciences of the United States of America* **105**, 961-966.

Desanti, G. E., Cowan, J. E., Baik, S., Parnell, S. M., White, A. J., Penninger, J. M., Lane, P. J., Jenkinson, E. J., Jenkinson, W. E. and Anderson, G. (2012). Developmentally regulated availability of RANKL and CD40 ligand reveals distinct mechanisms of fetal and adult cross-talk in the thymus medulla. *J Immunol* **189**, 5519-5526.

Dudakov, J. A., Hanash, A. M., Jenq, R. R., Young, L. F., Ghosh, A., Singer, N. V., West, M. L., Smith, O. M., Holland, A. M., Tsai, J. J., et al. (2012). Interleukin-22 drives endogenous thymic regeneration in mice. *Science* **336**, 91-95.

Dumont-Lagacé, M., Brochu, S., St-Pierre, C. and Perreault, C. (2014). Adult thymic epithelium contains nonsenescent label-retaining cells. *Journal of immunology (Baltimore, Md. : 1950)* **192**, 2219.

Erickson, M., Morkowski, S., Lehar, S., Gillard, G., Beers, C., Dooley, J., Rubin, J. S., Rudensky, A. and Farr, A. G. (2002). Regulation of thymic epithelium by keratinocyte growth factor. *Blood* **100**, 3269-3278.

Fischer, A. and Gessler, M. (2007). Delta-Notch--and then? Protein interactions and proposed modes of repression by Hes and Hey bHLH factors. *Nucleic Acids Res* **35**, 4583-4596.

Flanagan, S. P. (1966). 'Nude', a new hairless gene with pleiotropic effects in the mouse. *Genet Res* **8**, 295-309.

Frank, D., Fotheringham, L., Brewer, J., Muglia, L., Tristani-Firouzi, M., Capecchi, M. and Moon, A. (2002). An Fgf8 mouse mutant phenocopies human 22q11 deletion syndrome. *Development* **129**, 4591-4603.

Fujimoto, Y., Tu, L., Miller, A. S., Bock, C., Fujimoto, M., Doyle, C., Steeber, D. A. and Tedder, T. F. (2002). CD83 expression influences CD4+ T cell development in the thymus. *Cell* **108**, 755-767.

Gardiner, Jr., Jackson, A. L., Gordon, J., Lickert, H., Manley, N. and Basson, M. A. (2012). Localised inhibition of FGF signalling in the third pharyngeal pouch is required for normal thymus and parathyroid organogenesis. *Development* **139**, 3456-3466.

Gilbert, S. F. (2010). *Developmental Biology*: Sinauer Associates.

Gilchrist, D. S., Ure, J., Hook, L. and Medvinsky, A. (2003). Labeling of hematopoietic stem and progenitor cells in novel activatable EGFP reporter mice. *Genesis* **36**, 168-176.

Gill, J., Malin, M., Hollander, G. A. and Boyd, R. (2002). Generation of a complete thymic microenvironment by MTS24(+) thymic epithelial cells. *Nat Immunol* **3**, 635-642.

Godfrey, D. I., Zlotnik, A. and Suda, T. (1992). Phenotypic and functional characterization of c-kit expression during intrathymic T cell development. *J Immunol* **149**, 2281-2285.

Goldfarb, Y., Kadouri, N., Levi, B., Sela, A., Herzig, Y., Cohen, R. N., Hollenberg, A. N. and Abramson, J. (2016). HDAC3 Is a Master Regulator of mTEC Development. *Cell Rep* **15**, 651-665.

Gordon, J., Bennett, A., Blackburn, C. and Manley, N. (2001). Gcm2 and Foxn1 mark early parathyroid- and thymus-specific domains in the developing third pharyngeal pouch. *Mechanisms Of Development* **103**, 141-143.

Gordon, J. and Manley, N. R. (2011). Mechanisms of thymus organogenesis and morphogenesis. *Development (Cambridge, England)* **138**, 3865.

Gordon, J., Patel, S. R., Mishina, Y. and Manley, N. R. (2010). Evidence for an early role for BMP4 signaling in thymus and parathyroid morphogenesis. *Developmental Biology* **339**, 141-154.

Gordon, J., Wilson, V. A., Blair, N., Sheridan, J., Farley, A., Wilson, L., Manley, N. and Blackburn, C. (2004). Functional evidence for a single endodermal origin for the thymic epithelium. *Nat. Immunol.* **5**, 546-553.

Gordon, J., Xiao, S., Hughes, B., 3rd, Su, D. M., Navarre, S. P., Condie, B. G. and Manley, N. R. (2007). Specific expression of lacZ and cre recombinase in fetal thymic epithelial cells by multiplex gene targeting at the Foxn1 locus. *BMC Dev Biol* **7**, 69.

Graf, D., Nethisinghe, S., Palmer, D. B., Fisher, A. G. and Merkenschlager, M. (2002). The developmentally regulated expression of Twisted gastrulation reveals a role for bone morphogenetic proteins in the control of T cell development. *J Exp Med* **196**, 163-171.

Gratton, M. O., Torban, E., Jasmin, S. B., Theriault, F. M., German, M. S. and Stifani, S. (2003). Hes6 promotes cortical neurogenesis and inhibits Hes1 transcription repression activity by multiple mechanisms. *Mol Cell Biol* **23**, 6922-6935.

Gray, D., Abramson, J., Benoist, C. and Mathis, D. (2007). Proliferative arrest and rapid turnover of thymic epithelial cells expressing Aire. *The Journal of Experimental Medicine* **204**, 2521-2528.

Gray, D. H. D., Seach, N., Ueno, T., Milton, M. K., Liston, A., Lew, A. M., Goodnow, C. C. and Boyd, R. L. (2006). Developmental kinetics, turnover, and stimulatory capacity of thymic epithelial cells. *Blood* **108**, 3777.

Greenwald, I. (1998). LIN-12/Notch signaling: lessons from worms and flies. *Genes Dev* **12**, 1751-1762.

Guillemot, F., Lo, L. C., Johnson, J. E., Auerbach, A., Anderson, D. J. and Joyner, A. L. (1993). Mammalian achaete-scute homolog 1 is required for the early development of olfactory and autonomic neurons. *Cell* **75**, 463-476.

Hager-Theodorides, A. L., Outram, S. V., Shah, D. K., Sacedon, R., Shrimpton, R. E., Vicente, A., Varas, A. and Crompton, T. (2002). Bone morphogenetic protein 2/4 signaling regulates early thymocyte differentiation. *J Immunol* **169**, 5496-5504.

Haljasorg, U., Bichele, R., Saare, M., Guha, M., Maslovskaja, J., Kond, K., Remm, A., Pihlap, M., Tomson, L., Kisand, K., et al. (2015). A highly conserved NF-kappaB-responsive enhancer is critical for thymic expression of Aire in mice. *Eur J Immunol* **45**, 3246-3256.

Hamazaki, Y., Fujita, H., Kobayashi, T., Choi, Y., Scott, H., Matsumoto, M. and Minato, N. (2007). Medullary thymic epithelial cells expressing Aire represent a unique lineage derived from cells expressing claudin. *Nat. Immunol.* **8**, 304-311.

Hamazaki, Y., Sekai, M. and Minato, N. (2016). Medullary thymic epithelial stem cells: role in thymic epithelial cell maintenance and thymic involution. *Immunol Rev* **271**, 38-55.

Han, H., Tanigaki, K., Yamamoto, N., Kuroda, K., Yoshimoto, M., Nakahata, T., Ikuta, K. and Honjo, T. (2002). Inducible gene knockout of transcription factor recombination signal binding protein-J reveals its essential role in T versus B lineage decision. *Int Immunol* **14**, 637-645.

Hartman, B. H., Reh, T. A. and Bermingham-McDonogh, O. (2010). Notch signaling specifies prosensory domains via lateral induction in the developing mammalian inner ear. *Proc Natl Acad Sci U S A* **107**, 15792-15797.

Hauri-Hohl, M., Zuklys, S., Hollander, G. A. and Ziegler, S. F. (2014). A regulatory role for TGF-beta signaling in the establishment and function of the thymic medulla. *Nat Immunol* **15**, 554-561.

Heinonen, K., Vanegas, Jr., Brochu, S., Shan, J. D., Vainio, S. J. and Perreault, C. (2011). Wnt4 regulates thymic cellularity through the expansion of thymic epithelial cells and early thymic progenitors. *Blood* **118**, 5163-5173.

Hetzer-Egger, C., Schorpp, M., Haas-Assenbaum, A., Balling, R., Peters, H. and Boehm, T. (2002). Thymopoiesis requires Pax9 function in thymic epithelial cells. *Eur J Immunol* **32**, 1175-1181.

Hikosaka, Y., Nitta, T., Ohigashi, I., Yano, K., Ishimaru, N., Hayashi, Y., Matsumoto, M., Matsuo, K., Penninger, J. M., Takayanagi, H., et al. (2008). The Cytokine RANKL Produced by Positively Selected Thymocytes Fosters Medullary Thymic Epithelial Cells that Express Autoimmune Regulator. *Immunity* **29**, 438-450.

Hirata, H., Yoshiura, S., Ohtsuka, T., Bessho, Y., Harada, T., Yoshikawa, K. and Kageyama, R. (2002). Oscillatory expression of the bHLH factor Hes1 regulated by a negative feedback loop. *Science (New York, N.Y.)* **298**, 840.

Hollander, G., Gill, J., Zuklys, S., Iwanami, N., Liu, C. and Takahama, Y. (2006). Cellular and molecular events during early thymus development. *Immunol Rev* **209**, 28-46.

Honey, K., Nakagawa, T., Peters, C. and Rudensky, A. (2002). Cathepsin L regulates CD4+ T cell selection independently of its effect on invariant chain: a role in the generation of positively selecting peptide ligands. *J Exp Med* **195**, 1349-1358.

Hoppe, P. S., Coutu, D. L. and Schroeder, T. (2014). Single-cell technologies sharpen up mammalian stem cell research. *Nat Cell Biol* **16**, 919-927.

Hu, Z., Lancaster, J. N. and Ehrlich, L. I. (2015). The Contribution of Chemokines and Migration to the Induction of Central Tolerance in the Thymus. *Front Immunol* **6**, 398.

Imayoshi, I., Isomura, A., Harima, Y., Kawaguchi, K., Kori, H., Miyachi, H., Fujiwara, T., Ishidate, F. and Kageyama, R. (2013). Oscillatory control of factors determining multipotency and fate in mouse neural progenitors. *Science* **342**, 1203-1208.

Itoi, M., Kawamoto, H., Katsura, Y. and Amagai, T. (2001). Two distinct steps of immigration of hematopoietic progenitors into the early thymus anlage. *Int Immunol* **13**, 1203-1211.

Jenkinson, W. E., Jenkinson, E. J. and Anderson, G. (2003). Differential requirement for mesenchyme in the proliferation and maturation of thymic epithelial progenitors. *J Exp Med* **198**, 325-332.

Jensen, J., Pedersen, E. E., Galante, P., Hald, J., Heller, R. S., Ishibashi, M., Kageyama, R., Guillemot, F., Serup, P. and Madsen, O. D. (2000). Control of endodermal endocrine development by Hes-1. *Nat Genet* **24**, 36-44.

Jerome, L. A. and Papaioannou, V. E. (2001). DiGeorge syndrome phenotype in mice mutant for the T-box gene, Tbx1. *Nat Genet* **27**, 286-291.

Jiang, R., Lan, Y., Chapman, H. D., Shawber, C., Norton, C. R., Serreze, D. V., Weinmaster, G. and Gridley, T. (1998). Defects in limb, craniofacial, and thymic development in Jagged2 mutant mice. *Genes & development* **12**, 1046.

Kajiura, F., Sun, S., Kuroda, N., Han, H., Li, Y., Matsushima, A., Mitani, T., Matsumoto, M., Izumi, K., Bando, Y., et al. (2004). NF-κB-Inducing Kinase Establishes Self-Tolerance in A Thymic Stroma-Dependent Manner. *Journal of Immunology* **172**, 2067-2075.

Kiernan, A. E. (2013). Notch signaling during cell fate determination in the inner ear. *Semin Cell Dev Biol* **24**, 470-479.

Kiernan, A. E., Cordes, R., Kopan, R., Gossler, A. and Gridley, T. (2005). The Notch ligands DLL1 and JAG2 act synergistically to regulate hair cell development in the mammalian inner ear. *Development* **132**, 4353-4362.

Klein, L., Kyewski, B., Allen, P. and Hogquist, K. (2014). Positive and negative selection of the T cell repertoire: what thymocytes see (and don't see). In *Nat. Rev. Immunol.*, pp. 377-391.

Klug, D., Carter, C., Gimenez-Conti, I. and Richie, E. (2002). Thymocyte-independent and thymocyte-dependent phases of epithelial patterning in the fetal thymus. *Journal Of Immunology* **169**, 2842-2845.

Klug, D. B., Carter, C., Crouch, E., Roop, D., Conti, C. J. and Richie, E. R. (1998). Interdependence of Cortical Thymic Epithelial Cell Differentiation and T-Lineage Commitment. *Proceedings of the National Academy of Sciences of the United States of America* **95**, 11822-11827.

Koch, U., Fiorini, E., Benedito, R., Besseyrias, V., Schuster-Gossler, K., Pierres, M., Manley, N. R., Duarte, A., Macdonald, H. R. and Radtke, F. (2008). Delta-like 4 is the essential, nonredundant ligand for Notch1 during thymic T cell lineage commitment. *J Exp Med* **205**, 2515-2523.

Krangel, M. S. (2009). Mechanics of T cell receptor gene rearrangement. *Curr Opin Immunol* **21**, 133-139.

Krueger, A., Zietara, N. and Lyszkiewicz, M. (2017). T Cell Development by the Numbers. *Trends Immunol* **38**, 128-139.

Kvell, K., Fejes, A. V., Parnell, S. M. and Pongracz, J. E. (2014). Active Wnt/beta-catenin signaling is required for embryonic thymic epithelial development and functionality ex vivo. *Immunobiology* **219**, 644-652.

Le Douarin, N. M. and Jotereau, F. V. (1975). Tracing of cells of the avian thymus through embryonic life in interspecific chimeras. *J Exp Med* **142**, 17-40.

Li, X. Y., Zhai, W. J. and Teng, C. B. (2015). Notch Signaling in Pancreatic Development. *Int J Mol Sci* **17**.

Lindsay, E. A., Vitelli, F., Su, H., Morishima, M., Huynh, T., Pramparo, T., Jurecic, V., Ogunrinu, G., Sutherland, H. F., Scambler, P. J., et al. (2001). Tbx1 haploinsufficieny in the DiGeorge syndrome region causes aortic arch defects in mice. *Nature* **410**, 97-101.

Lio, C. W. and Hsieh, C. S. (2008). A two-step process for thymic regulatory T cell development. *Immunity* **28**, 100-111.

Lio, C. W. and Hsieh, C. S. (2011). Becoming self-aware: the thymic education of regulatory T cells. *Curr Opin Immunol* **23**, 213-219.

Lkhagvasuren, E., Sakata, M., Ohigashi, I. and Takahama, Y. (2013). Lymphotoxin beta receptor regulates the development of CCL21-expressing subset of postnatal medullary thymic epithelial cells. *J Immunol* **190**, 5110-5117.

Luc, S., Luis, T. C., Boukarabila, H., Macaulay, I., Buza-Vidas, N., Bouriez-Jones, T., Lutteropp, M., Won, P. S., Loughran, S. J., Mead, A., et al. (2012). The earliest thymic T cell progenitors sustain B cell and myeloid lineage potential. *Nat. Immunol.* **13**, 412-419.

Luis, T. C., Luc, S., Mizukami, T., Boukarabila, H., Thongjuea, S., Woll, P. S., Azzoni, E., Giustacchini, A., Lutteropp, M., Bouriez-Jones, T., et al. (2016). Initial seeding of the embryonic thymus by immune-restricted lympho-myeloid progenitors. *Nat Immunol* **17**, 1424-1435.

Macatee, T. L., Hammond, B. P., Arenkiel, B. R., Francis, L., Frank, D. U. and Moon, A. M. (2003). Ablation of specific expression domains reveals discrete functions of ectoderm- and endoderm-derived FGF8 during cardiovascular and pharyngeal development. *Development* **130**, 6361-6374.

Male, D. K., Brostoff, J. and Roitt, I. M. (2013). *Immunology,With STUDENT CONSULT Online Access,8: Immunology*: Elsevier/Saunders.

Manley, N. R. and Capecchi, M. R. (1995). The role of Hoxa-3 in mouse thymus and thyroid development. *Development* **121**, 1989-2003.

Masuda, K., Germeraad, W. T. V., Satoh, R., Itoi, M., Ikawa, T., Minato, N., Katsura, Y., van Ewijk, W. and Kawamoto, H. (2009). Notch activation in thymic epithelial cells induces development of thymic microenvironments. *Molecular Immunology* **46**, 1756-1767.

Matsumoto, A., Onoyama, I., Sunabori, T., Kageyama, R., Okano, H. and Nakayama, K. I. (2011). Fbxw7-dependent degradation of Notch is required for control of "stemness" and neuronal-glial differentiation in neural stem cells. *J Biol Chem* **286**, 13754-13764.

Mayer, C. E., Zuklys, S., Zhanybekova, S., Ohigashi, I., Teh, H. Y., Sansom, S. N., Shikama-Dorn, N., Hafen, K., Macaulay, I. C., Deadman, M. E., et al. (2015). Dynamic spatio-temporal contribution of single beta5t+ cortical epithelial precursors to the thymus medulla. *Eur J Immunol*.

Miller, J. F. (1961). Immunological function of the thymus. *Lancet* **2**, 748-749.

Moore-Scott, B. A. and Manley, N. R. (2005). Differential expression of Sonic hedgehog along the anterior-posterior axis regulates patterning of pharyngeal pouch endoderm and pharyngeal endoderm-derived organs. *Dev Biol* **278**, 323-335.

Mori, K., Itoi, M., Tsukamoto, N. and Amagai, T. (2010). Foxn1 is essential for vascularization of the murine thymus anlage. *Cell Immunol* **260**, 66-69.

Morrissey, P. J., McKenna, H., Widmer, M. B., Braddy, S., Voice, R., Charrier, K., Williams, D. E. and Watson, J. D. (1994). Steel factor (c-kit ligand) stimulates the in vitro growth of immature CD3-/CD4-/CD8- thymocytes: synergy with IL-7. *Cell Immunol* **157**, 118-131.

Mouri, Y., Yano, M., Shinzawa, M., Shimo, Y., Hirota, F., Nishikawa, Y., Nii, T., Kiyonari, H., Abe, T., Uehara, H., et al. (2011). Lymphotoxin signal promotes thymic organogenesis by eliciting RANK expression in the embryonic thymic stroma. *Journal of immunology (Baltimore, Md. : 1950)* **186**, 5047.

Mourikis, P. and Tajbakhsh, S. (2014). Distinct contextual roles for Notch signalling in skeletal muscle stem cells. *BMC Dev Biol* **14**, 2.

Murata, S., Sasaki, K., Kishimoto, T., Niwa, S., Hayashi, H., Takahama, Y. and Tanaka, K. (2007). Regulation of CD8+ T cell development by thymus-specific proteasomes. *Science* **316**, 1349-1353.

Murtaugh, L. C., Stanger, B. Z., Kwan, K. M. and Melton, D. A. (2003). Notch signaling controls multiple steps of pancreatic differentiation. *Proc Natl Acad Sci U S A* **100**, 14920-14925.

Nakagawa, T., Roth, W., Wong, P., Nelson, A., Farr, A., Deussing, J., Villadangos, J. A., Ploegh, H., Peters, C. and Rudensky, A. Y. (1998). Cathepsin L: critical role in Ii degradation and CD4 T cell selection in the thymus. *Science* **280**, 450-453.

Nehls, M., Kyewski, B., Messerle, M., Waldschutz, R., Schuddekopf, K., Smith, A. J. and Boehm, T. (1996). Two genetically separable steps in the differentiation of thymic epithelium. *Science* **272**, 886-889.

Nehls, M., Pfeifer, D., Schorpp, M., Hedrich, H. and Boehm, T. (1994). New member of the winged-helix protein family disrupted in mouse and rat nude mutations. *Nature* **372**, 103-107.

Neves, H., Dupin, E., Parreira, L. and Le Douarin, N. M. (2012). Modulation of Bmp4 signalling in the epithelial-mesenchymal interactions that take place in early thymus and parathyroid development in avian embryos. *Dev Biol* **361**, 208-219.

Nicolas, M., Wolfer, A., Raj, K., Kummer, J. A., Mill, P., van Noort, M., Hui, C. C., Clevers, H., Dotto, G. P. and Radtke, F. (2003). Notch1 functions as a tumor suppressor in mouse skin. *Nat Genet* **33**, 416-421.

Nitta, T., Ohigashi, I., Nakagawa, Y. and Takahama, Y. (2011). Cytokine crosstalk for thymic medulla formation. *Current Opinion in Immunology* **23**, 190-197.

Nowell, C. S., Bredenkamp, N., Tetelin, S., Jin, X., Tischner, C., Vaidya, H., Sheridan, J., Stenhouse, F., Heussen, R., Smith, A., et al. (2011). Foxn1 Regulates Lineage Progression in Cortical and Medullary Thymic Epithelial Cells But Is Dispensable for Medullary Sublineage Divergence. *Plos Genetics* **7**.

Nowotschin, S., Xenopoulos, P., Schrode, N. and Hadjantonakis, A. K. (2013). A bright single-cell resolution live imaging reporter of Notch signaling in the mouse. *BMC Dev Biol* **13**, 15.

Ohigashi, I., Zuklys, S., Sakata, M., Mayer, C. E., Hamazaki, Y., Minato, N., Hollander, G. A. and Takahama, Y. (2015). Adult Thymic Medullary Epithelium Is Maintained and Regenerated by Lineage-Restricted Cells Rather Than Bipotent Progenitors. *Cell Rep* **13**, 1432-1443.

Ohigashi, I., Zuklys, S., Sakata, M., Mayer, C. E., Zhanybekova, S., Murata, S., Tanaka, K., Holländer, G. A. and Takahama, Y. (2013). Aire- expressing thymic medullary epithelial cells originate from β5t- expressing progenitor cells. *Proceedings of the National Academy of Sciences of the United States of America* **110**, 9885.

Ohuchi, H., Hori, Y., Yamasaki, M., Harada, H., Sekine, K., Kato, S. and Itoh, N. (2000). FGF10 acts as a major ligand for FGF receptor 2 IIIb in mouse multi-organ development. *Biochem Biophys Res Commun* **277**, 643-649.

Okubo, T., Kawamura, A., Takahashi, J., Yagi, H., Morishima, M., Matsuoka, R. and Takada, S. (2011). Ripply3, a Tbx1 repressor, is required for development of the pharyngeal apparatus and its derivatives in mice. *Development* **138**, 339-348.

Onder, L., Nindl, V., Scandella, E., Chai, Q., Cheng, H.-W., Caviezel-Firner, S., Novkovic, M., Bomze, D., Maier, R., Ludewig, B., et al. (2015). Alternative NF-κB signaling regulates mTEC differentiation from podoplanin-expressing presursors in the cortico-medullary junction. *European Journal of Immunology*.

Osada, M., Ito, E., Fermin, H. A., Vazquez-Cintron, E., Venkatesh, T., Friedel, R. H. and Pezzano, M. (2006). The Wnt signaling antagonist Kremen1 is required for development of thymic architecture. *Clin Dev Immunol* **13**, 299-319.

Osada, M., Jardine, L., Misir, R., Andl, T., Millar, S. E. and Pezzano, M. (2010). DKK1 Mediated Inhibition of Wnt Signaling in Postnatal Mice Leads to Loss of TEC

Progenitors and Thymic Degeneration (DKK1 and Thymic Degeneration). *PLoS ONE* **5**, e9062.

Palmer, D. B. (2013). The effect of age on thymic function. *Front Immunol* **4**, 316.

Panin, V. M., Papayannopoulos, V., Wilson, R. and Irvine, K. D. (1997). Fringe modulates Notch-ligand interactions. *Nature* **387**, 908-912.

Pantelouris, E. M. (1968). Absence of thymus in a mouse mutant. *Nature* **217**, 370-371.

Pantelouris, E. M. and Hair, J. (1970). Thymus dysgenesis in nude (nu nu) mice. *J Embryol Exp Morphol* **24**, 615-623.

Parent, A. V., Russ, H. A., Khan, I. S., LaFlam, T. N., Metzger, T. C., Anderson, M. S. and Hebrok, M. (2013). Generation of functional thymic epithelium from human embryonic stem cells that supports host T cell development. *Cell Stem Cell* **13**, 219-229.

Patel, Sr., Gordon, J., Mahbub, F., Blackburn, C. and Manley, N. (2006). Bmp4 and Noggin expression during early thymus and parathyroid organogenesis. *Gene Expr. Patterns* **6**, 794-799.

Payne, J. L. and Wagner, A. (2015). Mechanisms of mutational robustness in transcriptional regulation. *Front Genet* **6**, 322.

Petcherski, A. G. and Kimble, J. (2000). Mastermind is a putative activator for Notch. In *Curr Biol*, pp. R471-473. England.

Peters, H., Neubuser, A., Kratochwil, K. and Balling, R. (1998). Pax9-deficient mice lack pharyngeal pouch derivatives and teeth and exhibit craniofacial and limb abnormalities. *Genes Dev* **12**, 2735-2747.

Petrovic, J., Formosa-Jordan, P., Luna-Escalante, J. C., Abello, G., Ibanes, M., Neves, J. and Giraldez, F. (2014). Ligand-dependent Notch signaling strength orchestrates lateral induction and lateral inhibition in the developing inner ear. *Development* **141**, 2313-2324.

Picelli, S., Bjorklund, A. K., Faridani, O. R., Sagasser, S., Winberg, G. and Sandberg, R. (2013). Smart-seq2 for sensitive full-length transcriptome profiling in single cells. *Nat Methods* **10**, 1096-1098.

Rebay, I., Silver, S. J. and Tootle, T. L. (2005). New vision from Eyes absent: transcription factors as enzymes. *Trends Genet* **21**, 163-171.

Reeh, K. A. G., Cardenas, K. T., Bain, V. E., Laurent, M., Richie, E. R., Liu, Z. and Manley, N. R. (2014). Ectopic TBX1 suppresses thymic epithelial cell differentiation and proliferation during thymus organogenesis. *Development (Cambridge)* **141**, 2950-2958.

Revest, J., Suniara, R., Kerr, K., Owen, J. and Dickson, C. (2001). Development of the thymus requires signaling through the fibroblast growth factor receptor R2-IIIb. *Journal Of Immunology* **167**, 1954-1961.

Rodewald, H. R., Paul, S., Haller, C., Bluethmann, H. and Blum, C. (2001). Thymus medulla consisting of epithelial islets each derived from a single progenitor. *Nature* **414**, 763-768.

Rossi, S., Jenkinson, W., Anderson, G. and Jenkinson, E. (2006). Clonal analysis reveals a common progenitor for thymic cortical and medullary epithelium. *Nature* **441**, 988-991.

Rossi, S. W., Chidgey, A. P., Parnell, S. M., Jenkinson, W. E., Scott, H. S., Boyd, R. L., Jenkinson, E. J. and Anderson, G. (2007a). Redefining epithelial progenitor potential in the developing thymus. *Eur J Immunol* **37**, 2411-2418.

Rossi, S. W., Kim, M.-Y., Leibbrandt, A., Parnell, S. M., Jenkinson, W. E., Glanville, S. H., McConnell, F. M., Scott, H. S., Penninger, J. M., Jenkinson, E. J., et al. (2007b). RANK signals from CD4 + 3 − inducer cells regulate development of Aire-expressing

epithelial cells in the thymic medulla. *The Journal of Experimental Medicine* **204**, 1267-1272.

Ruzinova, M. B. and Benezra, R. (2003). Id proteins in development, cell cycle and cancer. *Trends Cell Biol* **13**, 410-418.

Saldana, J. I., Solanki, A., Lau, C. I., Sahni, H., Ross, S., Furmanski, A. L., Ono, M., Hollander, G. and Crompton, T. (2016). Sonic Hedgehog regulates thymic epithelial cell differentiation. *J Autoimmun* **68**, 86-97.

Satoh, R., Kakugawa, K., Yasuda, T., Yoshida, H., Sibilia, M., Katsura, Y., Levi, B., Abramson, J., Koseki, Y., Koseki, H., et al. (2016). Requirement of Stat3 Signaling in the Postnatal Development of Thymic Medullary Epithelial Cells. *PLoS Genet* **12**, e1005776.

Scott, I. C., Steiglitz, B. M., Clark, T. G., Pappano, W. N. and Greenspan, D. S. (2000). Spatiotemporal expression patterns of mammalian chordin during postgastrulation embryogenesis and in postnatal brain. *Dev Dyn* **217**, 449-456.

Sekai, M., Hamazaki, Y. and Minato, N. (2014). Medullary Thymic Epithelial Stem Cells Maintain a Functional Thymus to Ensure Lifelong Central T Cell Tolerance. *Immunity* **41**, 753-761.

Shah, D. K., Hager-Theodorides, A. L., Outram, S. V., Ross, S. E., Varas, A. and Crompton, T. (2004). Reduced thymocyte development in sonic hedgehog knockout embryos. *J Immunol* **172**, 2296-2306.

Shah, D. K. and Zuniga-Pflucker, J. C. (2014). An overview of the intrathymic intricacies of T cell development. *J Immunol* **192**, 4017-4023.

Sheridan, J. M., Taoudi, S., Medvinsky, A. and Blackburn, C. C. (2009). A novel method for the generation of reaggregated organotypic cultures that permits juxtaposition of defined cell populations. *Genesis* **47**, 346-351.

Shih, H. P., Kopp, J. L., Sandhu, M., Dubois, C. L., Seymour, P. A., Grapin-Botton, A. and Sander, M. (2012). A Notch-dependent molecular circuitry initiates pancreatic endocrine and ductal cell differentiation. *Development* **139**, 2488-2499.

Soza-Ried, C., Bleul, C. C., Schorpp, M. and Boehm, T. (2008). Maintenance of thymic epithelial phenotype requires extrinsic signals in mouse and zebrafish. *J Immunol* **181**, 5272-5277.

Su, D., Ellis, S., Napier, A., Lee, K. and Manley, N. R. (2001). Hoxa3 and pax1 regulate epithelial cell death and proliferation during thymus and parathyroid organogenesis. *Dev Biol* **236**, 316-329.

Su, D. M. and Manley, N. R. (2000). Hoxa3 and pax1 transcription factors regulate the ability of fetal thymic epithelial cells to promote thymocyte development. *J Immunol* **164**, 5753-5760.

Su, D. M., Navarre, S., Oh, W. J., Condie, B. G. and Manley, N. R. (2003). A domain of Foxn1 required for crosstalk-dependent thymic epithelial cell differentiation. *Nat Immunol* **4**, 1128-1135.

Sun, X., Xu, J., Lu, H., Liu, W., Miao, Z., Sui, X., Liu, H., Su, L., Du, W., He, Q., et al. (2013). Directed differentiation of human embryonic stem cells into thymic epithelial progenitor-like cells reconstitutes the thymic microenvironment in vivo. *Cell Stem Cell* **13**, 230-236.

Swann, J. B., Happe, C. and Boehm, T. (2017). Elevated levels of Wnt signaling disrupt thymus morphogenesis and function. *Sci Rep* **7**, 785.

Tai, X., Erman, B., Alag, A., Mu, J., Kimura, M., Katz, G., Guinter, T., McCaughtry, T., Etzensperger, R., Feigenbaum, L., et al. (2013). Foxp3 transcription factor is proapoptotic and lethal to developing regulatory T cells unless counterbalanced by cytokine survival signals. *Immunity* **38**, 1116-1128.

Takaba, H., Morishita, Y., Tomofuji, Y., Danks, L., Nitta, T., Komatsu, N., Kodama, T. and Takayanagi, H. (2015). Fezf2 Orchestrates a Thymic Program of Self-Antigen Expression for Immune Tolerance. *Cell* **163**, 975-987.

Takada, K., Kondo, K. and Takahama, Y. (2017). Generation of Peptides That Promote Positive Selection in the Thymus. *J Immunol* **198**, 2215-2222.

Takahama, Y., Ohigashi, I., Baik, S. and Anderson, G. (2017). Generation of diversity in thymic epithelial cells. *Nat Rev Immunol* **17**, 295-305.

Tan, S. H. and Nusse, R. (2017). In vivo lineage tracing reveals Axin2-expressing, long-lived cortical thymic epithelial progenitors in the postnatal thymus. *PLoS One* **12**, e0184582.

Tsai, P. T., Lee, R. A. and Wu, H. (2003). BMP4 acts upstream of FGF in modulating thymic stroma and regulating thymopoiesis. *Blood* **102**, 3947-3953.

Uddin, M. M., Ohigashi, I., Motosugi, R., Nakayama, T., Sakata, M., Hamazaki, J., Nishito, Y., Rode, I., Tanaka, K., Takemoto, T., et al. (2017). Foxn1-beta5t transcriptional axis controls CD8+ T-cell production in the thymus. *Nat Commun* **8**, 14419.

Ueno, T., Saito, F., Gray, D. H., Kuse, S., Hieshima, K., Nakano, H., Kakiuchi, T., Lipp, M., Boyd, R. L. and Takahama, Y. (2004). CCR7 signals are essential for cortex-medulla migration of developing thymocytes. *J Exp Med* **200**, 493-505.

Ulyanchenko, S., O'Neill, K. E., Medley, T., Farley, A. M., Vaidya, H. J., Cook, A. M., Blair, N. F. and Blackburn, C. C. (2016). Identification of a Bipotent Epithelial Progenitor Population in the Adult Thymus. *Cell Rep* **14**, 2819-2832.

van Ewijk, W., Shores, E. W. and Singer, A. (1994). Crosstalk in the mouse thymus. *Immunology Today* **15**, 214-217.

Van Ewijk, W., Terhorst, C., Wang, B. and Holländer, G. (2000). Stepwise development of thymic microenvironments in vivo is regulated by thymocyte subsets. *Development* **127**, 1583-1591.

van Ewijk, W., Wang, B., Hollander, G., Kawamoto, H., Spanopoulou, E., Itoi, M., Amagai, T., Jiang, Y. F., Germeraad, W. T., Chen, W. F., et al. (1999). Thymic microenvironments, 3-D versus 2-D? *Semin Immunol* **11**, 57-64.

Visan, I., Yuan, J. S., Tan, J. B., Cretegny, K. and Guidos, C. J. (2006). Regulation of intrathymic T-cell development by Lunatic Fringe- Notch1 interactions. *Immunol Rev* **209**, 76-94.

Vitelli, F., Huynh, T. and Baldini, A. (2009). Gain of function of Tbx1 affects pharyngeal and heart development in the mouse. *Genesis* **47**, 188-195.

Wallin, J., Eibel, H., Neubuser, A., Wilting, J., Koseki, H. and Balling, R. (1996). Pax1 is expressed during development of the thymus epithelium and is required for normal T-cell maturation. *Development* **122**, 23-30.

Wei, Q. and Condie, B. G. (2011). A focused in situ hybridization screen identifies candidate transcriptional regulators of thymic epithelial cell development and function. *PLoS One* **6**, e26795.

Wong, K., Lister, N., Barsanti, M., Lim, J., Hammett, M., Khong, D. M., Siatskas, C., Gray, D., Boyd, R. and Chidgey, A. P. (2014). Multilineage Potential and Self-Renewal Define an Epithelial Progenitor Cell Population in the Adult Thymus. *Cell Reports* **8**, 1198-1209.

Wortis, H. H., Nehlsen, S. and Owen, J. J. (1971). Abnormal development of the thymus in "nude" mice. *J Exp Med* **134**, 681-692.

Wu, L., Sun, T., Kobayashi, K., Gao, P. and Griffin, J. D. (2002). Identification of a family of mastermind-like transcriptional coactivators for mammalian notch receptors. *Mol Cell Biol* **22**, 7688-7700.

Xu, P. X., Zheng, W., Laclef, C., Maire, P., Maas, R. L., Peters, H. and Xu, X. (2002). Eya1 is required for the morphogenesis of mammalian thymus, parathyroid and thyroid. *Development* **129**, 3033-3044.

Yamasaki, S. and Saito, T. (2007). Molecular basis for pre- TCR- mediated autonomous signaling. *Trends in Immunology* **28**, 39-43.

Zou, D., Silvius, D., Davenport, J., Grifone, R., Maire, P. and Xu, P. X. (2006). Patterning of the third pharyngeal pouch into thymus/parathyroid by Six and Eya1. *Dev Biol* **293**, 499-512.

Zuklys, S., Gill, J., Keller, M. P., Hauri-Hohl, M., Zhanybekova, S., Balciunaite, G., Na, K.-J., Jeker, L. T., Hafen, K., Tsukamoto, N., et al. (2009). Stabilized beta-catenin in thymic epithelial cells blocks thymus development and function. *Journal of immunology (Baltimore, Md. : 1950)* **182**, 2997.

Zuklys, S., Handel, A., Zhanybekova, S., Govani, F., Keller, M., Maio, S., Mayer, C. E., Teh, H. Y., Hafen, K., Gallone, G., et al. (2016). Foxn1 regulates key target genes essential for T cell development in postnatal thymic epithelial cells. *Nat Immunol* **17**, 1206-1215.